CHAPTER 3

A First-Generation Receptor Site for the Detection of Bacterial Spores

3.1 Introduction

To design an effective receptor site for a given analyte, we consider certain basic criteria: (1) the receptor site must exhibit an obvious, measurable response upon analyte binding, meaning there must be a clear and distinguishable difference between the two states of analyte bound or unbound; (2) the receptor site should have a very high affinity for the analyte of interest, on the order of $K \sim 10^9$ or greater;[1] (3) binding kinetics should be proportional to the rate of analyte release and consistent with timescales for field work in situ; (4) the receptor site should be resistant to local changes in the environment, such as pH and temperature variations; and (5) the binding of receptor site to analyte should be highly selective, even in complex matrices containing common environmental interferents.

All four luminescent $Ln(DO2A)^+$ binary complexes (Ln = Sm, Eu, Tb and Dy) meet this first requirement in improving lanthanide-based detection of dipicolinate. Based on quantum yield measurements, the $Tb(DO2A)^+$ complex has the greatest sensitization efficiency (Section 2.3.2) and would produce the greatest signal-to-noise ratio as a sensor. We therefore gear our analysis around characterizing the binding properties and robust qualities of $Tb(DO2A)^+$ in order to validate this complex as an effective DPA receptor site. Where appropriate, studies of the entire series will be performed to determine if lanthanide ionic radius has a significant influence.

Binding and kinetics studies will unveil the $Ln(DO2A)^+$ complex with the greatest affinity for dipicolinate and establish dependence of binding rate on lanthanide ionic radius. The effects of modifications to the dipicolinate ligand can be assessed using structural isomers and targeted substitutions. Temperature and pH dependence

experiments will determine if the DO2A ligand can make dipicolinate detection more robust. The impact of both cationic and anionic interferents on DPA detection by the $Tb(DO2A)^{+}$ receptor site will be investigated. Finally, we will apply the $Tb(DO2A)^{+}$ complex to detection of bacterial spores, both in controlled conditions and environmental samples.

3.2 Binding Studies

Various studies will be performed to determine the binding affinities of the luminescent lanthanide complexes for the dipicolinate anion. Binding stoichiometry is established using the Jobs method of continuous variations. Association constants for both the Ln^{3+} and the $Ln(DO2A)^{+}$ complexes for DPA^{2-} will be calculated, the latter with a novel competition experiment. A brief kinetics investigation will also delve into the speed and selectivity of dipicolinate binding.

3.2.1 Jobs Plots

A method of continuous variations will be employed to determine the binding stoichiometries of various lanthanide complexes. The concentrations of two components are varied inversely to produce a range of ratios between the two, with the total concentration held constant. Following spectroscopic analysis, the resulting Jobs Plot reveals any correlation between the components as a function of mole fraction (Figure 3.1). As the maximum response occurs when the mole fraction of the reactants is closest to the actual stoichiometric mole ratio, the binding stoichiometry can be estimated using this approach.[2] In our case, the two components are the lanthanide ion and the

dipicolinate ligand, with the macrocyclic protecting ligand in excess to ensure lanthanide complexation under constant ionic strength. The Jobs method can be applied to a wide variety of measurements (temperature, absorbance, conductivity, etc.); we utilize emission intensity as our metric to qualify lanthanide-dipicolinate binding ratios. Partially hydrolyzed lanthanide species are known to adhere to glass surfaces,[3] so these studies will be performed in disposable acrylate cuvettes (transmission range: 280–900 nm, ~ 70% transmission at 278 nm, reported variation < 1% between cuvettes).

We will use the Jobs method to determine optimal binding stoichiometries for the $Ln(DO2A)^{+}$ complex (Ln = Eu, Tb and Dy) with dipicolinate. We will also investigate several macrocyclic ligands for the terbium case: DO2A, DO3A, DOTA and hexacyclen (Figure 3.2). We anticipate that the two hexadentate ligands (DO2A and hexacyclen) will allow for dipicolinate binding to the lanthanide, with a binding ratio of approximately 1:1 for Tb:DPA. The DO3A and DOTA ligands, which are hepta- and octadentate, respectively, should restrict dipicolinate association to the lanthanide as less than three coordination sites remain available for binding.

Experimental Section

Materials. The following chemicals were purchased and used as received: trichloromethane (chloroform) (Mallinckrodt), DOTA (*1,4,7,10*-tetraazacyclododecane-*1,4,7,10*-tetraacetate) (Macrocyclics), DPA (dipicolinic acid, pyridine-*2,6*,-dicarboxylic acid) (Aldrich), dysprosium(III) chloride hydrate (Alfa Aesar), ether anhydrous (Acros Organics), ethyl alcohol (200-proof) (Acros Organics), europium(III) chloride hexahydrate (Aldrich), hexacyclen (hexamine, 18-azacrown-6, *1,4,7,10,13,16*-hexaaza-

cyclooctadecane) trisulfate (Aldrich), hydrochloric acid (36.5–38.0% in water) (EMD Chemicals), sodium hydroxide pellets (Mallinckrodt), terbium(III) chloride hexahydrate (Alfa Aesar). All lanthanide salts were 99.9% pure or greater, all solvents were ACS certified or HPLC grade, and all other salts were 97% pure or greater. Water was deionized to a resistivity of 18.2 MΩ-cm using a Purelab® Ultra laboratory water purification system (Siemens Water Technologies, Warrendale, PA). DO2A was prepared as previously described (Section 2.2.1).

The *1,4,7,10*-tetraazacyclododecane-*1,4,7*-triacetate (DO3A) ligand was prepared by hydrolysis of *1,4,7,10*-tetraazacyclododecane-*1,4,7*-tri(*tert*-butyl acetate) (DO3A-tBu-ester) (Macrocyclics, Dallas, TX) following a method adapted from the DO2A protocol. The DO3A-tBu-ester (0.9757 g, 1.90 mmol), a slightly off-white powder, was dissolved in 20.0 mL of 20% hydrochloric acid in a roundbottom flask and refluxed for 24 hours with stirring in an oil bath (115 °C). The hydrochloric acid was removed by rotary evaporation under vacuum (~ 50 mbar) in a hot water bath (60 °C) to give an off-white solid. The deprotected ligand was then rinsed using a fine frit (Pyrex, 15 mL, ASTM 4-5.5F, No. 36060) and vacuum filtration with the following in sequence: 20 mL of absolute ethanol (200-proof), 4 mL of diethyl ether, 8 mL of an ethanol-ether (1:1) mixture, and three 8-mL aliquots of ether. The solid was dried in a dessicator under vacuum for 7 days to produce DO3A·1.7HCl·2.8H_2O (0.4632 g, 1.02 mmol) in 53.56% yield. Anal. Calcd (found) for $C_{12}H_{24}N_4O_4$·1.7HCl·2.8H_2O (fw = 456.20): C, 36.86 (36.86); H, 6.69 (6.69); N, 12.28 (12.10). Purity was confirmed with thin-layer chromatography (TLC) using ethanol and chloroform and analysis with a handheld UVGL-25 multiband UV lamp (UVP, Upland, CA) in short wave (254 nm) mode.

It should be noted that subsequent attempts to synthesize DO3A using this same procedure resulted in a brown, viscous substance, presumably decomposition products according to analysis with NMR and mass spectroscopy. It is hypothesized that the hot plate heating the oil bath from the first, successful attempt did not maintain a constant temperature of 115 °C through the 24-hour reflux period, and in fact the reaction might have taken place at a lower temperature. An alternative deprotection procedure with milder reaction conditions was used for later batches (see Section 5.2.2).

Methods. All samples were prepared in triplicate from stock solutions to a final volume of 4.00 mL in disposable acrylate cuvettes (Spectrocell, Oreland, PA) with a 1 cm path length and were allowed to equilibrate for at least 5 days prior to analysis. The concentrations of $LnCl_3$ (Dy, Eu or Tb) and DPA were varied inversely in 1.0-μM increments from 0 to 12.0 μM with 100 μM ligand (DO2A, DO3A, DOTA or EDTA). Solution pH was maintained either by 1.0 mM NaOH (pH 9.0) or 100 mM CHES buffer (pH 9.4) to ensure that the ligands were sufficiently deprotonated for optimum binding.[4-7]

Luminescence spectral analysis was performed by a Fluorolog Fluorescence Spectrometer (Horiba Jobin-Yvon, Edison, NJ). To prevent second-order diffraction of the source radiation, all measurements were taken with a 350-nm colorless sharp cutoff glass filter (03 FCG 055, Melles Griot, Covina, CA). The solution pH was measured using a calibrated handheld pH/mV/temperature meter (Model IQ150, I. Q. Scientific Instruments, Loveland, CO) following data collection. All reported spectra were obtained as a ratio of corrected signal to corrected reference (S_c/R_c) to eliminate the effect of varying background radiation in the sample chamber; intensities are in units of counts per second per microampere (cps/μA).

Results and Discussion

Dipicolinate exhibits no detectable fluorescence (Section 2.3.1), and the emission of the lanthanide without a chromophore is negligible (Section 1.2); we therefore can attribute any significant change in emission intensity to the formation of a lanthanide-dipicolinate complex. The binding affinity of the lanthanide for the macrocycle is very high (Table 3.1),[5, 8, 9] so we can assume that all Ln^{3+} is bound as the lanthanide-macrocycle binary complex when the concentration of macrocycle is in excess. As the lanthanide mole fraction is increased, the emission intensity increases as more of the free dipicolinate binds to the lanthanide, producing a positive slope. Following complete complexation of all lanthanide-macrocycle species with dipicolinate, an increased mole fraction of the lanthanide will result in a decreasing amount of total ternary complex (the dipicolinate concentration is decreasing to maintain a constant total concentration), producing a negative slope. The point at which the biphasic curve shifts from positive to negative slope represents the optimal binding stoichiometry of the lanthanide binary complex to the dipicolinate ligand.

For the DO2A complex, the optimal binding stoichiometry occurs at a terbium mole fraction of 0.5, as would be expected if the $Tb(DO2A)^{+}$ and DPA^{2-} species were binding in a one-to-one fashion (Figure 3.3). The hexacyclen ligand, in contrast, shows nonlinear behavior and the greatest intensity at a Tb mole fraction below 0.5. This implies that an increased concentration of dipicolinate is necessary to completely form the ternary complex, most likely due to steric effects or poor association between the lanthanide and the larger binding cavity of this ligand.[10] The curving behavior of this Jobs plot is also indicative of low to moderate stability.[11] As lanthanides tend to be

oxophilic in character (see Section 1.1), this may be evidence of reduced Tb-hexacyclen binding affinity due to the replacement of two O-donors with two N-donors in the hexacyclen ligand.

The DO3A and DOTA ligands, which should exclude dipicolinate from the lanthanide coordination sphere, both show a binding stoichiometry of approximately 1:3 for Tb:DPA. This suggests that dipicolinate has a strong affinity for the Tb^{3+} cation, and when in excess is able to overcome steric hindrance and partially displace the strongly bound macrocyclic ligand. The Jobs plots of these ligands also show flattening around the maxima, indicating the presence of multiple species in solution. These are most likely the Tb(macrocycle) complex and multiple Tb(macrocycle)(dipicolinate) complexes, with various conformations possible as the dipicolinate forces one or two of the macrocycle carboxyl arms to decouple from the lanthanide.

Jobs plots with various lanthanides and DO2A show a potential relationship between stability and lanthanide ionic radius (Figure 3.4). Europium and terbium have identical binding stoichiometries to DPA with the DO2A ligand in excess, but the dysprosium case indicates the formation of $Dy(DPA)_3$ at low Dy mole fraction. This may be due to the smaller ionic radius of this lanthanide compared to Eu^{3+} and Tb^{3+}, such that there is reduced interaction between the Dy^{3+} cation and the DO2A ligand cavity.

Binding stoichiometry studies using the Jobs method of continuous variations indicate that, as expected, the hexadentate DO2A ligand is the ideal candidate to protect the lanthanide ion from solvent and leave sufficient space available for the tridentate dipicolinate chromophore to bind. We now focus on further characterization of the $Ln(DO2A)^+$ species as sensing complexes for DPA.

3.2.2 Calculation of Dipicolinate Association Constants

The primary measure of receptor site efficacy is binding affinity for the target analyte. Ideal sensing complexes have nanomolar sensitivity or better.[1] However, most titrimetric techniques for experimentally determining association constants, such as the Benesi-Hildebrand method,[12] break down under conditions where (1) binding constants are large ($> 10^9\ M^{-1}$), (2) the system contains more than two components, or (3) changes in absorbance or luminescence are small.[13, 14] We therefore developed and tested a binding affinity by competition (BAC) assay to determine DPA to binary complex binding constants.

Ternary $Ln(DO2A)(DPA)^-$ complex solutions (of crystallographically characterized TBA·Ln(DO2A)(DPA)) are titrated with $LnCl_3$; increased Ln^{3+} concentration results in a shift in equilibrium population from $Ln(DO2A)(DPA)^-$ to $Ln(DO2A)^+$ and $Ln(DPA)^+$, which is monitored via a ligand field sensitive transition using fluorescence spectroscopy (see Figure 3.5). A best fit of luminescence intensity titration data to a two-state thermodynamic model yields the competition equilibrium constant (K_c), which in conjunction with independent measurement of the $Ln(DPA)^+$ formation constant (K_a) allows calculation of the ternary complex formation constant (K_a'). In general, the BAC assay can be employed to determine ligand binding constants in systems were the lanthanide platform (usually a binary complex) is stable and the ligand bound versus unbound states can be spectroscopically distinguished.

Experimental Section

Materials. Dysprosium(III) chloride hydrate (Alfa Aesar), europium(III) chloride hexahydrate (Aldrich), samarium(III) chloride (Alfa Aesar), sodium acetate trihydrate (Mallinckrodt) and terbium(III) chloride hexahydrate (Alfa Aesar) were purchased and used as received. All lanthanide salts were 99.9% pure or greater and all other salts were 97% pure or greater. DO2A was prepared as previously described (Section 2.2.1). Dried, fully characterized TBA·Ln(DO2A)(DPA) crystals (Section 2.2.1) were used to produce a 1:1:1 ratio of Ln:DO2A:DPA in solution. Water was deionized to a resistivity of 18.2 MΩ-cm using a Purelab® Ultra laboratory water purification system.

Methods. All samples were prepared to a final volume of 3.50 mL from stock solutions in disposable acrylate cuvettes (Spectrocell, Oreland, PA) with a 1 cm path length and were allowed to equilibrate for at least 7 days. Luminescence spectral analysis was performed by a Fluorolog Fluorescence Spectrometer with a 350-nm cutoff filter as previously described (Section 3.2.1). The solution pH was measured using a calibrated handheld IQ150 pH/mV/temperature meter (I. Q. Scientific Instruments) following data collection. Sample temperature was monitored using a handheld Fluke 62 Mini Infrared Thermometer (Fluke Corp, Everett, WA).

Calculation of K_a. Initially, a Microlab 500 Series Autotitrator (Hamilton Co., Reno, NV) with Instrument Control software was used to adjust the concentrations of terbium and dipicolinate in a single cuvette for in situ luminescence monitoring. However, results were inconsistent in all titrations involving DPA, most likely due to retention of this species within the titrator tubing. An alternative approach using disposable acrylate cuvettes, with one cuvette per concentration point prepared

individually in triplicate, yielded reproducible results and allowed for pH measurement of each data point. This method will be used for all future titrimetric assays.

Association constants for Ln^{3+} to DPA^{2-} (Ln = Sm, Eu, Tb and Dy) were determined via titration of Ln^{3+} against 10.0 nM DPA in 0.2 M sodium acetate (pH 7.4). A linear fit similar to that of the one-step equilibrium model of Jones and Vullev[15] was applied as $[Ln^{3+}] > [DPA^{2-}]$, and the binding affinity of the binary complex (K_a) was calculated using the following linear relationship:

$$\log\left(\frac{R}{C_{Ln}}\right) = \log(1-R) + \log K_a$$
$$R = \frac{[LnDPA]_{eq}}{[LnDPA]_{eq} + [DPA]_{eq}} \qquad [3.1]$$

where C_{Ln} is the total concentration of the lanthanide and R is the normalized integrated emission intensity (see Appendix A for derivation).

Calculation of K_a'. Samples were prepared using solvated $Ln(DO2A)(DPA)^-$ crystals and lanthanide chloride salts in 0.2 M sodium acetate (pH 7.4), such that the concentration of $Ln(DO2A)(DPA)^-$ was 1.0 μM and the concentration of free Ln^{3+} ranged from 1.0 nM to 1.0 mM. The use of X-ray quality, solvated TBA·Ln(DO2A)(DPA) crystals in this work demonstrates a major advantage, especially at low concentrations; the precise measure of the initial concentration of $Ln(DO2A)(DPA)^-$ could not be achieved without this important step. As Ln^{3+} was added, the shift in equilibrium $Ln(DO2A)(DPA)^-$ and $Ln(DPA)^+$ concentrations was monitored via a ligand field sensitive transition in the emission spectrum using luminescence spectroscopy. Emission spectra (λ_{ex} = 278 nm) were integrated over the most ligand-field-sensitive peak (Sm: $^4G_{5/2} \rightarrow {}^6H_{7/2}$, 580–625 nm; Eu: $^5D_0 \rightarrow {}^7F_4$, 675–710 nm;

Tb: $^5D_4 \rightarrow {}^7F_4$, 570–600 nm; Dy: $^4F_{9/2} \rightarrow {}^6H_{13/2}$, 555–595 nm) to produce curves of observed integrated intensity (I_{obs}) against the log of excess free lanthanide (log $[Ln^{3+}]_{xs}$). A best fit to a two-state thermodynamic model using the Curve Fitting Tool in Matlab® yielded the competition equilibrium constant (K_c) by equation 3.2.

$$I_{obs} = \left(1 - \frac{[Ln(DPA)^+]_{eq}}{[Ln(DO2A)(DPA)^-]_T}\right) I_{max} + \left(\frac{[Ln(DPA)^+]_{eq}}{[Ln(DO2A)(DPA)^-]_T}\right) I_{min}$$

where [3.2]

$$[Ln(DPA)^+]_{eq} = \frac{[Ln^{3+}]_T + \left(\begin{array}{l}\left\{[Ln^{3+}]_T - 2\left(1 - K_C^{-1}\right)[Ln(DO2A)(DPA)^-]_T\right\}^2 \\ + 4K_C^{-1}\left(1 - K_C^{-1}\right)\left([Ln(DO2A)(DPA)^-]_T\right)^2\end{array}\right)^{1/2}}{2\left(1 - K_C^{-1}\right)}$$

The total concentrations of free lanthanide ($[Ln^{3+}]_T$) and ternary complex ($[Tb(DO2A)(DPA)^-]_T$) are known from initial conditions. Following independent measurement of the $Ln(DPA)^+$ formation constant (K_a) at identical pH and temperature, the ternary complex formation constant K_a' was calculated using the relation in equation 3.3 (see Appendix B for derivation).

$$K_C = \frac{K_a}{K_a'} \qquad [3.3]$$

Results and Discussion

The serial dilution method used for calculation of K_a, though not as ubiquitous as that of Jones and Vullev, presents certain advantages. Both were derived from the same one-step Tb-DPA equilibration model, but Jones and Vullev made the assumption that

[Ln] >> [DPA] to cancel a term and arrive at the final equation used for the linear fit (see Supporting Information of reference 15). As the intrinsic luminescence of the Ln^{3+} species alone presents an upper bound (which usually occurs in the millimolar regime), this high lower bound limiting the lanthanide concentration means that there is a very small range where this fit can be applied. In contrast, our fit makes no such assumption, and only requires that [Tb] ≥ [DPA] to be valid. Therefore, a broader data set can be applied to this fit, allowing for more accurate binding constant measurement (see Figure 3.6).

Secondly, though the linear fit provided by the Jones and Vullev method produces a value *n* for the slope that can be used to approximate the number of DPA moieties bound to the lanthanide, i.e., $Tb(DPA)_n$, this allows for more possible error in terms of the fit when the coordination number is already known. In other words, a value of n = 0.93 would be considered close enough to 1, and one might assume that the y-intercept of such a fit would therefore be an accurate measure of the K_a for TbDPA. However, a difference of 7% in the slope of this fit can produce a y-intercept that is off by nearly 10%, and this error would not be included in the reported value of K_a. In our fitting technique, the slope is set to unity, so the only parameter that can be shifted to fit the data is that of the quantity of interest – the y-intercept, or the value of K_a. We therefore have more confidence in our calculated values of K_a than in those of other methods.

Using the solvated TBA·Ln(DO2A)(DPA) crystals to achieve an optimized 1:1:1 ratio of Ln/DO2A/DPA, we were able to perform titrations over 6 orders of magnitude, with added $[Ln^{3+}]_{xs}$ ranging from 1.0 nM to 1.0 mM. The shift from ternary to binary complex was easily observed via luminescence spectroscopy in this range. Titration of

free Ln^{3+} in buffer over the same concentration range resulted in negligible intensity increase, confirming that the intensity change observed is due to the transition from ternary to mono-DPA complex.

Our calculated values of K_a and K_a' for various lanthanide complexes (Ln = Sm, Eu, Tb and Dy) appear in Table 3.2. The association constant K_a for the terbium case is in agreement with the formation constant obtained by Jones and Vullev at a similar pH and ionic strength.[15] As seen in Figures 3.7 and 3.8, the addition of the DO2A ligand enhances the binding affinity of the Ln^{3+} ion for the DPA^{2-} analyte by at least an order of magnitude. This result is quite intriguing, as this trend does not follow predictions based on total charges of the binding species. Specifically, upon addition of the DO2A ligand, the dipicolinate receptor site decreases from a net +3 charge of the lanthanide alone to a binary complex with a total charge of only +1. As binding interactions with lanthanides tend to be electrostatic in character (Section 1.1), this should have resulted in a decrease in binding affinity. We postulate that the lanthanide-macrocycle platform increases the positive charge of the binding site through the electron-withdrawing N and O moieties of the macrocycle, which allows for greater compatibility with the negative surface of the dipicolinate moiety. This property of 'ligand enhancement' in analyte binding affinity will be further explored in the Conclusions section at the end of the chapter.

Another interesting discovery was that the binding affinity of the $Tb(DO2A)^+$ binary complex is even more effective and nearly an order of magnitude greater than the other three lanthanides. The calculated association constant for $Tb(DO2A)^+$ to DPA^{2-} is also several orders of magnitude greater than that of Tb(EDTA).[16] Both DO2A and EDTA are hexadentate and leave three remaining sites available for dipicolinate

binding,[17] but closer examination of the geometry of those sites may provide an explanation for the discrepancy in binding affinity. A crystal structure of the Tb(EDTA) complex reveals that the three coordination sites are adjacent, but arranged in a trigonal fashion (Figure 3.9). The dipicolinate ligand is a linear molecule, and requires three adjacent *linear* sites available on the lanthanide to bind properly. The DO2A ligand, with its more rigid azacrown backbone and two carboxyl arms, coordinates to the lanthanide with the appropriate geometry. The floppy EDTA ligand must undergo reorganization around the Tb^{3+} ion to accommodate the dipicolinate ligand, and therefore the binding affinity is lower for the Tb(EDTA) complex. This is supported by a study involving picolinic acid, dipicolinic acid and various terbium polycarboxylate ligands, where in many cases the ligand entered a forced conformational change to facilitate chromophore binding and form the ternary complex.[18]

The binding affinity by competition (BAC) assay can be employed to quantify ternary lanthanide complex formation under conditions where the lanthanide-macrocycle platform is stable and the concentrations of the two states of the receptor site – bound and vacant – can be measured. In our case, the binary and ternary complexes of interest are spectroscopically resolvable. The BAC assay is especially useful in high binding regimes, where direct measures of ligand binding, such as the Benesi-Hildebrand method, break down. A similar luminescence-based study has demonstrated calculation of europium-macrocycle stability constants based on lifetime measurements,[19] also in the high binding constant regime. However, this technique is only valid for two components and where lifetimes of the two species of interest are discernable, and cannot be applied to environmental samples. Our assay, in contrast, can be applied to equilibria with more

than two components and can be implemented in a variety of conditions such as those expected in environmental samples. As long as K_a and K_a' are measured in identical conditions, the change in binding affinity can be calculated quantitatively. The BAC assay allows for the unambiguous measure of relative stability, to guide us toward a superior sensor for bacterial spores via DPA-triggered Tb^{3+} luminescence.

3.2.3 Binding Rates and Kinetics

Another important quality of an effective receptor site is rapid binding to the analyte of interest. To determine the rate of dipicolinate binding by the $Ln(DO2A)^+$ complexes, time courses and a brief kinetics study will be performed. Various studies have shown that macrocyclic ligands can take hours to even days to completely coordinate the lanthanide.[5, 6, 20] The carboxylate groups coordinate first, followed by the lanthanide moving into the macrocycle cavity in a concerted rearrangement that may take several steps to produce the final thermodynamically stable complex.[21] However, once the lanthanide-macrocycle binary complex is formed, we believe dipicolinate binding will occur rapidly as little or no reorganization of the macrocycle is necessary.

Experimental Section

Materials. CAPS (*N*-cyclohexyl-*3*-aminopropanesulfonic acid) buffer (Alfa Aesar), DPA (dipicolinic acid, pyridine-*2,6,*-dicarboxylic acid) (Aldrich), dysprosium(III) chloride hydrate (Alfa Aesar), europium(III) chloride hexahydrate (Aldrich), MOPS (*3*-(*N*-morpholino)ethanesulfonic acid) buffer (Alfa Aesar), samarium(III) chloride (Alfa Aesar), sodium acetate trihydrate (Mallinckrodt) and terbium(III) chloride hexahydrate

(Alfa Aesar) were purchased and used as received. All lanthanide salts were 99.9% pure or greater and all other salts were 97% pure or greater. DO2A was prepared as previously described (Section 2.2.1). Water was deionized to a resistivity of 18.2 MΩ-cm using a Purelab® Ultra laboratory water purification system.

Methods. Unless otherwise specified, all experiments were performed at 25 °C in disposable acrylate cuvettes with a 1 cm path length. Sample injection during spectral acquisition was performed in the dark to prevent signal bleaching or damage to the photomultiplier tube of the fluorescence spectrometer.

Time courses. A 3.80 mL solution of 1.05 μM $Tb(DO2A)^+$ in 0.1 M buffer was placed in an acrylate cuvette in the spectrofluorometer sample chamber. A time course was initiated (λ_{ex} = 278 nm, λ_{em} = 544 nm), and after an appropriate baseline was obtained (~ 200 s) a 200-μL aliquot of 20.0 μM DPA was injected to produce a final concentration of 1.0 μM DPA in a 4.00 mL solution of 1.0 μM $Tb(DO2A)^+$. Ternary complex formation was confirmed with an analogous setup and emission scans every 5 minutes. This was performed in MOPS (pH 7.4) and CAPS (pH 10.4) to determine if OH^- is more difficult to displace from the Tb^{3+} coordination sphere than H_2O.

Kinetics study. Solutions of 1.0 and 10.0 μM Ln(DO2A)(DPA), where Ln = Sm, Eu, Tb and Dy, were injected with various aliquots of 4.0 mM $GdCl_3$ in 0.2 M NaOAc, pH 7.5, using the same time course method described above. Emission intensity at the λ_{max} for each lanthanide was monitored as a function of time (λ_{Sm} = 600 nm, λ_{Eu} = 614 nm, λ_{Tb} = 544 nm, λ_{Dy} = 575 nm).

Stability over time. The same series of cuvettes prepared for the calculation of K_a' (Section 3.2.2) were stored at room temperature and analyzed again after 5 and 11

months. Cuvettes that had lost an appreciable amount of solvent (> 0.5 mL) due to evaporation were refilled back to the 4.00 mL volume by mass using nanopure water (18.2 MΩ-cm resistivity). Sample pH was determined after collection of each data set.

Results and Discussion

Though others have noted that complex formation involving macrocyclic ligands can occur on the order of several hours to even days, we have found that DPA binding is rapid at neutral to high pH provided that the $Tb(DO2A)^+$ binary complex is already formed in solution, as would be the case for a receptor site (see Figure 3.10). The rate of DPA complexation is slightly longer at higher pH (~ 10 s as compared to 3 s); this is attributed to the negatively charged OH^- moieties being more difficult to displace from the Tb^{3+} coordination sphere than neutral H_2O molecules. However, as complete DPA binding occurs on the order of seconds in both cases, the applicability of the $Tb(DO2A)^+$ complex as a dipicolinate sensor in real-time is confirmed.

An initial experiment competing 10 μM $Tb(DO2A)(DPA)^-$ with 10 μM Eu^{3+} in 0.2 M NaOAc, pH 7.4, validated the hypothesis that the DO2A ligand is not labile over the course of the experiment, as only $Eu(DPA)^+$ is produced (see Figure 3.11), described in equilibrium 3.4.

$$Tb(DO2A)(DPA)^- + Eu^{3+} \rightleftharpoons Tb(DO2A)^+ + EuDPA^+ \qquad [3.4]$$

The DO2A ligand does not begin to dissociate from the Tb^{3+} ion and bind to the Eu^{3+} ion for several weeks, as evidenced by formation of the $Eu(DO2A)(DPA)^-$ complex from the characteristic emission spectrum.

The kinetics study involving competition of $Ln(DO2A)(DPA)^-$ against Gd^{3+} produced decay curves that were fit to a monoexponential model. Gadolinium does not luminesce under excitation at 278 nm, and therefore as the Gd^{3+} competes with the $Ln(DO2A)^+$ complex and removes the dipicolinate ligand to form $Gd(DPA)^+$, the luminescence intensity will decrease to zero. This is illustrated in equilibrium 3.5 with the observable rate described by equation 3.6.

$$Ln(DO2A)(DPA)^- + Gd^{3+} \underset{k_{-1}}{\overset{k_1}{\rightleftharpoons}} Ln(DO2A)^+ + GdDPA^+ \qquad [3.5]$$

$$k_{obs} = k_1 - k_{-1} \qquad [3.6]$$

Results indicate that the observed rate of DPA loss by the ternary complex (k_{obs}) is a function of lanthanide ionic radius, with the smallest lanthanide (dysprosium) exhibiting the slowest rate (see Figure 3.12). We postulate this is due to effective shielding of the smaller lanthanides by the DO2A and DPA ligands, reducing ligand exchange rates for these species. This is also substantiated by the higher dipicolinate binding affinities for the $Tb(DO2A)^+$ and $Dy(DO2A)^+$ binary complexes (log K_a' = 9.25 and 8.79, respectively) as compared to the Eu and Sm complexes (Section 3.2.2).

For the terbium and europium ternary complexes, kinetics experiments involving gadolinium were more thoroughly explored, and a relationship between the observed luminescence decay rate (k_{obs}) and gadolinium concentration was established. These decay curves were also fit to a monoexponential model, though we found it interesting that as the Gd^{3+} concentration increased, the rate of luminescence decay decreased in a logarithmic fashion (see Figure 3.13). It must be noted, however, that only in the limit of 1000-fold Gd^{3+} concentration versus ternary complex does the luminescence drop

completely to zero; for all cases where [Gd^{3+}] < 1 mM, a population of $Tb(DO2A)(DPA)^-$ or $Eu(DO2A)(DPA)^-$ persisted. This indicates that the rate of DPA abstraction by Gd^{3+} is limited by concentration, and that the affinity of Gd^{3+} for dipicolinate is significantly less than that of the $Tb(DO2A)^+$ and $Eu(DO2A)^+$ complexes, as expected.

Once formed, the $Tb(DO2A)(DPA)^-$ ternary complex remains stable in solution for extended periods of time, approaching a year or more, with negligible loss in dipicolinate binding affinity (Figure 3.14). The emission intensity of the complex also does not decrease over time or repeated spectral analysis, indicating substantial resistance to photobleaching.

3.3 DPA Derivatives

In order to better understand the binding behavior of dipicolinate, the coordination geometries of various DPA analogues with Tb^{3+} and $Tb(DO2A)^+$ will be explored. Structural isomers and related pyridines, in which one or more of the carboxyl arms of the dipicolinate are moved around the pyridine ring or removed altogether, and DPA species with targeted substitutions in the para-position, will all be investigated to determine what factors are most important for effective chelation to the lanthanide or lanthanide complex.

3.3.1 Structural Isomers and Related Pyridines

Three structural isomers will be utilized in this study: pyridine-*2,4*-dicarboxylic acid (2,4-DPA), pyridine-*3,5*-dicarboxylic acid (3,5-DPA) and dipicolinate itself (pyridine-*2,6*-dicarboxylic acid, DPA). Picolinic acid (Pic) and pyridine (Pyr), which

have one and both carboxyl arms removed, respectively, are also included. As DPA usually coordinates in a tridentate fashion with the two carboxyl arms and the pyridine amine involved, shifting one or both of the carboxyl moieties around the ring will result in multiple bidentate chelation possibilities (Figure 3.15).

Lanthanides tend to be oxophilic, but evidence from complexes with azacrown ligands suggests that neutral N donors may be slightly preferred to neutral O donors.[22] Though admittedly formal neutrality of ligands is not the most important factor governing complexation, this may still suggest that nitrogen can be an effective chelator and can compete with oxygen in some cases. By comparison of the relative stabilities of the various isomers and pyridine species, we can learn whether the carboxyl or the amine substituent is more important in lanthanide chelation.

Experimental Section

Materials. DPA (dipicolinic acid, pyridine-*2,6*,-dicarboxylic acid) (Aldrich), 2,4-DPA (pyridine-*2,4*-dicarboxylic acid) monohydrate (Aldrich), 3,5-DPA (pyridine-*3,5*-dicarboxylic acid) (Aldrich), EDTA (ethylenediaminetetraacetic acid) (Aldrich), MOPS (*3*-(*N*-morpholino)ethanesulfonic acid) buffer (Alfa Aesar), picolinic acid (pyridine-*2*-carboxylic acid, Pic) (Aldrich), pyridine (Pyr) (J.T. Baker), terbium(III) chloride hexahydrate (Alfa Aesar) and sodium acetate trihydrate (Mallinckrodt) were purchased and used as received. All lanthanide salts were 99.9% pure or greater, all DPA derivatives and pyridines were 98% pure or greater, and all other salts were 97% pure or greater. DO2A and DO3A were prepared as previously described (Sections 2.2.1 and

3.2.1). Water was deionized to a resistivity of 18.2 MΩ-cm using a Purelab® Ultra laboratory water purification system.

Methods. Unless otherwise specified, all samples were prepared to a final volume of 4.00 mL in disposable acrylate cuvettes with a 1 cm path length. Luminescence spectral analysis was performed by a Fluorolog Fluorescence Spectrometer with a 350-nm cutoff filter as previously described (Section 3.2.1).

Pyridines. Stock solutions of DPA, Pic and Pyr were prepared volumetrically in clean 100-mL volumetric flasks. Solutions of 10.0 μM Tb(ligand) were prepared in 0.2 M NaOAc buffer, pH 5.5, and allowed to equilibrate for one hour prior to analysis. For the picolinate study, 10.0 μM solutions of Tb(Pic), $Tb(Pic)_4$ (100.0 μM Pic; saturation number of 4 Pic ligands on the lanthanide assumes bidentate coordination), Tb(Pic)(DO2A) and Tb(Pic)(DO3A) were prepared in 0.1 M MOPS buffer, pH 7.2, and allowed to equilibrate for 24 hours before analysis.

Structural isomers. Solutions of 10.0 μM dipicolinate species (DPA, 2,4-DPA and 3,5-DPA) and picolinate in 1.0 mM Tb(ligand), where ligand is DO2A, DO3A, DOTA or EDTA, were prepared in 50 mM MOPS buffer, pH 7.5, and allowed to equilibrate for 5 days prior to analysis.

DFT calculations. The equilibrium geometry, orbitals and energies of the minimized pyridine, picolinate and dipicolinate derivatives were refined by the semi-empirical PM3 method using the Titan® software package (Wavefunction, Inc.; Schrödinger, Inc.). Electron density maps were generated for the highest occupied molecular orbital (HOMO) of each species.

Results and Discussion

Pyridine has no detectable emission when in solution with terbium (Figure 3.16), indicating either very low binding affinity or little to no energy transfer. This is expected, as relatively few lanthanide complexes with monodentate nitrogen donors exist (Section 1.1), and without any carboxyl moieties to donate to binding, pyridine has little appeal to the oxophilic lanthanide. Picolinate has some coordination to Tb^{3+} as evidenced by excitation spectra, but dipicolinate exhibits the greatest intensity by a significant margin. This indicates that lanthanide sensitization is directly proportional to chromophore denticity, as anticipated, at least in the mono- to tridentate regime.

The excitation of terbium picolinate exhibits two peaks similar to the terbium dipicolinate spectrum, attributed to $\pi \rightarrow \pi^*$ transitions. However, the terbium picolinate maxima (268 and 273 nm) are blue-shifted by approximately 5 nm compared to the dipicolinate case. This may indicate reduced terbium sensitization efficiency as greater energy is required to produce lanthanide emission, possibly due to a shift in electron density back onto the pyridine ring. This is supported by simulations using the Titan® software package, which depict more of the electron density localized around the ring in the Pic structure than DPA (Figure 3.15).

Emission intensities of picolinate with $Tb(DO2A)^+$ and Tb(DO3A) are nearly identical (Figure 3.17), indicating that the Pic anion has a similar affinity for the binary complex in both cases. This suggests that picolinate coordinates to the Tb^{3+} ion in a bidentate fashion, most likely via a carboxyl oxygen and the pyridine nitrogen, which would not be hindered by the heptadentate DO3A ligand as the lanthanide is nine-coordinate. Coordination in an η-fashion through both oxygens of the single carboxyl

moiety is possible, though increased distance from the pyridine ring would severely reduce energy transfer efficiency (Section 1.2).[23] Further, a published crystal structure of hydrated dysprosium picolinate reports chelation via the nitrogen atom and one carboxyl oxygen of the picolinate ion.[24] The dipicolinate anion, in contrast, suffers a large decrease in emission intensity for the Tb(DO3A) case, as tridentate chelation is not possible without disruption of one of the DO3A carboxylate arms. High resolution emission spectra of the Tb(DO2A)(Pic) and Tb(DO3A)(Pic)$^-$ complexes also display different Stark splittings (Figure 3.18), consistent with a change in the composition and/or symmetry of the lanthanide coordination sphere (Section 2.4.1).

The emission spectra of the 2,4-DPA and DPA ternary complexes with Tb(DO2A)$^+$ and Tb(DO3A) have similar intensities, suggesting these two species coordinate with similar affinity (Figure 3.17). Loss of intensity by approximately half with the DO3A complex in both cases indicates steric hindrance when only two coordination sites are available on the terbium; as the 2,4-DPA derivative has only two possible coordination modes, both of them bidentate, this implies that the option with the greater 'bite' is favored. We therefore postulate that the 2,4-DPA species is coordinating via the two carboxyl arms to the terbium, with the pyridine amine not directly involved in binding. This is also supported by the difference in emission intensity between the 2,4-DPA and Pic ternary complexes with Tb(DO2A)$^+$; if the 2,4-DPA species was coordinating through the pyridine amine and one carboxyl arm as the Pic ligand does, these intensities should be much more similar.

In contrast, the 3,5-DPA emission spectra are about an order of magnitude lower in intensity than the 2,6- and 2,4-dipicolinate derivatives, indicating weak coordination

and/or lanthanide sensitization. Further, the DO3A complex has the greatest intensity for this isomer. This suggests bidentate coordination in a manner of low surface area with respect to the lanthanide. Most likely, the 3,5-DPA is coordinating via one of the carboxyl groups and the pyridine nitrogen. Such coordination is unusual, considering the potential for bidentate binding with the two carboxyl groups on the opposite side of the pyridine ring. Perhaps the pyridine nitrogen is more significant than supposed when it comes to lanthanide coordination.

All attempts at crystallization of these species were unsuccessful, and the only reported crystal structures of lanthanides with these dipicolinate derivatives are of polymeric species obtained under hydrothermal conditions,[25] which cannot be directly related to solution studies. Obviously more thorough analysis is required before accurate binding models can be proposed, but we have established through our brief investigation that the chelation properties of dipicolinate and related pyridines to lanthanides are not trivial, and that the pyridine nitrogen may play a significant part in dictating both binding motif and lanthanide sensitization.

3.3.2 Targeted Substitution

To determine the effect of electrostatics on dipicolinate binding interactions with the lanthanide, various spectroscopic and stability experiments were performed with a 4-substituted dipicolinate analogue, specifically *4*-fluoro-pyridine-*2,6*-dicarboxylic acid (F-DPA). With a highly electron-withdrawing group in the 4-position on the dipicolinate ligand, we anticipate decreased electron density on the chelating side of the DPA. Assuming the interaction between the lanthanide cation and the dipicolinate anion is

electrostatic in nature, this should manifest in decreased binding affinity and changes in intramolecular bond distances for complexes involving the F-DPA ligand.

A previous study[26] reported a trend of energy transfer efficiency to the Tb^{3+} ion with 4-substituted dipicolinate ligands as follows:

$$NH_2 > OH > NHAc > Cl > H \sim Br$$

We assume that the 4-fluoro-substituted DPA ligand will behave similarly to the 4-chloro-substituted species, and should therefore have a greater energy transfer efficiency than the unmodified DPA chelator.

Experimental Section

Materials. Acetone (J. T. Baker), DPA (dipicolinic acid, pyridine-*2,6*-dicarboxylic acid) (Aldrich), MOPS (*3*-(*N*-morpholino)ethanesulfonic acid) buffer (Alfa Aesar), sodium hydroxide (NaOH 50% in water) (Mallinckrodt), sodium hydroxide pellets (Mallinckrodt), terbium(III) chloride hexahydrate (Alfa Aesar) and tetrabutylammonium hydroxide (TBAOH 10% in *2*-propanol) (TCI America) were purchased and used as received. The terbium salt was 99.9% pure, DPA was 98% pure, all solvents were ACS certified or HPLC grade, and all other salts were 97% pure or greater. DO2A was prepared as previously described (Section 2.2.1). F-DPA (*4*-fluoro-pyridine-*2,6*-dicarboxylic acid) was synthesized by CB Research & Development, Inc., from the *4*-oxo-dipicolinate in five steps (Project code CIT-1000CB-b, Lots KW-5-133 and KW-5-155) (Figure 3.19) with a reported purity of > 95% and melting point of > 250 °C. Water was deionized to a resistivity of 18.2 MΩ-cm using a Purelab® Ultra laboratory water purification system.

Methods. Unless otherwise specified, all samples were prepared in triplicate to a final volume of 3.50 mL in disposable acrylate cuvettes with a 1 cm path length. Luminescence spectral analysis was performed by a Fluorolog Fluorescence Spectrometer with a 350-nm cutoff filter as previously described (Section 3.2.1).

Spectroscopy. Solutions of 10.0 μM terbium mono-dipicolinate (with Tb in 10% excess) and tris-dipicolinate (with 1:10 Tb:dipicolinate), where dipicolinate is DPA or F-DPA, were prepared in nanopure H_2O (18.2 MΩ-cm resistivity). The Tb(DO2A)(DPA)$^-$ and Tb(DO2A)(F-DPA)$^-$ ternary complexes were prepared to 10.0 μM in 1.0 mM NaOH, pH 9. All solutions were allowed to equilibrate for 90 hours prior to analysis. Absorbance measurements were made in quartz cuvettes (1 cm path length) using a Cary 50 Bio UV/Visible Spectrophotometer (Varian, Inc., Palo Alto, CA).

Binding studies. A Jobs method of continuous variations was performed as previously described (Section 3.2.1) with the concentrations of F-DPA and Tb(DO2A)$^+$ inversely varied from 0 to 12 μM in 1.0 mM NaOH, pH 9.0. Samples were allowed to equilibrate for 2 days prior to analysis. The binding affinity of F-DPA for Tb^{3+} was calculated using the one-step equilibration model previously described (equation 3.1), with 10.0 nM F-DPA and the concentration of $TbCl_3$ ranging from 10.0 nM to 1.0 μM in 0.2 M NaOAc, pH 7.6 at 25 °C. Each trial was fit separately and the three values of log K_a averaged to produce the final result.

pH dependence. Samples of 10.0 μM Tb(DO2A)(DPA)$^-$ or Tb(DO2A)(F-DPA) were prepared in 0.1 M buffer. Five buffers were used: MES (pK_a = 6.1), MOPS (pK_a = 7.2), TAPS (pK_a = 8.4), CHES (pK_a = 9.3) and CAPS (pK_a = 10.4), with pH adjustment

to within 0.1 of the pK_a value using 50% NaOH added dropwise. Emission spectra were obtained after an equilibration time of 21 hours.

Crystallization. Crystals of TBA·Tb(DO2A)(F-DPA) were obtained after several attempts following the same procedure as the normal ternary complex crystallization (Section 2.2.1) using similar reactant masses and solvent volumes and a new frit. Crystal formation was observed after sitting at room temperature for 3 days. Suitable crystals were utilized for X-ray diffraction studies at the Beckman Institute X-ray Crystallography Facility (Caltech).

X-ray crystallography. Crystals were mounted on a glass fiber using Paratone oil and then placed on the diffractometer under a nitrogen stream. Diffraction data were collected at 100 ± 2 K on a Bruker KAPPA APEX II diffractometer equipped with graphite monochromated MoKα radiation (λα = 0.71073 Å). The structure was solved by direct methods using SHELXS-97[27] and refined by full-matrix least-squares calculations on F^2 against all reflections using the SHELXL-97 program package.[28, 29] Non-hydrogen atoms were refined anisotropically. Due to disorder at the halogen site, the fluorine was refined isotropically, and fluorine and chlorine were restrained to a total occupancy of unity. The hydrogen atoms were introduced in calculated positions. CCDC reference number 761002. Crystal and refinement data are collected in Table 3.3. Complete crystallographic data, including asymmetric unit contents, atomic coordinates, bond distances and angles, and anisotropic displacement parameters, are listed in Appendix F.

Results and Discussion

Excitation spectra of the F-DPA and DPA ternary complexes reveal a blue-shift with respect to the fluorinated dipicolinate species of approximately 5–6 nm, similar to the picolinate complex (Figure 3.20). This could be due to reduced coupling of the substituted dipicolinate and the lanthanide as a result of shifted electron density towards the fluorine moiety, away from the chelating face of the ligand. Though we do see more pronounced Stark splitting in the F-DPA ternary complex (Figure 3.21), there is no evidence of a heavy-atom effect in terms of enhancement of luminescence intensity or spin-orbit coupling.[30] The Jobs plot (Figure 3.22) indicates a clear 1:1 binding stoichiometry of the $Tb(DO2A)^{+}$ binary complex and F-DPA.

The binding affinity of F-DPA^{2-} for Tb^{3+} was calculated using the same procedure as the dipicolinate ligand (Section 3.2.2) in identical conditions. The binding constant for the 4-fluoro-substituted ligand ($\log K_a = 7.10 \pm 0.04$) is less than that of the normal dipicolinate ligand ($\log K_a = 7.41 \pm 0.03$). This is consistent with the hypothesis that the electron density in the F-DPA ligand is shifted away from the chelating side of the ligand, thereby reducing electrostatic attraction between the F-DPA and the lanthanide. The $Tb(DO2A)(F\text{-}DPA)^{-}$ complex also exhibits a slight pH dependence (Figure 3.23), with the emission intensity decreasing by more than 10% below pH 7. This could also support reduced electron density near the carboxyl moieties, making them more easily protonated as pH decreases.

Crystallographic analysis indicates that the crystal structure is composed of approximately 63% $Tb(DO2A)(Cl\text{-}DPA)^{-}$ and 37% $Tb(DO2A)(F\text{-}DPA)^{-}$, where Cl-DPA is *4*-chloro-pyridine-*2,6*-dicarboxylic acid. Given that the F-DPA starting material is

approximately 10% Cl-DPA by elemental analysis (meaning the initial F-DPA purity was not 95% as reported) and the likelihood of halogen exchange on the dipicolinate is very low in this temperature and pressure regime,[31] this result indicates a preference for the chloro-substituted dipicolinate ligand in the crystallization protocol. Most likely, the larger chlorine atom is more thermodynamically favored in the unit cell. Contrary to expectations, no significant deviation is observed in the dipicolinate-lanthanide intramolecular distances; instead, certain C-C and C-O bonds within the F-DPA ligand appear to have lengthened or shortened to accommodate the halogen in the 4-position (Figure 3.24). However, as the crystal structure is not purely F-DPA, little conclusions can be drawn from such an analysis.

Due to the F/Cl discrepancy between solution studies and crystallographic analysis, calculation of K_a' using the BAC assay with solvated crystals was not attempted. Pure crystals of either Tb(DO2A)(F-DPA)$^-$ or Tb(DO2A)(Cl-DPA)$^-$ are necessary for binding constant calculation, and require a 4-substituted dipicolinate starting material with purity greater than 90%.

Overall, spectroscopic and binding studies of the 4-fluoro-subsituted dipicolinate chromophore indicate that electrostatic effects play a significant role in lanthanide chelation and stability. Introduction of an electron-withdrawing group in a position opposite of the tridentate binding site results in an observable decrease in binding affinity and an increased susceptibility to protonation.

3.4 Effects of pH and Temperature

Ideal sensing complexes should be highly resistant to pH and temperature variations in the local environment. Temperature studies can also provide information regarding the thermodynamics of our system through isolation of enthalpic and entropic effects. The protonation constants of dipicolinate are known (Table 3.4); we are interested in the pH regime where the DPA is fully deprotonated (pH > 5.2)[15] and binding affinity is dictated by pH effects on the $Tb(DO2A)^+$ complex alone. Potential factors that may affect dipicolinate binding include protonation/deprotonation of the DO2A macrocycle, the hydration state of the lanthanide, the difference in exchange rates between H_2O and OH^- in the binary complex binding site, and the propensity for lanthanides to form hydroxide precipitates at high pH.[32, 33]

3.4.1 pH Dependence Studies

Various pH dependence studies will be conducted over a range from 6.1 to 10.4 to determine the extent of ternary complex stability. This will be performed both with Jobs plots and deconvolution of emission spectra to determine the dominant species in solution. The change in dipicolinate binding affinity for the europium binary complex (K_a') can also be monitored over a smaller pH regime (6.1 to 8.0) where high concentrations of free europium can be maintained in solution. Previous work indicates that macrocyclic ligands, due to their high binding affinities with lanthanides, can hinder bridging interactions with hydroxyl species that might lead to insoluble oligomers and thus stabilize these metals in basic conditions, at least temporarily.[34] We therefore anticipate that the DO2A ligand should impart some degree of resistance to changes in

pH, as evidenced by minimal intensity variation and reduced precipitation compared to the analogous Ln^{3+} species.

Experimental Section

Materials. The following chemicals were purchased and used as received: CAPS (*N*-cyclohexyl-*3*-aminopropanesulfonic acid) buffer (Alfa Aesar), CHES (*N*-cyclohexyl-*2*-aminoethanesulfonic acid) buffer (Alfa Aesar), DPA (dipicolinic acid, pyridine-*2,6,*-dicarboxylic acid) (Aldrich), dysprosium(III) chloride hydrate (Alfa Aesar), europium(III) chloride hexahydrate (Aldrich), MES monohydrate (*2*-(*N*-morpholino)ethanesulfonic acid monohydrate) buffer (Alfa Aesar), MOPS (*3*-(*N*-morpholino)-propanesulfonic acid) buffer (Alfa Aesar), samarium(III) chloride (Alfa Aesar), sodium acetate trihydrate (Mallinckrodt), sodium hydroxide (NaOH 50% in water) (Mallinckrodt), TAPS (*N*-tris(hydroxymethyl)methyl-*3*-aminopropanesulfonic acid) buffer (TCI America) and terbium(III) chloride hexahydrate (Alfa Aesar). All lanthanide salts were 99.9% pure or greater, all other salts were 99% pure or greater, and all buffers were at least 98% pure. DO2A was prepared as previously described (Section 2.2.1). Water was deionized to a resistivity of 18.2 MΩ-cm using a Purelab® Ultra laboratory water purification system.

Methods. Unless otherwise specified, all samples were prepared in triplicate to a final volume of 3.50 mL in disposable acrylate cuvettes with a 1 cm path length. Luminescence spectral analysis was performed by a Fluorolog Fluorescence Spectrometer with a 350-nm cutoff filter as previously described (Section 3.2.1). The

solution pH was measured using a calibrated handheld IQ150 pH/mV/temperature meter (I. Q. Scientific Instruments) following data collection.

Jobs plots. The concentrations of $LnCl_3$ (Ln = Tb, Eu) and DPA were varied inversely from 0 to 12.0 μM in 1.0-μM increments with 100 μM DO2A in 0.1 M buffer. Five buffers were used: MES (pK_a = 6.1), MOPS (pK_a = 7.2), TAPS (pK_a = 8.4), CHES (pK_a = 9.3) and CAPS (pK_a = 10.4), with pH adjustment to within 0.1 of the pK_a value using 50% NaOH added dropwise. Solutions were allowed to equilibrate for 7 days prior to analysis.

Speciation study. For each lanthanide, samples were prepared from 4.00 mM stock solutions of $LnCl_3$, DPA and DO2A to contain 10.0 μM $Ln(DO2A)(DPA)^-$ or $Ln(DPA)^+$ in 0.1 M buffer (MES, MOPS, TAPS, CHES and CAPS). Emission spectra were obtained after an equilibration time of 7 days. Normalized spectra were deconvoluted into a linear combination of the three standard emission profiles for $Ln(DPA)^+$, $Ln(DPA)_3^{3-}$ and $Ln(DO2A)(DPA)^-$ using the Solver function in Excel® based on the most ligand field sensitive peak in each spectrum. Transitions used in calculation: Sm ($^4G_{5/2} \rightarrow {}^6H_{7/2}$, 580–625 nm), Eu ($^5D_0 \rightarrow {}^7F_4$, 675–710 nm), Tb ($^5D_4 \rightarrow {}^7F_4$, 570–600 nm), Dy ($^4F_{9/2} \rightarrow {}^6H_{13/2}$, 555–595 nm). The resulting percentage of mono, tris or ternary complex in each emission spectrum was then used to determine the average number of DPA molecules bound per lanthanide.

pH dependence of K_c. Samples were prepared using solvated $Eu(DO2A)(DPA)^-$ crystals ($TBA{\cdot}Eu(DO2A)(DPA){\cdot}4.0H_2O{\cdot}3.0C_3H_8O$, FW = 1098.2 g/mol) and $EuCl_3$ in 0.1 M buffer such that the concentration of $Eu(DO2A)(DPA)^-$ was 1.0 μM and the concentration of free Eu^{3+} ranged from 1.0 nM to 1.0 mM. Four buffers were used: MES

(pH 6.1), NaOAc (pH 7.4), MOPS (pH = 7.5) and TAPS (pH = 8.0). Higher pH buffers were attempted, but precipitate was observed in cuvettes containing high concentrations of $EuCl_3$, assumed to be $Eu(OH)_3$. With the concentration of europium in solution not accurately known, the data could not be appropriately fit and was therefore discarded.

As Eu^{3+} was added, the shift in equilibrium $Eu(DO2A)(DPA)^-$ and $Eu(DPA)^+$ concentrations was monitored via the ligand field sensitive $^5D_0 \rightarrow {}^7F_4$ transition (675–710 nm) in the emission spectrum using luminescence spectroscopy. Emission spectra (λ_{ex} = 278 nm) were integrated to produce curves of observed integrated intensity (I_{obs}) against the log of excess free europium (log $[Eu^{3+}]_{xs}$). These were then fit to the two-state thermodynamic model derived previously (Section 3.2.2) using the Curve Fitting Tool in Matlab® to yield the competition equilibrium constant (K_c) for each pH value.

Results and Discussion

Jobs plots of the $Tb(DO2A)(DPA)^-$ and $Eu(DO2A)(DPA)^-$ complexes indicate formation of the $Ln(DPA)_3^{3-}$ species at low Ln mole fraction when the pH reaches 7.2 or below (Figures 3.25 and 3.26). This indicates that the DO2A ligand may be easier to displace in acidic conditions, as would be expected considering the protonation constants of this and the dipicolinate species.[6, 15] However, this only occurs when DPA is in excess to $Ln(DO2A)^+$, which would be unlikely in any situation where this complex might be applied to detect bacterial spores. When the $Ln(DO2A)^+$ receptor site complex is equal to or greater than the concentration of DPA, we see near perfect linearity over the entire pH range (pH 6.1 to 10.4).

In the speciation study, the number of DPA molecules bound per lanthanide was calculated using the luminescence transition with the most obvious change in band splitting (i.e., the 'ligand field sensitive' peak) for the three complexes, $Ln(DPA)^{+}$, $Ln(DPA)_3^{3-}$ and $Ln(DO2A)(DPA)^{-}$, and solving each pH dependence emission spectrum as a best fit of a linear combination of these three profiles. With the DO2A ligand bound, a ratio of one DPA molecule per lanthanide is maintained over the entire pH range, meaning all four lanthanide ternary complexes remained stable (Figure 3.27). In contrast, the $Ln(DPA)^{+}$ complexes began to form the tris $Ln(DPA)_3^{3-}$ species at high pH as evidenced by the Ln:DPA ratio approaching 1:3, indicating precipitation of some of the lanthanide as $Ln(OH)_3$. This suggests that the addition of the DO2A ligand prevents precipitation of the trivalent lanthanide cation and confers additional stability to the complex.

A clear pH dependence of the binding affinity for dipicolinate was observed over the range 6.1 to 8.0 for the europium complex (Figure 3.28). As no analogous K_a values for the association of Eu^{3+} to DPA^{2-} were derived (except at pH 7.5 as shown in Section 3.2.2), we did not calculate K_a' values and instead focus our analysis on the competition constant K_c. The competition constant, which is proportional to K_a and inversely proportional to K_a' (equation 3.3), decreases as the pH becomes more basic. This indicates that the binding affinity of the Eu^{3+} ion for dipicolinate is decreasing and/or the binding affinity of the $Eu(DO2A)^{+}$ complex for dipicolinate is increasing. In either case, the DO2A ligand stabilizes the complex in more basic conditions, and allows for greater relative dipicolinate binding in comparison to the Eu^{3+} ion alone.

These pH dependence studies have also demonstrated an important point in terms of using lanthanides and lanthanide complexes as sensors for bacterial spores. In every lanthanide studied, the luminescence intensity of the $Ln(DPA)^+$ complex varies significantly with pH, due largely to the precipitation of $Ln(OH)_3$ and the resulting formation of the more strongly luminescent $Ln(DPA)_n$ species, where n = 2 or 3. This means that unless the solution pH is known, there is no longer a direct correlation between luminescence intensity and dipicolinate concentration, and the number of bacterial spores cannot be quantified. With the $Ln(DO2A)^+$ complex, fortunately, the change in luminescence intensity over the pH range from 6.1 to 9.4 is no more than 5%, and therefore bacterial spore concentration can be determined directly from emission intensity with a high degree of confidence.

3.4.2 Temperature Dependence Study

The stabilities of complexes are governed by enthalpic (H) and entropic (S) changes as described in equation 3.7.

$$\Delta G = \Delta H - T\Delta S \qquad [3.7]$$

The changes in Gibbs free energy (ΔG) are related to temperature and stability constants (K) by equation 3.8,

$$\Delta G = -RT(\ln K) \qquad [3.8]$$

where R is the universal gas constant (8.314 $J \cdot K^{-1} \cdot mol^{-1}$). We can therefore use the change in stability constant with temperature to calculate the changes in enthalpy (ΔH) and entropy (ΔS) using the Van ‘t Hoff equation (see equation 3.9).

$$\ln K = -\frac{\Delta H}{R}\left(\frac{1}{T}\right) + \frac{\Delta S}{R} \qquad [3.9]$$

A plot of the natural logarithm of the association constant (K_a or K_a') against the reciprocal of absolute temperature will therefore produce a linear relationship with slope equal to -ΔH/R and a y-intercept of ΔS/R.

Lanthanide ions are net structure promoters, and the enthalpy and entropy terms in complex formation will reflect the disruption of solvent structure as well as the combination of the ions.[35, 36] For both the $Ln(DPA)^+$ and the $Ln(DO2A)(DPA)^-$ complexes, ionic combination should outweigh disruption of the hydration structure and result in an exothermic enthalpic parameter (-ΔH). For entropy, displacement of three water molecules to allow one dipicolinate molecule to bind to the lanthanide should produce a positive entropy contribution (+ΔS).

Temperature has been shown to influence the water exchange dynamics of the $Eu(DO2A)^+$ complex in aqueous solution, resulting in a decrease in hydration number from 3 to 2 with increasing temperature.[20] As this will most likely decrease the positive surface area of the Ln^{3+} binding site, we anticipate a decrease in the binding affinity for dipicolinate with increasing temperature for $Ln(DO2A)^+$ complexes (Ln = Eu and Tb). The change in hydration structure may also cause variations in enthalpy and entropy for these systems.

Methods. The previously prepared sets of $Ln(DO2A)(DPA)^-$ and $Ln(DPA)^+$ cuvettes (Ln = Tb and Eu) used to calculate K_a and K_a' (Section 3.2.2) were heated or cooled to a specified temperature (equilibration time of ~ 24 hrs for each temperature point) in the range of 10–50 °C using a refrigerator (Marvel Scientific, Greenville, MI),

incubator (VWR International, West Chester, PA), or AccuBlock™ Digital Dry Bath (Labnet International, Edison, NJ). The sample chamber of the Fluorolog-3, which has a cuvette-holder that can be temperature-controlled, was connected to a Neslab RTE 7 Digital Plus water heater/chiller (Thermo Scientific, Waltham, MA) to maintain the desired temperature of the cuvette during scans. Sample temperature was monitored using a handheld Fluke 62 Mini Infrared Thermometer. The temperature of each cuvette was checked prior to and following each measurement, and these values were averaged over the set of cuvettes to produce the reported temperature. The solution pH was measured using a calibrated handheld IQ150 pH/mV/temperature meter following data collection. Association constants K_a and K_a' were calculated as described previously (Section 3.2.2) and plotted as ln K against 1/T in Kaleidagraph®. Enthalpic and entropic parameters were calculated using equation 3.6 from the slope and y-intercept, respectively, of a linear fit.

Results and Discussion

The temperature dependence study reveals a decrease in luminescence intensity for both Tb(DO2A)(DPA)$^-$ and Eu(DO2A)(DPA)$^-$ as temperature increases from 10 °C to 50 °C. This is consistent with previous temperature dependence studies of europium complexes,[20] and is most likely due to increased nonradiative deactivation through thermal population of vibrational modes.

The binding affinities of both Tb^{3+} and Eu^{3+} for dipicolinate, determined using the one-step equilibration model derived previously (equation 3.1), display a similar temperature dependence. In both cases, the value of K_a decreases by 0.7 logarithmic

units (Table 3.5), indicating a decrease in dipicolinate binding affinity. An Eyring-Polanyi plot of 1/T against ln K_a (Figure 3.29) yields an enthalpy of activation of -30.8 kJ/mol for the $Tb(DPA)^+$ association constant and -34.7 kJ/mol for the $Eu(DPA)^+$ system (Table 3.6). The negative value of enthalpy for both Tb^{3+} and Eu^{3+} suggests that the hydration sphere is only partially disrupted in the formation of $Ln(DPA)^+$ from the Ln^{3+} aquo species, and that the ionic combination to produce a net +1 complex is the dominant contributor, causing the net enthalpy to be exothermic. The increase in enthalpic destabilization for terbium over europium observed here is consistent with observed trends in lanthanide dipicolinate complexes, and may be due to secondary interactions involving the carboxyl arms of the dipicolinate ligand.[37]

The net entropy change in both the Tb and Eu cases is positive, consistent with the elimination of water molecules from the inner coordination sphere, with a slightly greater entropy value for the terbium case. Studies have shown variation in thermodynamics for the solvation steric effect of lanthanides based ionic radius,[38] so the observed differences in entropy are probably due to variation in ionic radius and/or charge density between the Tb^{3+} and Eu^{3+} cations.

Results of the equilibrium model fits (Figure 3.30) indicate a nonlinear temperature dependence on the stability of the $Tb(DO2A)(DPA)^-$ complex over the range from 10–50 °C and a slight trend for the Eu complex. Though a previous study involving $Eu(EDTA)^-$ reported an increase in binding affinity for citrate from 25 °C to 60 °C,[39] we see the opposite effect for the dipicolinate anion, with binding affinity decreasing more than half an order of magnitude as temperature increases (Table 3.5). This effect is most likely due to the reported decrease in hydration number of the $Eu(DO2A)^+$ complex from

3 to 2, possibly from expansion of the DO2A ligand reducing solvent exposure of the lanthanide. Calculations of enthalpy and entropy for each complex from plots of ln K_a' versus 1/T (Figure 3.31) are given in Table 3.6. Binding of dipicolinate generates less entropy for the europium case than for the terbium complex, supporting the theory of decreased hydration number at higher temperature for the $Eu(DO2A)^+$ complex. If only two waters must be displaced for dipicolinate to bind to $Eu(DO2A)^+$ compared to three for $Tb(DO2A)^+$, the entropy for the terbium case should be greater. The relative difference between these two entropy values and those of the corresponding $Ln(DPA)^+$ complexes are attributed to the elimination of water molecules from the inner hydration zone for the $Ln(DO2A)(DPA)^-$ complexes.[35]

As with the $Ln(DPA)^+$ case, the change in enthalpy for dipicolinate binding is more negative for the $Eu(DO2A)^+$ complex than the $Tb(DO2A)^+$ complex by approximately 5 kJ/mol, most likely due to differences in lanthanide ionic radius. Overall, the net change in enthalpy for the complexes involving DO2A is less than those without the ligand. We attribute this more endothermic enthalpy value to the change in ionic combination. In the $Ln(DPA)^+$ case, the binding of dipicolinate results in the net charge decreasing from +3 for the lanthanide aquo ion to +1 for the mono-dipicolinate complex. With DO2A bound, dipicolinate binds to the lanthanide macrocycle binary complex and reduces the net charge from +1 to –1. This should cause reorganization of polar solvent in the outer sphere to account for the change from positive to negative, so the change in enthalpy is less favorable.

We have established the dependence of dipicolinate binding affinity and emission intensity on temperature for europium and terbium complexes. While both $Ln(DPA)^+$

complexes present a clear temperature dependence, the addition of the DO2A ligand appears to disrupt this effect for the terbium case. Differences between the europium and terbium complexes are attributed to variations in lanthanide ionic radius and charge density, as well as evidence that the $Eu(DO2A)^+$ complex loses a solvent molecule at higher temperature. Our data indicate that this is not the case for the $Tb(DO2A)^+$ complex, which maintains a dipicolinate binding affinity near the nanomolar regime even at temperatures of 50 °C. We can therefore qualify the $Tb(DO2A)^+$ complex as robust to temperature variation, with the note that emission intensity is temperature dependent and appropriate adjustments should be made for in situ measurement of environmental samples to obtain an accurate dipicolinate concentration.

3.5 Interferent Studies

A primary concern when applying tailored receptor sites to in situ detection is the potential for undesired chelation of environmental interferents. For lanthanide-based sensors such as $Tb(DO2A)^+$ which rely on ionic interactions for analyte binding, the greatest threat is from charged species. Anions, particularly those containing oxygen and/or the ability to complex metal ions, could compete with dipicolinate for the oxophilic lanthanide receptor site and produce a false negative result. If these anionic interferents are aromatic and capable of transferring energy to the terbium, we might also encounter false positives. Alternatively, cationic interferents such as calcium or metal ions could bind to dipicolinate and prevent coordination to the lanthanide complex, producing a false negative result. We will investigate a plethora of cations and anions commonly found in environmental samples which may adversely affect dipicolinate

detection, including species that are known to quench Tb-DPA luminescence such as phosphate and carbonate.[40] We will also compare the efficacy of DO2A to other proposed interferent mitigation techniques.

3.5.1 Ion Screen

A screen was performed to test the robustness of the $Tb(DO2A)^{+}$ receptor site in the presence of common environmental interferents. The lanthanide complex and dipicolinate were kept at very low concentration, with the interferent concentration varied from three to six orders of magnitude in excess. To avoid any complexities introduced by the concomitant presence of buffer ions, solutions were unbuffered and instead the pH was adjusted to neutral using sodium hydroxide or hydrochloric acid. Any change in emission intensity, whether due to displacement of dipicolinate or some other mechanism such as precipitation of the lanthanide, would represent a vulnerability of the lanthanide complex to that interferent.

Experimental Section

Materials. The following chemicals were purchased and used as received: ammonium chloride (J.T. Baker), calcium chloride trihydrate (Aldrich), cesium chloride (MP Biomedicals), DPA (dipicolinic acid, pyridine-*2,6,*-dicarboxylic acid) (Aldrich), lithium chloride (Aldrich), magnesium chloride hexahydrate (Mallinckrodt), potassium chloride (Mallinckrodt), samarium(III) chloride (Alfa Aesar), sodium acetate trihydrate (Mallinckrodt), sodium bromide (J.T. Baker), sodium carbonate (Mallinckrodt), sodium chloride (EM Science), sodium citrate dihydrate (Mallinckrodt), sodium fluoride

(Aldrich), sodium hydroxide (NaOH 50% in water) (Mallinckrodt), sodium iodide hydrate (Alfa Aesar), sodium nitrate (Mallinckrodt), sodium phosphate tribasic dodecahydrate (BDH), anhydrous sodium sulfate (Mallinckrodt) and terbium(III) chloride hexahydrate (Alfa Aesar). All lanthanide salts were 99.9% pure or greater, all other salts were 99% pure or greater, and all buffers were at least 98% pure. DO2A was prepared as previously described (Section 2.2.1). Water was deionized to a resistance of 18.2 MΩ-cm using a Siemens Purelab® Ultra laboratory water purification system.

Methods. Unless otherwise specified, all samples were prepared in triplicate to a final volume of 3.50 mL in disposable acrylate cuvettes with a 1 cm path length. Luminescence spectral analysis was performed by a Fluorolog Fluorescence Spectrometer with a 350-nm cutoff filter as previously described (Section 3.2.1).

Cuvettes were prepared from 400 μM stock solutions to contain 0.10 μM $Tb(DO2A)(DPA)^-$ or $Tb(DPA)^+$ and an excess (100, 10, 1.0 or 0.10 mM) of one of the following ions: magnesium, calcium, lithium, sodium, potassium, ammonium, cesium, acetate, nitrate, fluoride, chloride, bromide, iodide, carbonate, sulfate, phosphate and citrate. All cations were chloride salts, and all anions were sodium salts. Solution pH was adjusted to ~ 7 with NaOH or HCl added dropwise. Solutions were allowed to equilibrate for 2 days prior to spectral analysis. The solution pH was measured using a calibrated handheld IQ150 pH/mV/temperature meter following data collection. Emission intensities were normalized to $Tb(DO2A)(DPA)^-$ or $Tb(DPA)^+$ control solutions of identical concentrations.

Results and Discussion

Addition of common cations and anions in large excess (10^3 to 10^6-fold) to submicromolar Tb(DO2A)$(DPA)^-$ at near neutral pH resulted in minimal emission intensity change for most ions in comparison to the $Tb(DPA)^+$ complex (Figures 3.32 and 3.33). For most potential ionic interferents, the inclusion of DO2A improved luminescence intensity to some degree ($\leq 10^2$-fold) when the ion concentration was up to six orders of magnitude greater than the Tb-DPA concentration (Figure 3.34). Carbonate interference was only observed at concentrations five orders of magnitude or greater than that of Tb-DPA; in this regime, DO2A improves dipicolinate sensing efficiency tenfold. Citrate interferes significantly with Tb-DPA complexation; this is reduced with the use of DO2A for concentrations up to five orders of magnitude greater than Tb-DPA. Further, as the resting concentration of citrate in extracellular fluid is around 130 μM,[41] where interference is almost completely mitigated by DO2A, we do not anticipate significant luminescence quenching from this interferent in environmental samples. DO2A complexation successfully eliminates phosphate interference for concentrations up to five orders of magnitude greater than Tb and DPA.

The inclusion of DO2A successfully improves Tb-DPA binding in the presence of a wide array of interfering ions, most up to concentrations five orders of magnitude greater than that of DPA. This indicates that the $Tb(DO2A)^+$ complex is able to selectively bind dipicolinate, even in the presence of similar oxygen-containing ligands such as acetate, carbonate and citrate.

3.5.2 Cation/Anion Competition Experiments

Cations and anions of particular interest from the ion screen were further explored via competition experiments. These included carbonate, sulfate, phosphate, calcium and potassium. Phosphate in particular has been shown to severely inhibit DPA^{2-} binding to Tb^{3+} in previous studies, completely quenching Tb luminescence via an unknown mechanism even when DPA is in excess.[15, 42] L-alanine was also investigated, as this amino acid is a commonly used germinant of *Bacillus* bacterial spores and is often present in high concentrations in various endospore viability assays.[43-45]

Experimental Section

Materials. Aluminum chloride hexahydrate (Aldrich), calcium chloride trihydrate (Aldrich), DPA (dipicolinic acid, pyridine-*2,6,*-dicarboxylic acid) (Aldrich), MOPS (*3*-(*N*-morpholino)ethanesulfonic acid) buffer (Alfa Aesar), potassium chloride (Mallinckrodt), sodium acetate trihydrate (Mallinckrodt), sodium carbonate (Mallinckrodt), sodium phosphate tribasic dodecahydrate (BDH), anhydrous sodium sulfate (Mallinckrodt) and terbium(III) chloride hexahydrate (Alfa Aesar) were purchased and used as received. All lanthanide salts were 99.9% pure or greater, all other salts were 99% pure or greater, and all buffers were at least 98% pure. DO2A was prepared as previously described (Section 2.2.1). Water was deionized to a resistance of 18.2 MΩ-cm using a Siemens Purelab® Ultra laboratory water purification system.

Methods. Carbonate, sulfate, phosphate, calcium and potassium were used in competition experiments against 0.1 μM $Tb(DO2A)(DPA)^-$ in 0.1 M MOPS (pH 7.5), where the concentration of the ion was varied from 1.0 nM to 0.1 M. For ions where

significant competition was observed, the data was fit using the Curve Fitting Tool in Matlab® with a chemical equilibrium model similar to that used for the BAC Assay (see Appendix C for derivation). For phosphate, an additional competition experiment was performed for 0.10 μM $Tb(DPA)^{+}$ with 0.10 mM aluminum chloride in 0.2 M NaOAc, pH 7.3, to compare the efficacy of DO2A in phosphate mitigation to a compound established in the literature.

Results and Discussion

Competition experiments were performed for selected ions (Figure 3.35); of those, only calcium demonstrated any significant competition with $Tb(DO2A)^{+}$ for dipicolinate, and only at ~ 10^4 excess (Figure 3.36). This was expected, as CaDPA is a stable neutral salt (log K_{CaDPA} = 4.05 [46]), and the mode by which most bacterial spores store the high concentrations of dipicolinic acid present in the spore cortex.[47] The data were fit to a two-state chemical equilibrium model similar to that used in the BAC assay, and competition constants were calculated for Ca^{2+} competing with the $Tb(DO2A)^{+}$ binary complex (log K_{cation} = 4.36 ± 0.23) and the Tb^{3+} ion alone (log K_{cation} = 3.68 ± 0.17) for DPA^{2-}. The addition of the DO2A ligand improves the stability of Tb-DPA binding by a factor of 4.7 compared to Tb^{3+} alone, increasing the range over which this receptor site can be used in environmental conditions.

Phosphate has been reported to severely quench Tb-DPA luminescence via an unknown mechanism even when DPA is in excess. This was supported in the competition experiment for phosphate with $Tb(DPA)^{+}$; however, application of DO2A successfully mitigated phosphate interference in the binding of DPA^{2-} to Tb^{3+} by more

than three orders of magnitude compared to Tb^{3+} alone (Figure 3.37). Aluminum chloride is reported to mitigate phosphate interference of Tb-DPA luminescence via precipitation of $AlPO_4$.[42, 48] Though the addition of aluminum chloride in micromolar concentrations does appear to improve Tb-DPA stability in the presence of phosphate, the effect is minor in comparison to that of nanomolar concentrations of DO2A.

L-alanine appears to detrimentally affect Tb-DPA luminescence, though the effect is not concentration-dependent. Emission intensity of the $Tb(DPA)^+$ complex varied by a margin of more than 11%, compared to less than 3% for the $Tb(DO2A)(DPA)^-$ complex (Figure 3.38). We therefore recommend the use of $Tb(DO2A)^+$ instead of Tb^{3+} in any endospore assays where the L-alanine germinant is used, regardless of germinant concentration.

The application of DO2A improves the resistance of the Tb-DPA luminescence assay to calcium interference nearly five-fold. The concentration of calcium must be at least 1000 times greater than that of DPA for the ion to affect luminescence intensity. The DO2A ligand also successfully mitigates phosphate interference of Tb-DPA luminescence, and exhibits great improvement over other compounds cited in the literature such as aluminum chloride. Further, DO2A reduces variation in luminescence intensity from germinants like L-alanine that are often used to trigger dipicolinate release from bacterial spores. We can therefore recommend the use of the $Tb(DO2A)^+$ binary complex over the Tb^{3+} ion in the sensitive, robust detection of endospores over a wide pH and temperature range, as well as in the presence of environmental interferents.

3.6 Applications

3.6.1 Bacterial Spore Study

With the superior stability and performance of the $Tb(DO2A)^{+}$ binary complex over Tb^{3+} alone verified experimentally, we have applied this novel DPA receptor site to the detection of bacterial spore samples. *Bacillus atrophaeus* spores have been well characterized in the literature[49-51] and represent spores found in typical environmental samples in their relative size and DPA content.[52, 53] We will compare the emission intensity and signal-to-noise ratios of dipicolinate detection using Tb^{3+} or $Tb(DO2A)^{+}$ for these spores, which will be physically lysed to release DPA into solution. We anticipate an improvement with the use of DO2A, as this ligand should reduce or eliminate any interfering effects from various other biomolecules (amino acids, proteins, nucleic acids, fatty acids, etc.) released from the lysed spores.

Experimental Section

Materials. Ethyl alcohol (Acros Organics), sodium acetate trihydrate (Mallinckrodt) and terbium(III) chloride hexahydrate (Alfa Aesar) were purchased and used as received. All lanthanide salts were 99.9% pure or greater and all other salts were at least 99% pure. DO2A was prepared as previously described (Section 2.2.1). *Bacillus atrophaeus* bacterial spores were purchased from Raven Biological Laboratories (Mesa Laboratories, Inc., Omaha, NE) and stored at 4 °C until use. Water was deionized to a resistance of 18.2 MΩ-cm using a Siemens Purelab® Ultra laboratory water purification system, and filter-sterilized using a Nalgene® MF75 sterile disposable filter unit containing a polyethersulfone (PES) membrane (0.2 μm pore size).

Methods. Sterile technique was used throughout the bacterial spore study, and controls were treated identically to samples containing spores. Samples were prepared in a SterilGARD III Advance Class II Biological Safety Cabinet (Model SG-403A, Baker Co., Sanford, ME) to minimize contamination.

Preparation of the spore suspension. Approximately 100 μL of a *Bacillus atrophaeus* spore stock suspension (approx. concentration 10^9 spores/mL) was diluted to 500 μL in a sterile microcentrifuge tube with cold filter-sterilized deionized water (18.2 MΩ-cm resistivity). The spores were washed twice via centrifugation (16,100 rcf for 20 min at 4 °C), decanting the supernatant and resuspending the pellet in 500 μL of cold filter-sterilized deionized water. The washed spores were diluted 1:50 using cold filter-sterilized deionized water to produce a suspension in the 10^7 spores/mL range (just visibly turbid). These suspensions were kept in ice until use.

Determination of spore concentration. Bacterial spore concentration was determined using a haemocytometer (Hausser Scientific Partnership, Horsham, PA), a glass microscope slide with a chamber of precisely known volume containing a laser-etched grid. The coverslip was cleaned with 70% ethanol and anchored to the haemocytometer using two 3.5-μL drops of deionized water. A 7-μL aliquot of the diluted spore suspension was slowly injected between the haeomocytometer grid and coverslip, ensuring no bubble formation. Enumeration was performed with phase-contrast microscopy using a Nikon Eclipse 80i microscope (Nikon Instruments, Inc., Melville, NY) with a Hamamatsu ORCA-ER Digital Camera (Model C4742-80, Hamamatsu Corporation, Bridgewater, NJ) under 40X magnification and a phase range setting of 2. The phase rings were aligned prior to counting. Once in focus, the number

of spores in a 16-square block was counted; this was repeated 8 times with different 16-square units. The enumeration procedure was repeated for three separate aliquots of the diluted spore suspension and the results averaged. The spore concentration (C_{spore}) was then calculated using the conversion in equation 3.10, to produce a result in units of spores per milliliter.

$$C_{spore} = \left(\frac{\text{Avg spores in}}{\text{16 squares}} \right) \times 25 \times 50{,}000 \qquad [3.10]$$

The calculation produced a concentration of 3.11 x 10^7 (± 6.11 x 10^6) spores/mL. The suspension was then diluted using cold filter-sterilized deionized water to a final concentration of 1.00 x 10^5 spores/mL.

Bacterial spore experiment. Samples were prepared in quintuplicate as follows: two 2.97 mL aliquots of the spore suspension were transferred to two microwave tubes and sealed using a crimper. Ten microwave tubes, along with two sets of controls containing filter-sterilized deionized water, were autoclaved at 134 ºC for 45 min using a Tuttnauer 3870 EA autoclave (Tuttnauer USA Co, Ltd., Hauppauge, NY) to lyse the spores and effect DPA release. The solution from each tube was transferred to a cuvette, to which either 30 μL of 100 μM $TbCl_3$ or $Tb(DO2A)^+$ was added to the lysed spore suspensions and the control solutions. The excitation and emission spectra were obtained following ~ 30 seconds of thorough mixing. The signal-to-noise (S/N) ratio was calculated by dividing the sample amplitude of the most intense peak (544 nm) by the control amplitude using equation 3.11. Signal amplitude was calculated by subtracting the maximum observed intensity in the range of 530–560 nm from the minimum observed intensity in that range.

$$S/N = \frac{Max_{Sample} - Min_{Sample}}{Max_{Control} - Min_{Control}} \quad [3.11]$$

The calculated S/N ratios for each of the five trials were averaged to produce the final values for Tb^{3+} and $Tb(DO2A)^{+}$.

Results and Discussion

The use of DO2A in the detection of dipicolinate from *B. atrophaeus* bacterial spores not only doubles the luminescence intensity, but also improves the signal-to-noise ratio threefold (Figure 3.39). As the concentration of terbium in this experiment was always in excess to the predicted DPA concentration released from the bacterial spores, meaning no multimeric $Tb(DPA)_n$ species ($n > 1$) could be formed, the observed increase in intensity is most likely the result of two mechanisms. First, we anticipated a minor improvement due to exclusion of water from the Tb^{3+} coordination sphere. This is confirmed by the slight intensity increase in the $Tb(DO2A)^{+}$ control compared to the Tb^{3+} control. However, the increase in luminescence intensity coupled to the significant enhancement of the signal-to-noise ratio is attributed largely to the improved binding affinity of the $Tb(DO2A)^{+}$ complex for dipicolinate.

It is important to note that this result was achieved for low concentrations of bacterial spores without any sample purification (filtration to remove cell debris, extraction, pH adjustment, etc.), minimizing sample preparation and enabling facile automation of this technique. We can therefore conclude that the $Tb(DO2A)^{+}$ complex is superior to the Tb^{3+} ion in rapid, reliable detection of bacterial spores via sensitized lanthanide luminescence.

3.6.2 Ice Core Experiments

With the successful application of the $Tb(DO2A)^+$ complex to the detection of bacterial spores in a laboratory setting, we will now apply this novel receptor site to the quantitation of bacterial spores in environmental samples. We will focus on ice core samples, as these tend to have a low spore concentration in a clean matrix. We will compare the efficacy of Tb^{3+} to $Tb(DO2A)^+$ to determine if the DO2A ligand can improve the limit of detection of bacterial spores in environmental samples.

The Greenland Ice Sheet Project 2 (GISP2) was an international study administered by the Office of Polar Programs (OPP) of the U.S. National Science Foundation (NSF) under the Arctic System Science (ARCSS) program. Under this project, an ice core was drilled over a five-year period starting in 1993 from the surface to the bedrock more than 3000 meters down, making it the deepest continuous ice core recovered in the world at the time.[54] The GISP2 ice core contains information of approximately the last 110,000 years, which includes the Holocene and part of the Pleistocene epochs.[55] We will investigate the bacterial spore content of four sections of this ice core in the hopes of understanding the viability and diversity of microorganisms over time.

Experimental Section

Materials. D-alanine (Aldrich), L-alanine (Aldrich), ethyl alcohol (Acros Organics), nitric acid 68–70% (EMD Chemicals, Inc.) and terbium(III) chloride hexahydrate (Alfa Aesar) were purchased and used as received. All lanthanide salts were 99.9% pure or greater, and all other salts were 98% pure or greater. DO2A was prepared

as previously described (Section 2.2.1). All solutions of lanthanide complex and/or germinant were filter-sterilized using sterile Acrodisc® 25 mm syringe filters with a 0.2 μm Supor® membrane (Pall Corporation, Ann Arbor, MI) prior to use. Ice cores from the Greenland Ice Sheet Project 2 (GISP2) were obtained from the National Ice Core Laboratory and stored at -80 °C until use. Specific ice cores used in study:

- Core GISP2D, Tube 158. Top depth 157.45 m, bottom depth 157.70 m. Cut MCA02. Length 0.25 m. Date 5 Jan 2007. Age 600 years.
- Core GISP2D, Tube 270. Top depth 269.43 m, bottom depth 269.68 m. Cut MCA02. Length 0.25 m. Date not specified. Age unknown.
- Core GISP2D, Tube 480. Top depth 480.15 m, bottom depth 480.40 m. Cut MCA02. Length 0.25 m. Date 5 Jan 2007. Age 2,000 years.
- Core GISP2D, Tube 835. Top depth 834.10 m, bottom depth 834.35 m. Cut MCA02. Length 0.25 m. Date 4 Jan 2007. Age 4,000 years.

Note that the reported date on the ice core sample is not the date of collection (1993–1998) but instead the date of cutting each section from the larger core.

Methods. Sterile technique was used in all protocols. All glassware was sterilized in a Cress™ C100-6B Electric Kiln (Cress MFG Co., Carson City, NV) at 500 °C for 4 hours prior to use. Water was deionized to a resistance of 18.2 MΩ-cm using a Siemens Purelab® Ultra laboratory water purification system, and filter-sterilized using a Nalgene® MF75 sterile disposable filter unit containing a polyethersulfone (PES) membrane (0.2 μm pore size).

Decontamination. To slowly increase the temperature, each ice core was removed from -80 °C storage and placed in a -25 °C freezer for 8 hours, followed by a transition to 0 °C for 2 hours. This prevented the decontamination solutions from simply freezing to the exterior of the core. Each ice core was then cut in half on a sterilized aluminum block kept at -80 °C until use. The shallower portion of the core was placed back in the -80 °C freezer. The deeper half of the ice core was dipped in a solution of bleach (6.15% sodium hypochlorite, 4 °C) for 10 seconds, and then three separate aliquots of filter-sterilized deionized water (4 °C) for 10 seconds each.

Melting and filtration. The decontaminated ice core was placed in a sterile 1-L beaker in a SterilGARD III Advance Class II Biological Safety Cabinet to melt. Melting was timed. Immediately following complete melting, the solution was filtered using a 0.1-μm 47 mm polycarbonate nucleopore track-etch filter membrane and vacuum filtration.

Resuspension. The filter was transferred to a sterile 15-mL polypropylene centrifuge tube containing 4.40 mL of filter-sterilized nanopure water (4 °C). The tube was vortexed for 1 min and then chilled on ice for 1 min. This was repeated four times. Twelve 225-μL aliquots of the solution were placed into sterile microcentrifuge tubes.

Germination. For each batch of 4 tubes, a 25-μL aliquot of one of the following was added:

- 10.0 μM $TbCl_3$ with 1.0 M L-alanine
- 10.0 μM $Tb(DO2A)^+$ with 1.0 M L-alanine
- 10.0 μM $TbCl_3$ with 1.0 M D-alanine
- 10.0 μM $Tb(DO2A)^+$ with 1.0 M D-alanine

The 12 tubes were then placed in an AccuBlock™ Digital Dry Bath (Labnet International) at 37 °C for 48 hours to induce germination. The solutions were then transferred to 0.6-mL quartz microcuvettes with a 1 cm path length. Quartz cells were washed with 50% nitric acid and rinsed ten times with filter-sterilized nanopure water (18.2 MΩ-cm resistivity) prior to each use. Luminescence spectral analysis was performed at 37 °C by a Fluorolog Fluorescence Spectrometer with a 350-nm cutoff filter as previously described (Section 3.2.1). Emission spectra were normalized to a 10.0 μM $Tb(DPA)^+$ standard solution, also in quartz.

DPA release. Following germination and spectral analysis, the solutions were transferred back into their respective microcentrifuge tubes and autoclaved at 134 °C for 45 minutes to lyse any remaining spores and effect complete DPA release. These solutions were transferred into quartz microcuvettes for luminescence spectral analysis.

Results and Discussion

Due to issues involving contamination of the L-alanine germinant with DPA (from the vendor Aldrich) and lack of sufficiently concentrated sample, no detectable signal for dipicolinate was observed either in excitation or emission spectra that could be attributed to bacterial spores in the ice core sample. Though the use of DO2A would most likely have reduced intensity variations from the high L-alanine concentration (Section 3.5.2) and produced an improved signal-to-noise ratio, we appear to be below the limit of detection for both the Tb^{3+} and $Tb(DO2A)^+$ species. Given the high binding affinity of the $Tb(DO2A)^+$ complex in these conditions (log K_a' = 9.25) and the assumption of an average dipicolinate content of 10^8 DPA molecules per spore, this

indicates that, if any bacterial spores are present in these ice core samples, they are most likely below a concentration of 100 spores/mL. Hence, though the $Tb(DO2A)^{+}$ complex demonstrates significant improvement over Tb^{3+} in the detection of bacterial spores, further optimization of dipicolinate binding affinity by this receptor site is necessary to reach the desired limit of detection to apply to environmental samples such as ice cores.

3.7 Conclusions

An investigation of $Ln(DO2A)^{+}$, where Ln = Sm, Eu, Tb and Dy, was performed to determine the efficacy of these binary complexes in sensitive, selective detection of bacterial spores via DPA-triggered Ln^{3+} luminescence. We based our analysis on five basic qualities of an effective receptor site: (1) the receptor site must present an obvious, measurable response upon analyte binding; (2) the binding affinity for the analyte of interest should be high, in the nanomolar regime or better; (3) binding should be rapid and compatible with the rate of analyte release in situ; (4) the receptor site should be resistant to pH and temperature changes; and (5) the binding affinity and selectivity should not be susceptible to environmental interferents. Of the lanthanide(macrocycle) complexes studied, the $Tb(DO2A)^{+}$ complex was the best match according to our criteria for the optimal dipicolinate receptor site.

One of the commonly exploited features of macrocyclic ligands is that of rendering several coordination sites inert to substitution and consequently limiting both the number and geometry of available binding sites.[56] The $Ln(DO2A)^{+}$ complex leaves exactly three adjacent, linearly-arranged coordination sites open for binding, ideal for the dipicolinate ligand. Work with pyridines and DPA derivatives suggests that the nitrogen

is integral to the strong binding observed, despite the usual preference of lanthanides for oxygen moieties. In comparison to other ligands such as hexacyclen, EDTA, DO3A and DOTA, which either coordinate to the lanthanide with less affinity or present a binding site with unfavorable size and/or geometry, the DO2A ligand produces the most effective lanthanide binary complex in terms of dipicolinate binding.

Binding affinity studies reveal an increase in dipicolinate complexation for the $Ln(DO2A)^{+}$ complex compared to the Ln^{3+} ion alone. This increase in binding affinity for the binary complex goes contrary to predictions based purely on net complex electrostatics, in that the DPA^{2-} analyte should be more strongly attracted to the tripositive Ln^{3+} species than the $Ln(DO2A)^{+}$ complex. Apparently, binding of the DO2A ligand affords an enhancement in DPA affinity that is substantial enough to counteract this loss of charge and still improve dipicolinate binding by an order of magnitude. Evidence of this 'ligand enhancement' can be found for various other lanthanide/ligand/analyte systems in the literature, and are tabulated in Table 3.7.[57-61] In each case, application of a chelating ligand improves binding affinity of the oxyanion analyte (picolinate, acetate and lactate) by around an order of magnitude, regardless of the type (cyclic or linear), denticity or charge of the ligand. We attribute this 'ligand enhancement' to a shift in electron density of the lanthanide upon ligand chelation, generating a binding site with a greater positive character due to the electron-withdrawing O and N moieties of the ligand. Though the net charge of the complex may have decreased, the *local* charge in the binding site may be even greater than the Ln^{3+} aquo case, where the nine solvent molecules are evenly distributed in the lanthanide coordination sphere and the electron density is still uniform. Though further

experimentation is required to support this theory, the existence of ligand enhancement is nevertheless a powerful tool in receptor site design. Any chemist seeking to improve the binding affinity of an oxyanion with a lanthanide cation *should utilize a helper ligand*, preferably one rich in nitrogen and oxygen.

The difference in binding affinity between the $Tb(DO2A)^{+}$ and $Dy(DO2A)^{+}$ complexes and the $Eu(DO2A)^{+}$ and $Sm(DO2A)^{+}$ species is most likely due to a phenomenon known as the "gadolinium break." Various studies of stability constants across the lanthanide series, such as those with acetate and anthranilate, indicate a change in stability constant around gadolinium.[62] Suggestions as to why this occurs include solvent exchange or the possibility of a mechanistic change occurring in the middle of the series. Evidence of the gadolinium break can also be seen in enzymatic inhibition studies,[63] and in a shift in hydration number from 9 for the larger lanthanides to 8 for the smaller lanthanides.[36, 64] An expansion of the Dy^{3+} coordination sphere from 8- to 9-coordinate is known to occur when two or more negatively charged ligands are coordinated,[6, 65] which may explain why the potentially 8-coordinate Dy^{3+} was able to accommodate the $DO2A^{2-}$ and DPA^{-2} ligands in a 9-coordinate motif.

The interesting aspect of the gadolinium break observed in our binding studies is that it appears to be *induced by ligation of DO2A*. The dipicolinate affinity for the Ln^{3+} ions exhibits little variation, but the analogous $Ln(DO2A)^{+}$ complexes show an obvious divide between those to the left of gadolinium (Sm, Eu) and those to the right (Tb, Dy). Another study concerning lanthanide(macrocycle) binary complexes also noted a similar trend, in this case using a chiral heptadentate DO3A derivative. The authors noticed an increase in the binding affinity of the terbium complex for certain oxy-anions (acetate,

bicarbonate and phosphate) in comparison to the analogous europium complex by about the same margin as we have observed for dipicolinate (Table 3.8).[60] As with our system, lifetime measurements of these complexes indicated no differences in hydration state that might explain the discrepancy. They attribute the affinity trend to a divergence of pK_a for the two complexes. If the pK_a of the europium complex were lower than that of the terbium complex, the presence of a population of hydroxylated species for the europium case would reduce the overall binding affinity due to a decrease in electrostatic attraction for this population of dipositive complex. Differences in pK_a values for Eu and Gd macrocyclic complexes with DOTA derivatives have been noted in the literature,[66] though it is not clear if this trend is extended to include Tb, or if these ligands can be directly compared to DO2A or others. We see no evidence of such a hydroxylated species in our pH dependence studies, which should have manifested in a change in stability of the $Eu(DO2A)(DPA)^-$ complex compared to the $Tb(DO2A)(DPA)^-$ complex at lower pH. We therefore cannot accept this hypothesis, and instead turn to ionization energy for a possible explanation.

The ability of a chelating ligand to perturb the electron density of a Ln^{3+} cation is dependent on (1) the number and arrangement of electron-withdrawing groups in the ligand and (2) the susceptibility of the lanthanide to polarization. The former property can be tuned by judicial choice of ligand; the latter is defined by how easily the electron density of the lanthanide can be externally influenced, one measure of which is ionization energy. A lanthanide with a low $Ln^{3+} \rightarrow Ln^{4+}$ ionization energy requires less energy to remove an electron, and is arguably more susceptible to perturbation by ligating species than a lanthanide with a high ionization energy. As shown in Figure 3.40, the Tb^{3+} ion

has the lowest 3+ → 4+ ionization energy of all the lanthanides investigated,[67] due primarily to the fact that the Tb^{4+} ion has an electronic configuration with an *exactly half-filled 4f-shell*. This lanthanide is therefore particularly susceptible to perturbation by an electronegative chelating ligand, as Tb^{3+} has the lowest energy barrier to losing an electron. Thus, the observed phenomenon of the ligand-induced gadolinium break is simply a manifestation of the half-shell effect, where lanthanides with the lowest ionization energies are the most significantly affected by electron density perturbations from a chelating helper ligand. In terms of receptor site design, this ligand-induced effect presents a strong case for using terbium as the lanthanide of choice in a sensing complex, as the Tb^{3+} ion will yield the greatest binding affinity increase when paired with a helper ligand.

The detection of bacterial spores via dipicolinate-triggered lanthanide luminescence has been improved in terms of detection limit, stability, and susceptibility to interferents by use of lanthanide-macrocycle binary complexes. The $Ln(DO2A)^{+}$ binary complexes bind dipicolinic acid, a major constituent of bacterial spores, with greater affinity and demonstrate significant improvement in bacterial spore detection. Of the four luminescent lanthanides studied (Sm, Eu, Tb and Dy), the terbium complex exhibits the greatest dipicolinate binding affinity (100-fold greater than Tb^{3+} alone, and 10-fold greater than other $Ln(DO2A)^{+}$ complexes) and highest quantum yield. Moreover, the inclusion of DO2A extends the pH range over which Tb-DPA coordination is stable, reduces the interference of calcium ions nearly five-fold, and mitigates phosphate interference 1000-fold compared to free terbium alone. In addition, detection of *Bacillus atrophaeus* bacterial spores was improved by the use of $Tb(DO2A)^{+}$, yielding a three-

fold increase in the signal-to-noise ratio over Tb^{3+}. However, initial experiments with Greenland ice core samples suggests further optimization is necessary to reach target limits of detection for very low concentrations of bacterial spores.

As a first-generation receptor site, the $Tb(DO2A)^{+}$ binary complex demonstrates improved dipicolinate binding affinity and enhanced resistance to pH, temperature and environmental interferents. We therefore conclude that the $Tb(DO2A)^{+}$ complex represents an excellent first step towards development of a rapid, robust DPA receptor for the detection of bacterial spores.

REFERENCES

(1) Nogrady, T.; Weaver, D. F. In *Medicinal Chemistry: A Molecular and Biochemical Approach*; Oxford University Press, 2005, pp 67-105.
(2) Job, P. *Comptes redus de l'Academie des sciences* **1925**, *180*, 928-930.
(3) Samuel, A. P. S.; Moore, E. G.; Melchior, M.; Xu, J.; Raymond, K. N. In *Lawrence Berkeley National Laboratory*; Lawrence Berkeley National Laboratory, 2009.
(4) Choppin, G. R.; Schaab, K. M. *Inorganica Chimica Acta* **1996**, *252*, 299-310.
(5) Chang, C. A.; Chen, Y.-H.; Chen, H.-Y.; Shieh, F.-K. *Journal Of The Chemical Society-Dalton Transactions* **1998**, 3243-3248.
(6) Huskens, J. *Inorganic Chemistry* **1997**, *36*, 1495-1503.
(7) Kimura, E.; Sakonaka, A.; Yatsunami, T.; Kodama, M. *Journal Of The American Chemical Society* **1981**, *103*, 3041-3045.
(8) Kim, W. D.; Hrncir, D. C.; Kiefer, G. E.; Sherry, A. D. *Inorganic Chemistry* **1995**, *34*, 2225-2232.
(9) Loncin, M. F.; Desreux, J. F.; Merciny, E. *Inorganic Chemistry* **1986**, *25*, 2646-2648.
(10) Mitewa, M.; Bontchev, P. R. *Coordination Chemistry Reviews* **1994**, *135/136*, 129-163.
(11) Gil, V. M. S.; Oliveira, N. C. *Journal of Chemical Education* **1990**, *67*, 473-478.
(12) Benesi, H. A.; Hildebrand, J. H. *Journal Of The American Chemical Society* **1949**, *71*, 2703-2707.
(13) Wang, R.; Yu, Z. W. *Acta Physico-Chimica Sinica* **2007**, *23*, 1353-1359.
(14) Yang, C.; Liu, L.; Mu, T. W.; Guo, Q. X. *Analytical Sciences* **2000**, *16*, 537-539.
(15) Jones, G.; Vullev, V. I. *Journal of Physical Chemistry A* **2002**, *106*, 8213-8222.
(16) Sanny, C. G.; Price, J. A. *Bioconjugate Chemistry* **1999**, *10*, 141-145.
(17) Horrocks Jr., W. D.; Sudnick, D. R. *Journal Of The American Chemical Society* **1979**, *101*, 334-340.
(18) Spaulding, L.; Brittain, H. G.; O'Connor, L. H.; Pearson, K. H. *Inorganic Chemistry* **1986**, *25*, 188-193.
(19) Wu, S. L.; Horrocks, W. D. *Analytical Chemistry* **1996**, *68*, 394-401.
(20) Yerly, F.; Dunand, Frank A.; Tóth, É.; Figueirinha, A.; Kovács, Z.; Sherry, A. D.; Geraldes, C. F. G. C.; Merbach, André E. *European Journal Of Inorganic Chemistry* **2000**, *2000*, 1001-1006.
(21) Moreau, J.; Guillon, E.; Pierrard, J.-C.; Rimbault, J.; Port, M.; Aplincourt, M. *Chemistry: A European Journal* **2004**, *10*, 5218-5232.
(22) Shestakova, A. K.; Chertkov, V. A.; Schneider, H.-J.; Lysenko, K. A. *Organic Letters* **2001**, *3*, 325-327.
(23) Abusaleh, A.; Meares, C. F. *Photochemistry and Photobiology* **1984**, *39*, 763-769.
(24) Jian-Fang, M.; Ning-Hai, H.; Jia-Zuan, N. *Polyhedron* **1996**, *15*, 1797-1799.
(25) Min, D.; Lee, S. W. *Inorganic Chemistry Communications* **2002**, *5*, 978-983.
(26) Lamture, J. B.; Hong Zhou, Z.; Kumar, S.; Wensel, T. G. *Inorganic Chemistry* **1995**, *34*, 864-869.
(27) Sheldrick, G. M. *Acta Crystallographica* **1990**, *A46*, 467-473.
(28) Sheldrick, G. M.; University of Göttingen: Göttingen, Germany, 1997.
(29) Sheldrick, G. M. *Acta Crystallographica* **2008**, *A64*, 112-122.
(30) McNaught, A. D.; Wilkinson, A., Eds. *IUPAC Compendium of Chemical Terminology*, 2nd ed.; Royal Society of Chemistry: Cambridge, UK, 1997.

(31) Werner, J. A.; Office, U. S. P. a. T., Ed.; The Dow Chemical Company (Midland, MI): United States, 1985.
(32) Moeller, T.; Kremers, H. E. *Journal Of Physical Chemistry* **1944**, *48*, 395-406.
(33) Arnaud, N.; Georges, J. *Analyst* **1999**, *124*, 1075-1078.
(34) Voss, D. A.; Buttrey-Thomas, L. A.; Janik, T. S.; Churchill, M. R.; Morrow, J. R. *Inorganica Chimica Acta* **2001**, *317*, 149-156.
(35) Choppin, G. R.; Strazik, W. F. *Inorganic Chemistry* **1965**, *4*, 1250-1254.
(36) Choppin, G. R.; Graffeo, A. J. *Inorganic Chemistry* **1965**, *4*, 1254-1257.
(37) Piguet, C.; Bunzli, J. C. G. *Chemical Society Reviews* **1999**, *28*, 347-358.
(38) Ishiguro, S.; Umebayashi, Y.; Komiya, M. *Coordination Chemistry Reviews* **2002**, *226*, 103-111.
(39) Mathur, J. N.; Cernochova, K.; Choppin, G. R. *Inorganica Chimica Acta* **2007**, *360*, 1785-1791.
(40) Barela, T. D.; Sherry, A. D. *Analytical Biochemistry* **1976**, *71*, 351-352.
(41) Parker, D.; Williams, J. A. G. In *Metal Ions in Biological Systems: The Lanthanides and Their Interrelations with Biosystems*; Sigel, A., Sigel, H., Eds.; Marcel Dekker, Inc.: New York, 2003; Vol. 40, pp 233-280.
(42) Pellegrino, P. M.; Fell, N. F.; Rosen, D. L.; Gillespie, J. B. *Analytical Chemistry* **1998**, *70*, 1755-1760.
(43) Akoachere, M.; Squires, R. C.; Nour, A. M.; Angelov, L.; Brojatsch, J.; Abel-Santos, E. *The Journal of Biological Chemistry* **2007**, *282*, 12112-12118.
(44) Gounina-Allouane, R.; Broussolle, V.; Carlin, F. *Food Microbiology* **2008**, *25*, 202-206.
(45) Titball, R. W.; Manchee, R. J. *Journal Of Applied Microbiology* **1987**, *62*, 269-273.
(46) Chung, L.; Rajan, K. S.; Merdinge.E; Grecz, N. *Biophysical Journal* **1971**, *11*, 469-482.
(47) Murrell, W. G. *The Bacterial Spore*; Academic Press: New York, 1969.
(48) Rosen, D. L. *Applied Optics* **2006**, *45*, 3152-3157.
(49) Fritze, D.; Pukall, R. *Int. J. Syst. Evol. Microbiol.* **2001**, *51*, 35-37.
(50) Setlow, P. *Journal Of Applied Microbiology* **2006**, *101*, 514-525.
(51) Kunst, F.; Ogasawara, N.; Moszer, I.; Albertini, A. M.; Alloni, G.; Azevedo, V.; Bertero, M. G.; Bessières, P.; Bolotin, A.; Borchert, S.; Borriss, R.; Boursier, L.; Brans, A.; Braun, M.; Brignell, S. C.; Bron, S.; Brouillet, S.; Bruschi, C. V.; Caldwell, B.; Capuano, V.; Carter, N. M.; Choi, S. K.; Codani, J. J.; Connerton, I. F.; Cummings, N. J.; Daniel, R. A.; Denizot, F.; Devine, K. M.; Düsterhöft, A.; Ehrlich, S. D.; Emmerson, P. T.; Entian, K. D.; Errington, J.; Fabret, C.; Ferrari, E.; Foulger, D.; Fritz, C.; Fujita, M.; Fujita, Y.; Fuma, S.; Galizzi, A.; Galleron, N.; Ghim, S.-Y.; Glaser, P.; Goffeau, A.; Golightly, E. J.; Grandi, G.; Guiseppi, G.; Guy, B. J.; Haga, K.; Haiech, J.; Harwood, C. R.; Hénaut, A.; Hilbert, H.; Holsappel, S.; Hosono, S.; Hullo, M.-F.; Itaya, M.; Jones, L.; Joris, B.; Karamata, D.; Kasahara, Y.; Klaerr-Blanchard, M.; Klein, C.; Kobayashi, Y.; Koetter, P.; Koningstein, G.; Krogh, S.; Kumano, M.; Kurita, K.; Lapidus, A.; Lardinois, S.; Lauber, J.; Lazarevic, V.; Lee, S.-M.; Levine, A.; Liu, H.; Masuda, S.; Mauël, C.; Médigue, C.; Medina, N.; Mellado, R. P.; Mizuno, M.; Moestl, D.; Nakai, S.; Noback, M.; Noone, D.; O'Reilly, M.; Ogawa, K.; Ogiwara, A.; Oudega, B.; Park, S.-H.; Parro, V.; Pohl, T. M.; Portetelle, D.; Porwollik, S.; Prescott, A. M.; Presecan, E.; Pujic, P.; Purnelle, B.; Rapoport, G.; Rey, M.; Reynolds, S.; Rieger, M.; Rivolta, C.; Rocha, E.; Roche, B.; Rose, M.; Sadaie, Y.; Sato, T.; Scanlan, E.; Schleich, S.; Schroeter, R.; Scoffone, F.; Sekiguchi, J.; Sekowska, A.; Seror, S. J.; Serror, P.; Shin, B.-S.; Soldo, B.; Sorokin, A.; Tacconi, E.; Takagi, T.; Takahashi, H.; Takemaru, K.; Takeuchi, M.; Tamakoshi, A.; Tanaka, T.; Terpstra, P.; Tognoni, A.; Tosato, V.; Uchiyama, S.; Vandenbol,

M.; Vannier, F.; Vassarotti, A.; Viari, A.; Wambutt, R.; Wedler, E.; Wedler, H.; Weitzenegger, T.; Winters, P.; Wipat, A.; Yamamoto, H.; Yamane, K.; Yasumoto, K.; Yata, K.; Yoshida, K.; Yoshikawa, H.-F.; Zumstein, E.; Yoshikawa, H.; Danchin, A. *Nature* **1997**, *390*, 249-256.

(52) Shafaat, H. S.; Ponce, A. *Applied and Environmental Microbiology* **2006**, *72*, 6808-6814.

(53) Sojka, B.; Ludwig, H. *Pharm. Ind.* **1997**, *59*, 355-359.

(54) Mayewski, P.; Bender, M. *Reviews of Geophysics* **1995**, *33*, 1287-1296.

(55) Stratigraphy, I. C. o.; International Union of Geological Sciences, 2009.

(56) Harrowfield, J. M. In *Metal Ions in Biological Systems: The Lanthanides and Their Interrelations with Biosystems*; Sigel, A., Sigel, H., Eds.; Marcel Dekker, Inc.: New York, 2003; Vol. 40, pp 105-159.

(57) Powell, J. E.; Ingemanson, J. W. *Inorganic Chemistry* **1968**, *7*, 2459-2461.

(58) Elkström, C.-G.; Nilsson, L.; Duncan, I. A.; Grenthe, I. *Inorganica Chimica Acta* **1980**, *40*, 91-98.

(59) Moeller, T.; Martin, D. F.; Thompson, L. C.; Ferrus, R.; Feistel, G. R.; Randall, W. J. *Chemical Reviews* **1965**, *65*, 1-50.

(60) Bruce, J. I.; Dickins, R. S.; Govenlock, L. J.; Gunnlaugsson, T.; Lopinski, S.; Lowe, M. P.; Parker, D.; Peacock, R. D.; B., P. J. J.; Aime, S.; Botta, M. *Journal Of The American Chemical Society* **2000**, *122*, 9674-9684.

(61) Kolat, R. S.; Powell, J. E. *Inorganic Chemistry* **1962**, *1*, 293-296.

(62) Silber, H. B.; Paquette, S. J. In *Metal Ions in Biological Systems: The Lanthanides and Their Interrelations with Biosystems*; Sigel, A., Sigel, H., Eds.; Marcel Dekker, Inc.: New York, 2003; Vol. 40, pp 69-104.

(63) Yang, Z.; Batra, R.; Floyd, D. L.; Hung, H.-C.; Chang, G.-G.; Tong, L. *Biochemical and Biophysical Research Communications* **2000**, *274*, 440-444.

(64) Kimura, T.; Kato, Y. *Journal Of Alloys And Compounds* **1998**, *278*, 92-97.

(65) Huskens, J.; Kennedy, A. D.; Van Bekkum, H.; Peters, J. A. *Journal Of The American Chemical Society* **1995**, *117*, 375-382.

(66) Aime, S.; Barge, A.; Bruce, J. I.; Botta, M.; Howard, J. A. K.; Moloney, J. M.; Parker, D.; De Sousa, A. S.; Woods, M. *Journal Of The American Chemical Society* **1999**, *121*, 5762-5771.

(67) Cotton, S. *Lanthanide and Actinide Chemistry*; John Wiley & Sons Ltd.: West Sussex, England, 2006.

Tb (μM)	DPA (μM)	Mole Fraction Tb	Ratio Tb:DPA
0	12	0.000	0:12
1	11	0.083	1:11
2	10	0.167	1:5
3	**9**	**0.250**	**1:3**
4	8	0.333	1:2
5	7	0.417	1:1.4
6	**6**	**0.500**	**1:1**
7	5	0.583	1.4:1
8	**4**	**0.667**	**2:1**
9	3	0.750	3:1
10	2	0.833	5:1
11	1	0.917	11:1
12	0	1.000	12:0

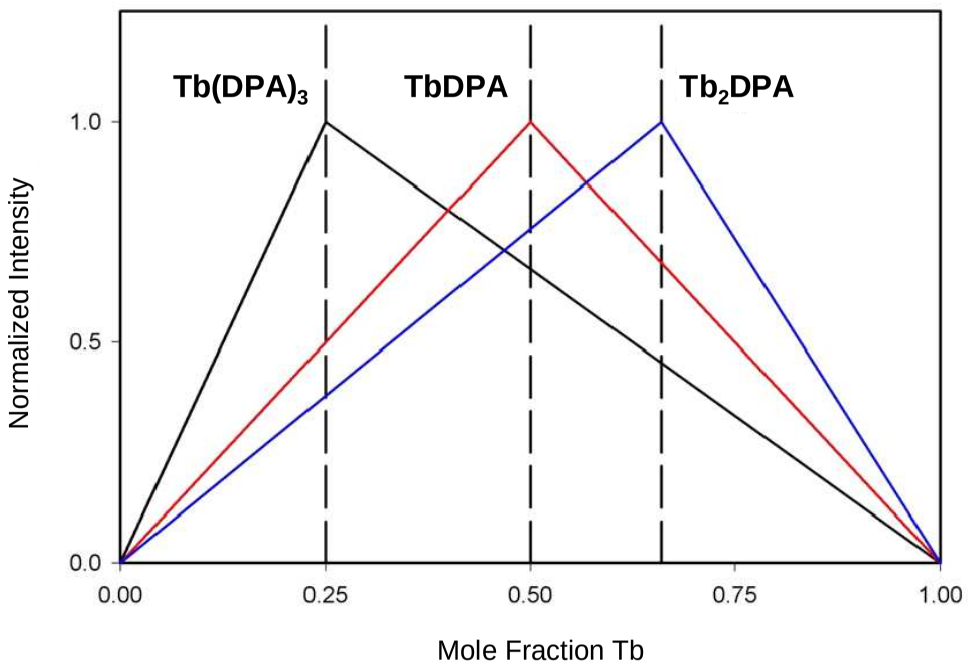

Figure 3.1. Method of continuous variations to determine optimal binding stoichiometry. The two components, in this case Tb and DPA, are varied inversely to produce various mole fractions (left). The best response (in this case, luminescence intensity) will be produced for the optimal ratio of the two (right).

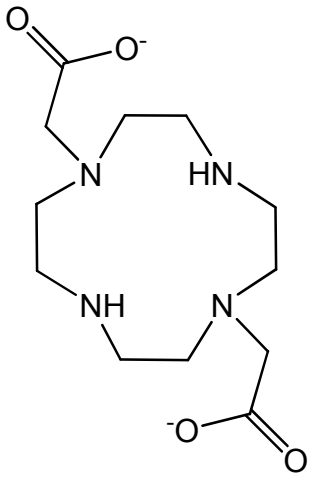

DO2A

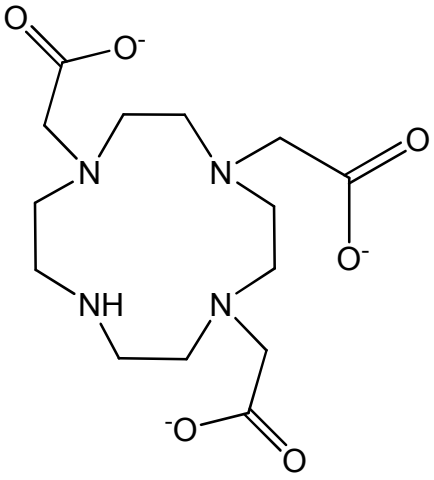

DO3A

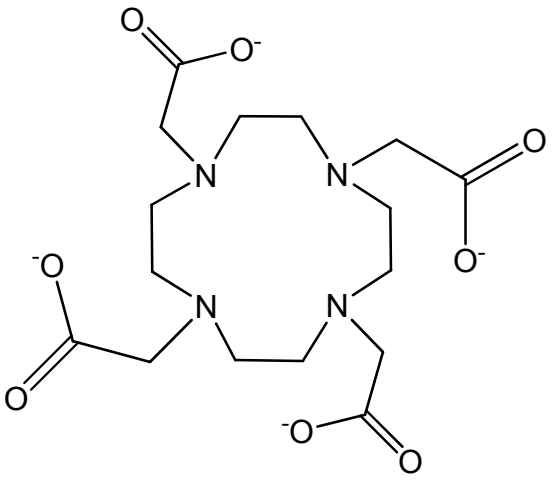

DOTA

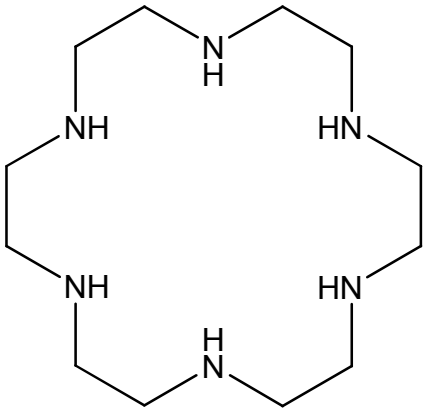

Hexacyclen

Figure 3.2. Macrocyclic ligands utilized for determining binding stoichiometries.

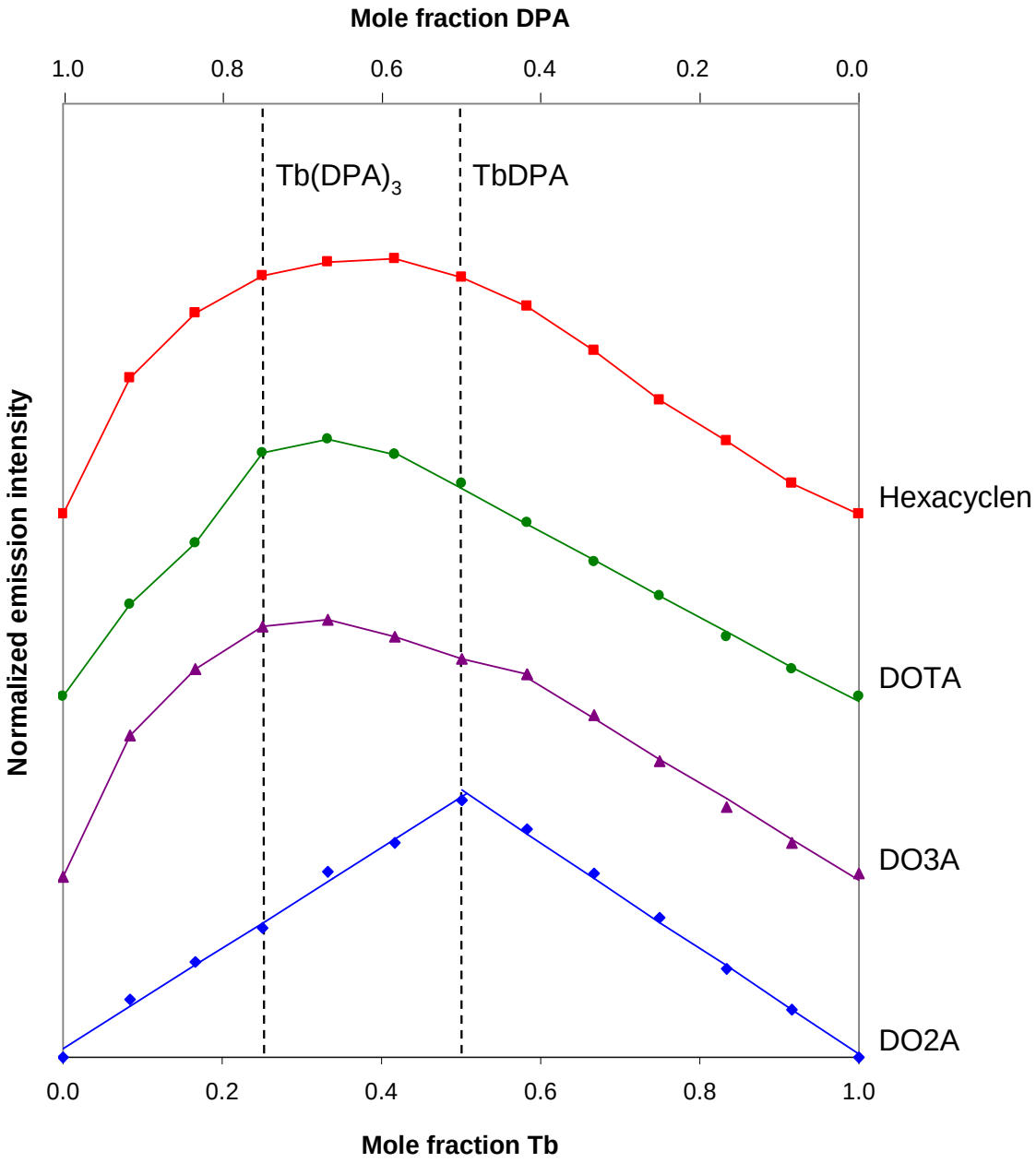

Figure 3.3. Jobs plots of various macrocyclic ligands in 1.0 mM NaOH, pH 8.1. The concentrations of Tb and DPA are varied inversely from 0 to 12 μM in 1 μM increments, with the macrocyclic ligand in excess (100 μM). Linear regions are fitted with trendlines, and significant Tb:DPA ratios are noted by dashed lines.

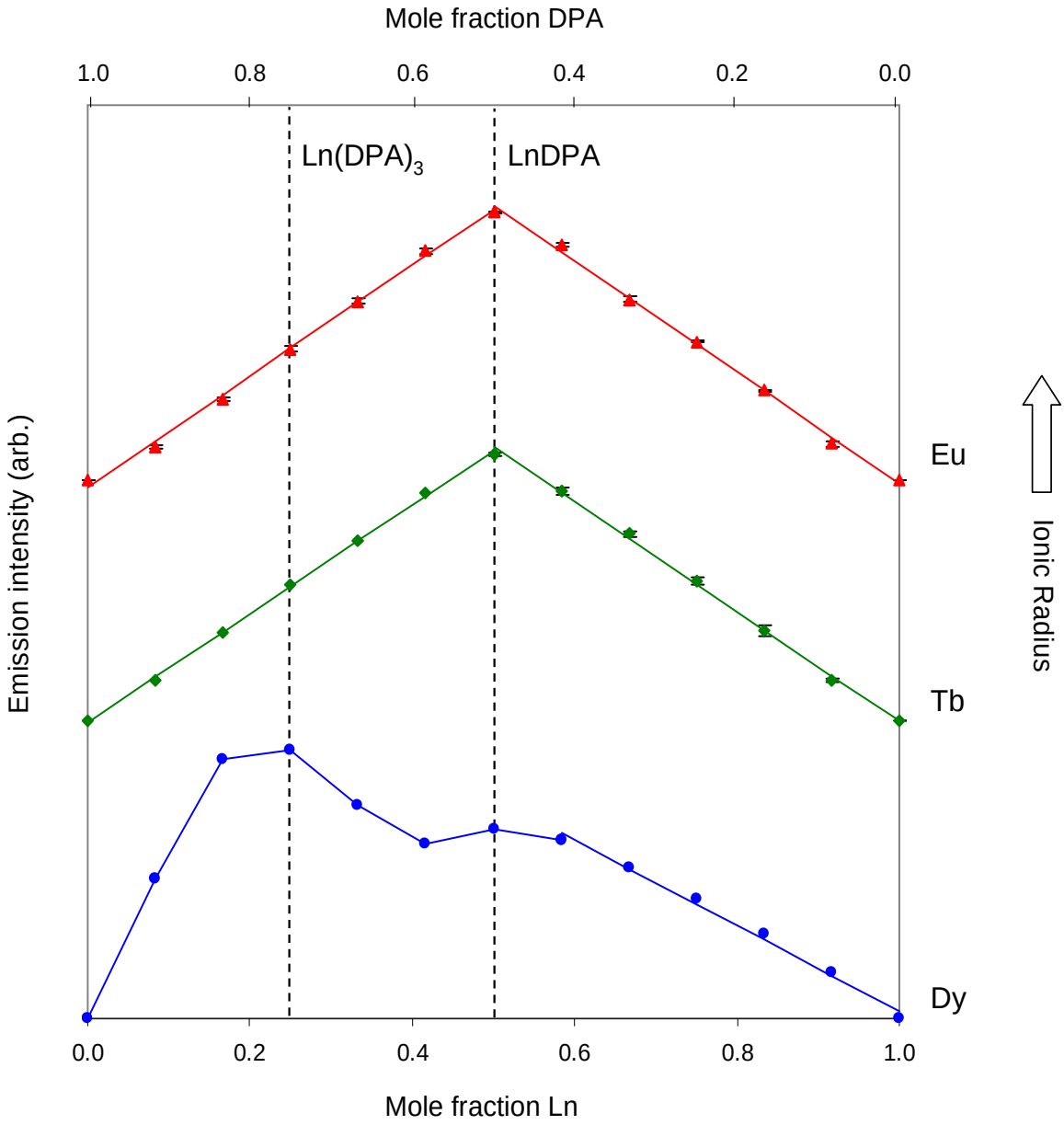

Figure 3.4. Jobs plots of various lanthanides in 100 mM CHES, pH 9.4. The concentrations of lanthanide and DPA are varied inversely from 0 to 12 μM in 1 μM increments, with DO2A in excess (100 μM).

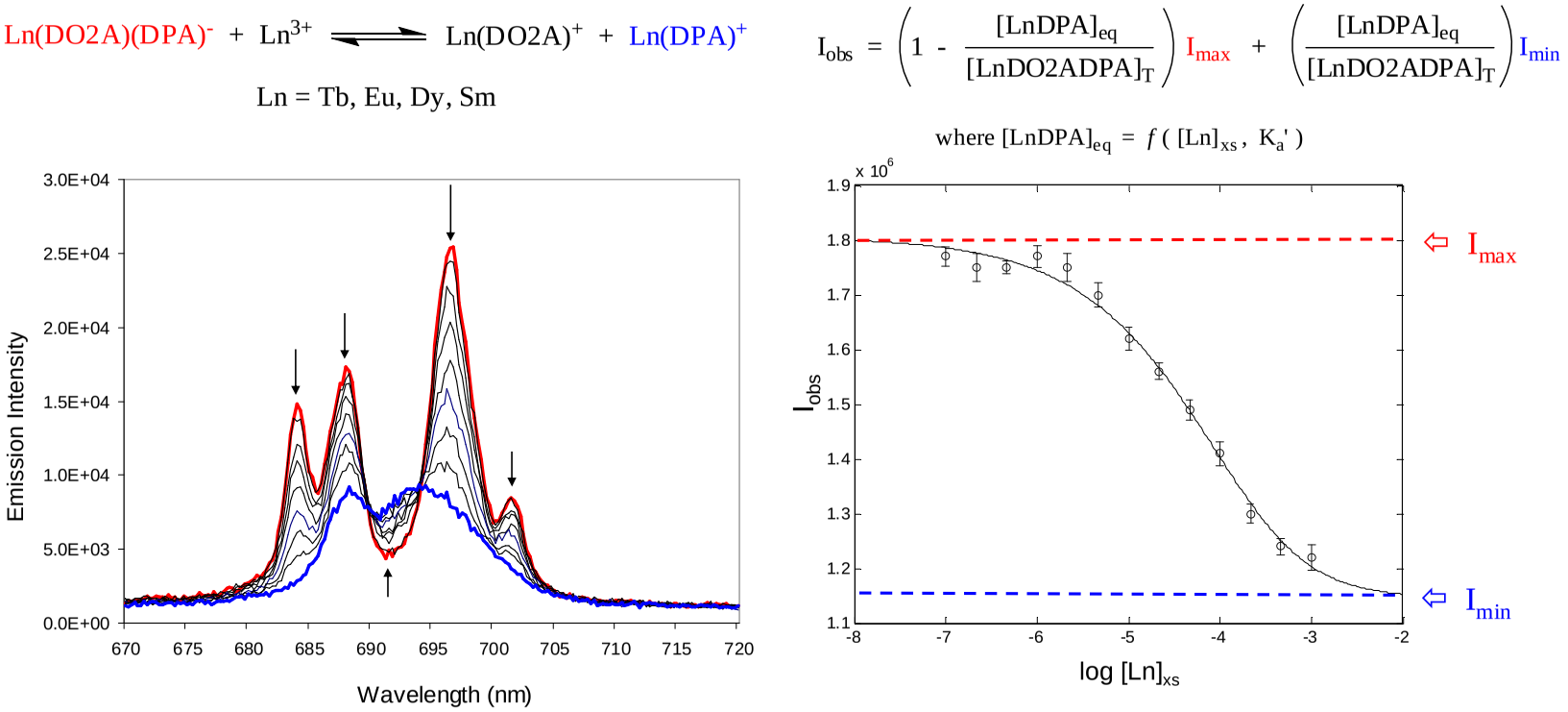

Figure 3.5. Binding affinity by competition (BAC) assay. The ternary complex (red) with the greatest luminescence is competed against free Ln^{3+}, which eventually strips the dipicolinate and forms the $Ln(DPA)^{+}$ complex (blue), whose luminescence is diminished due to solvent quenching (left). The luminescence of the Ln^{3+} and $Ln(DO2A)^{+}$ species is negligible, as these lack the DPA chromophore. The resulting curve (right) is then fitted to a model to produce an association constant (K_a') for $Ln(DO2A)^{+}$ to DPA^{2-}.

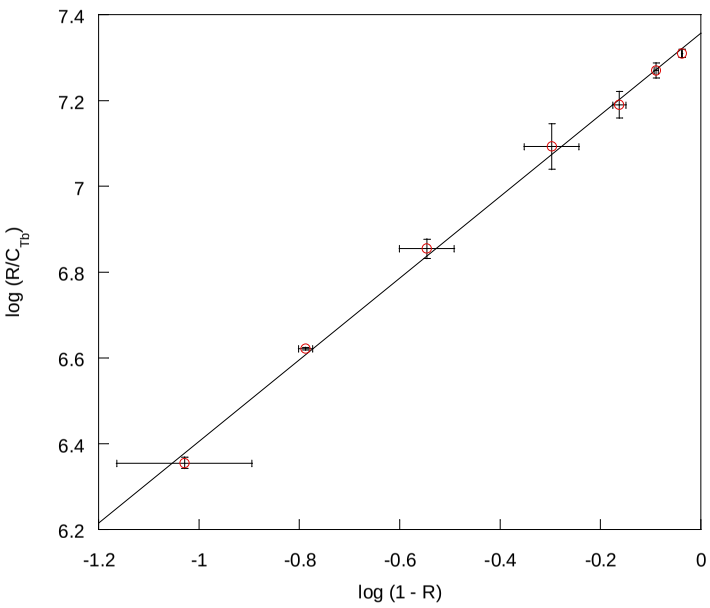

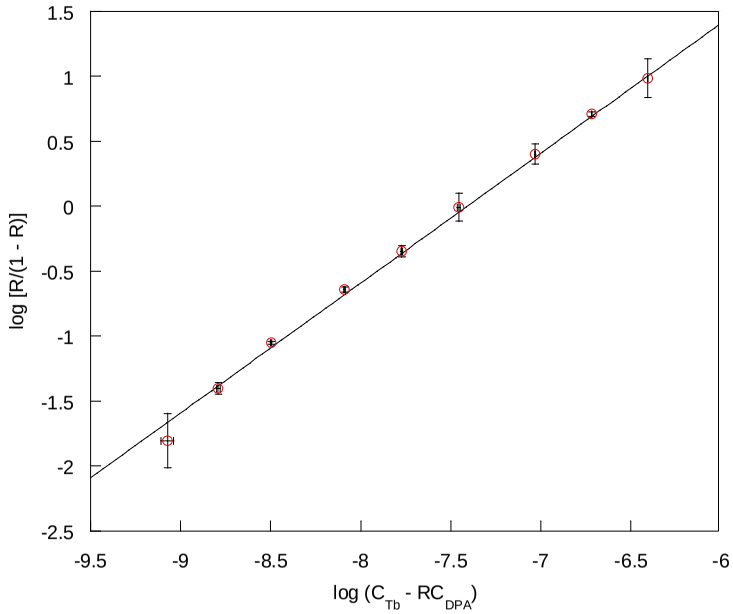

$\log (R/C_{Tb}) = n \log (1 - R) + \log K_a$

$\log [R/(1 - R)] = \log (C_{Tb} - RC_{DPA}) + \log K_a$

n = 0.932 (No. of DPA's per Tb)

No additional parameters used

$\log K_a = 7.35 \pm 0.03$

$\log K_a = 7.41 \pm 0.03$

Figure 3.6. Methods to calculate K_a. (A) Linear fit using the Jones and Vullev method to determine Tb^{3+}/DPA^{2-} binding affinity, 0.2 M NaOAc, pH 7.4, 25℃. (B) The exact same data set treated with our fitting model. Fewer constraints mean more data points can be used, producing a more accurate fit.

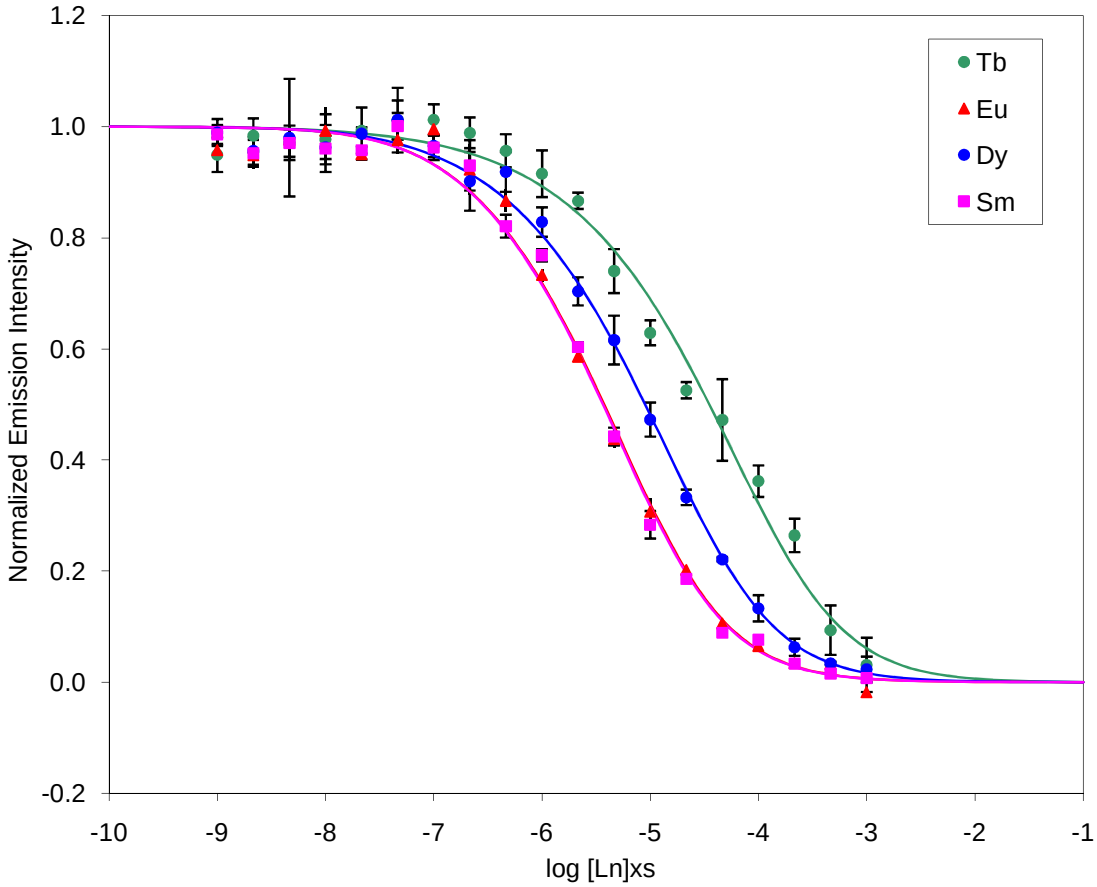

Figure 3.7. Lanthanide competition experiment. Binding affinity by competition (BAC) assay titration curves for Sm, Eu, Tb and Dy, 0.2 M NaOAc, pH 7.5.

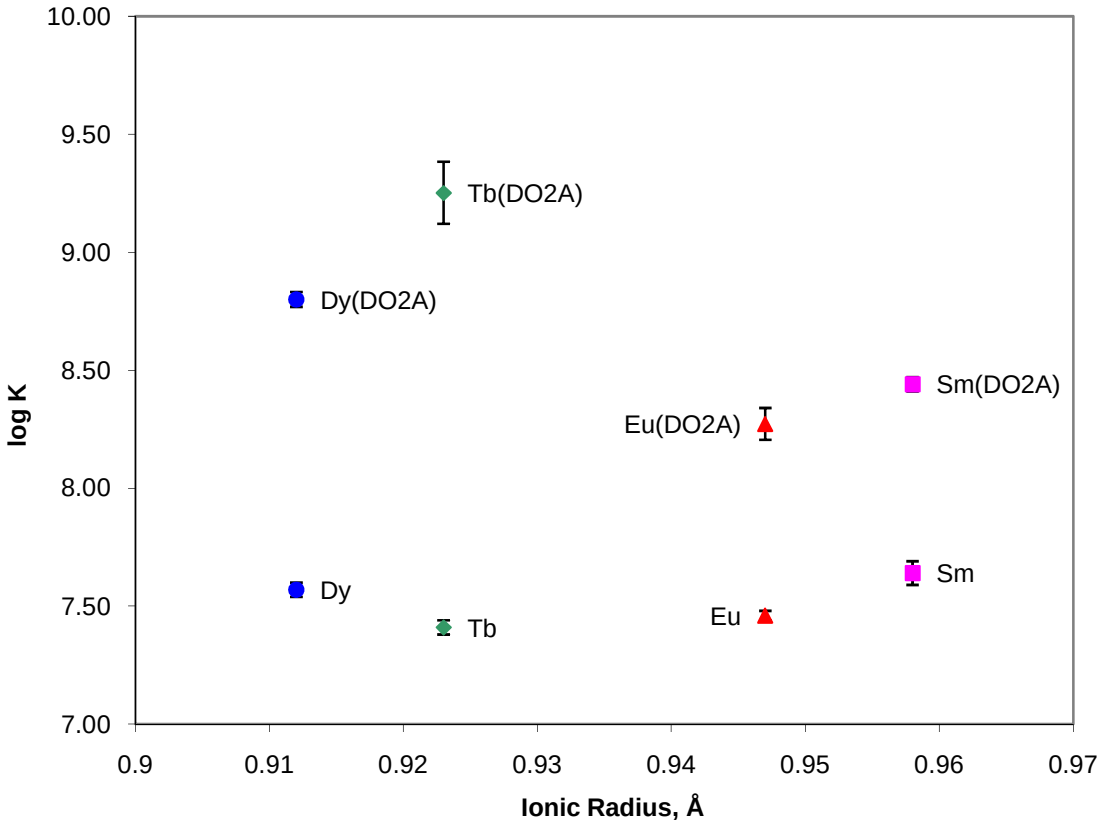

Figure 3.8. Plot of association constants for Ln^{3+} and $Ln(DO2A)^{+}$ to DPA^{2-} against lanthanide ionic radius, 0.2 M NaOAc, pH 7.5. The addition of DO2A enhances dipicolinate binding affinity by an order of magnitude for most lanthanides, and by nearly two orders of magnitude for terbium (green).

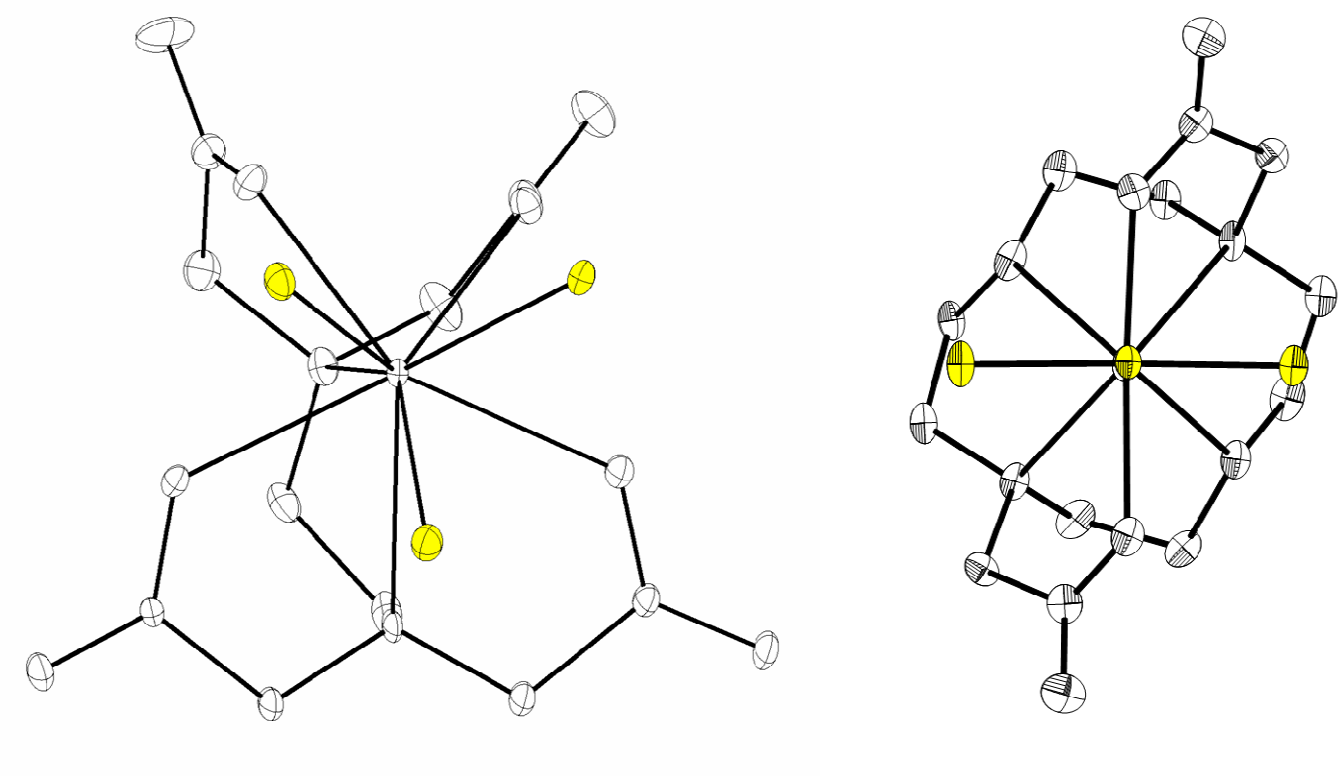

Figure 3.9. Crystal structures of Tb(EDTA)·NaOH·2H_2O and TBA·Tb(DO2A)(DPA), showing trigonal and linear coordination sites, respectively, available for dipicolinate binding (yellow). Thermal ellipsoids are at 50% probability; hydrogens and extraneous atoms omitted for clarity. Tb(EDTA)·NaOH·2H_2O crystallized out of deionized water (18.2 MΩ-cm resistivity) at 4℃.

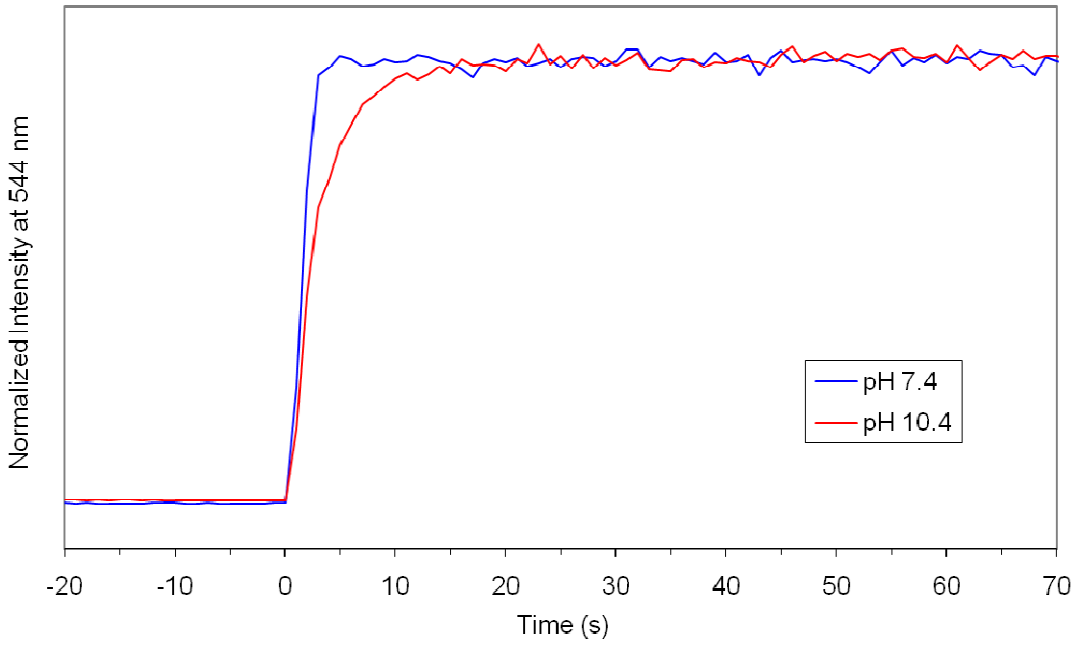

Figure 3.10. Time courses for binding of $Tb(DO2A)^{+}$ to DPA^{2-} at neutral and high pH. Both reach completion in seconds; the longer time required for the time course at high pH is attributed to displacement of hydroxyl groups from the terbium coordination sphere.

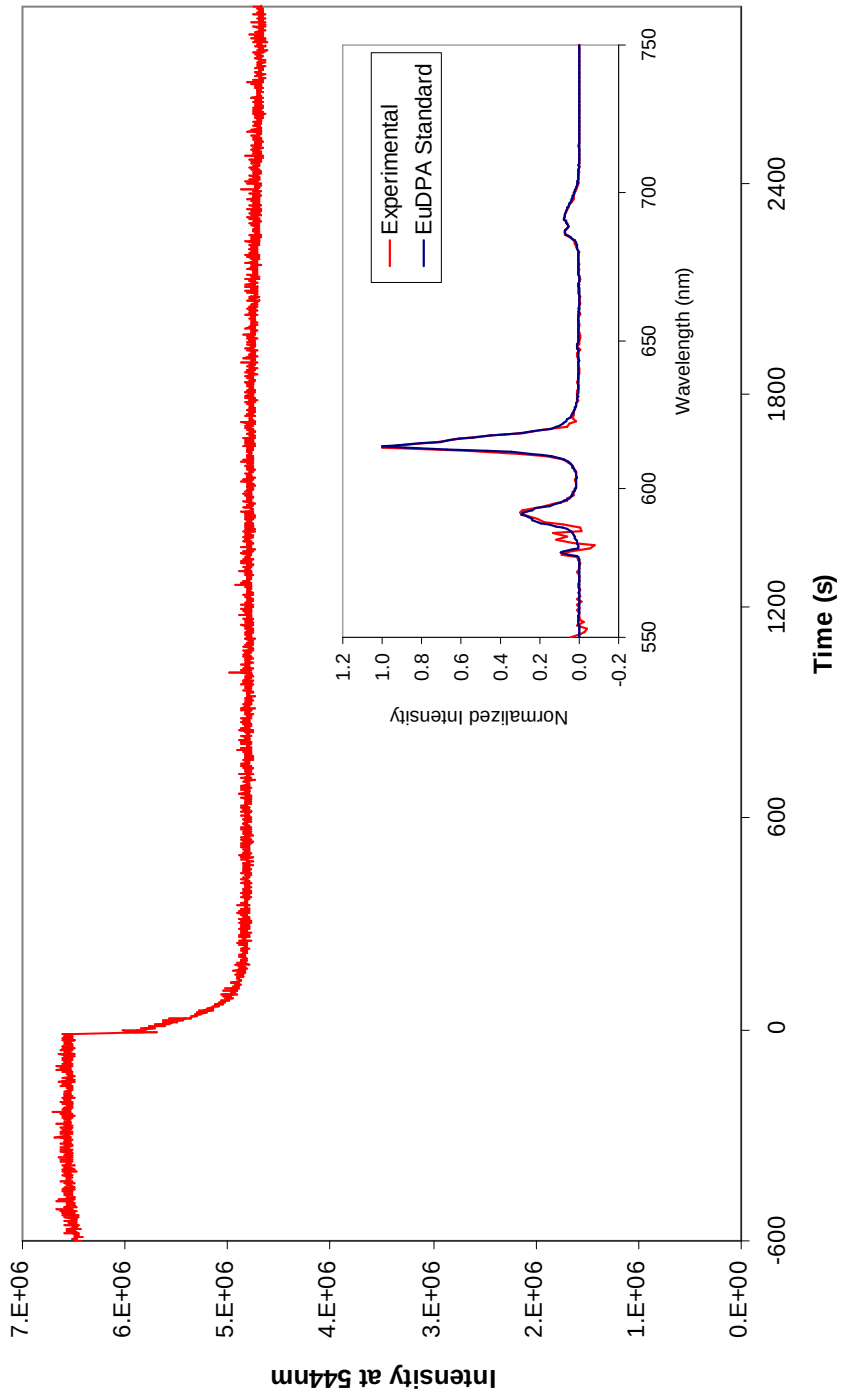

Figure 3.11. Kinetics experiment competing equimolar Tb(DO2A)(DPA)$^{-}$ against Eu^{3+}, 0.2 M NaOAc, pH 7.5, 25℃. $EuDPA^{+}$ is the only europium species produced (inset), supporting the assumption that DO2A remains bound to the terbium for the duration of the experiment.

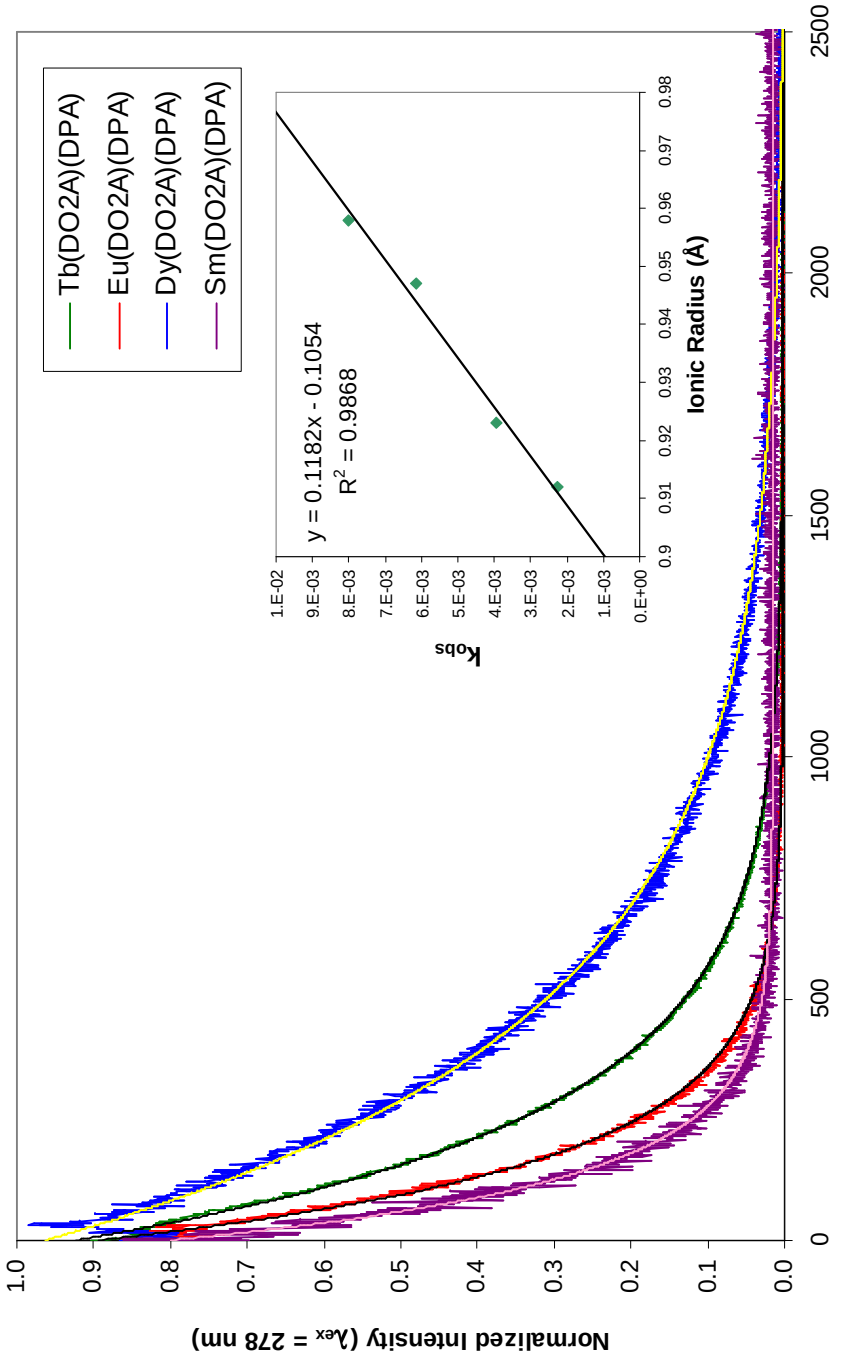

Figure 3.12. Kinetics decay curves of 1.0 μM Ln(DO2A)(DPA)$^{-}$ with 1.0 mM Gd^{3+} in 0.2 M NaOAc, pH 7.5, 25 ℃ (Ln = Sm, Eu, Tb and Dy). The rate of luminescence decay, fitted to a monoexponential model, tracks linearly with lanthanide ionic radius (inset).

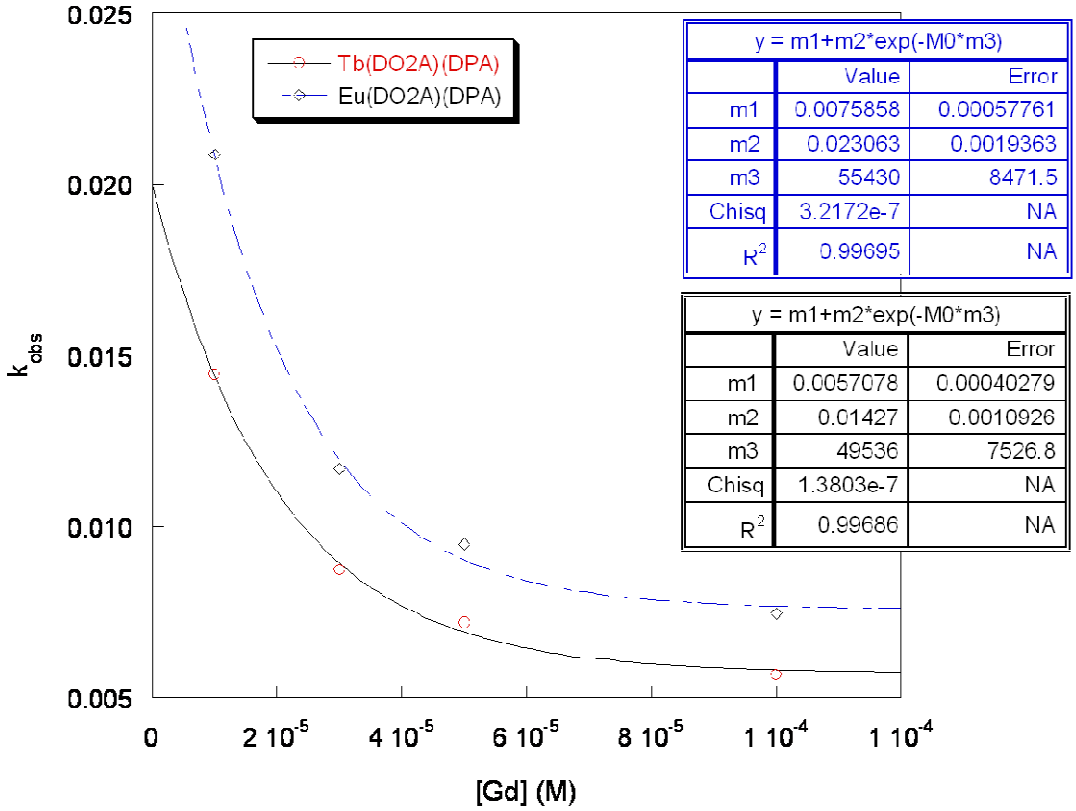

y = m1+m2*exp(-M0*m3)		
	Value	Error
m1	0.0075858	0.00057761
m2	0.023063	0.0019363
m3	55430	8471.5
Chisq	3.2172e-7	NA
R^2	0.99695	NA

y = m1+m2*exp(-M0*m3)		
	Value	Error
m1	0.0057078	0.00040279
m2	0.01427	0.0010926
m3	49536	7526.8
Chisq	1.3803e-7	NA
R^2	0.99686	NA

Figure 3.13. Kinetics experiments with $Tb(DO2A)(DPA)^-$ and $Eu(DO2A)(DPA)^-$ competed with Gd^{3+}, showing a decrease in the rate with increasing [Gd].

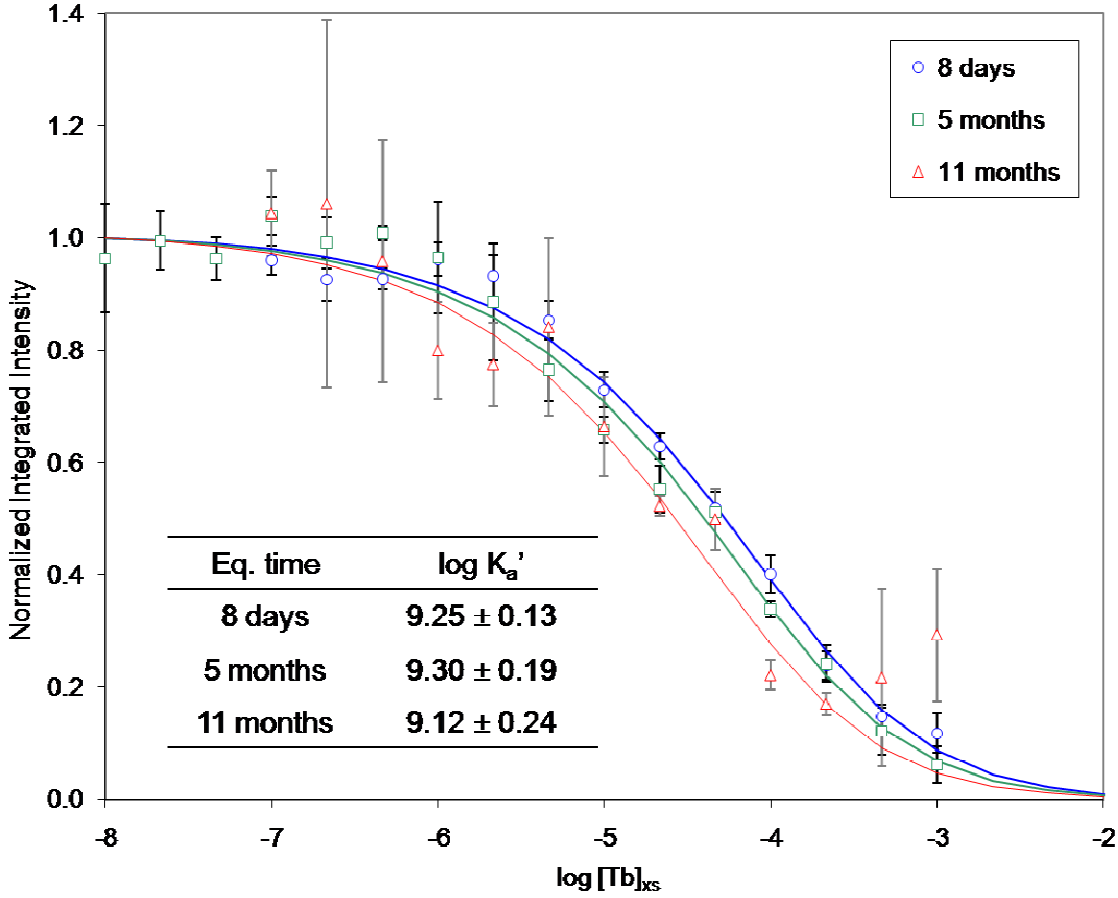

Figure 3.14. Stability of Tb(DO2A)(DPA)$^{-}$ over time, 0.2 M NaOAc, pH 7.5, 25 ℃. λ_{ex} = 278 nm, emission spectra integrated from 570–600 nm. Large error bars in 11 months data set (gray) are due to loss of solvent through evaporation.

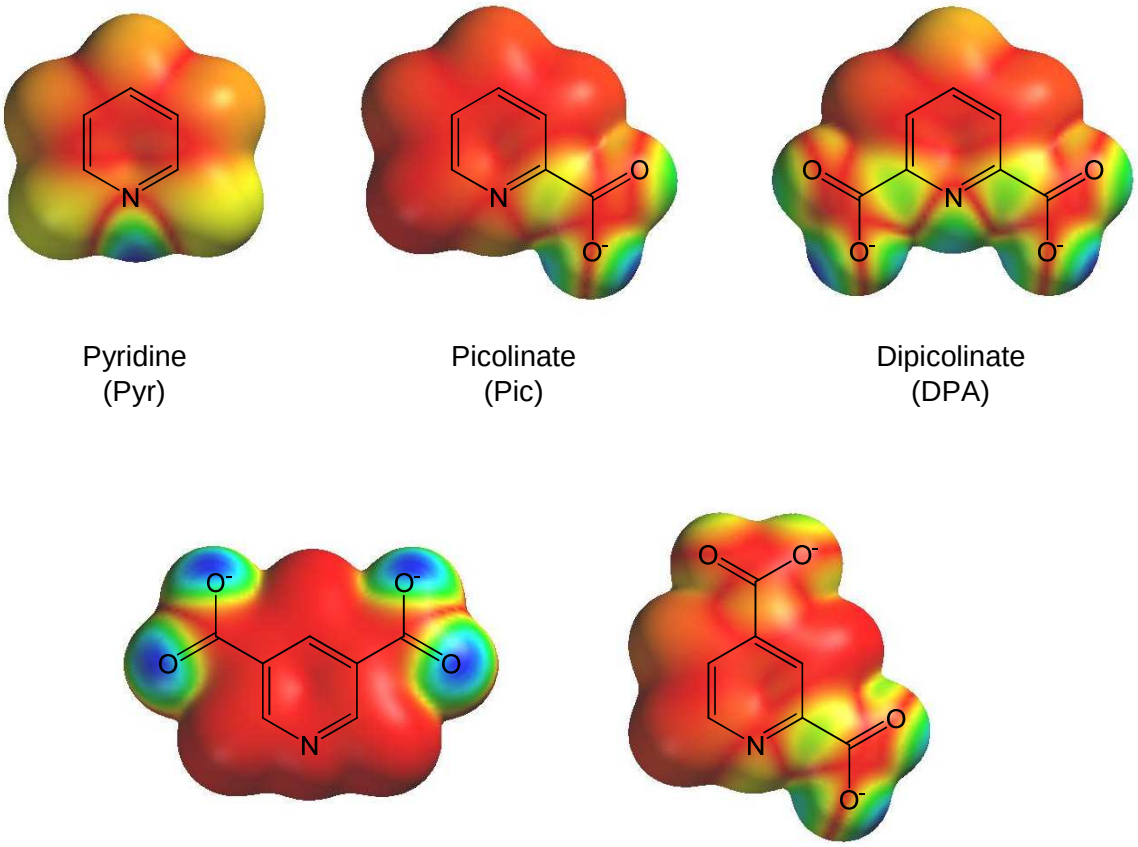

Figure 3.15. Structures of pyridine, picolinate, and three structural isomers of dipicolinate, overlaid with an electron density map of the highest occupied molecular orbital (HOMO) for each ligand. These chromophores were explored to better understand the binding properties of DPA. Electron density maps generated using Titan®; higher electron density is in blue, lower in red.

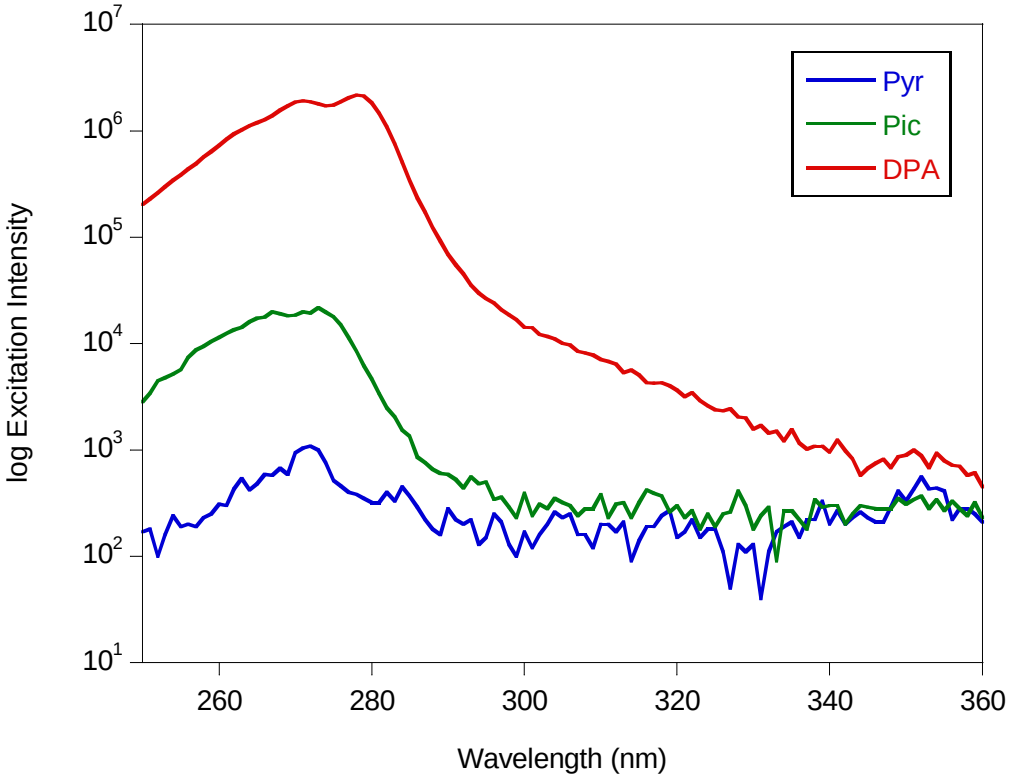

Figure 3.16. Excitation spectra (λ_{em} = 544 nm) of various terbium complexes, 10 μM in 0.2 M NaOAc, pH 5.5. Note the logarithmic y-axis. Pyridine (Pyr) has little detectable terbium sensitization, picolinate (Pic) is moderately effective, and dipicolinate (DPA) is most effective.

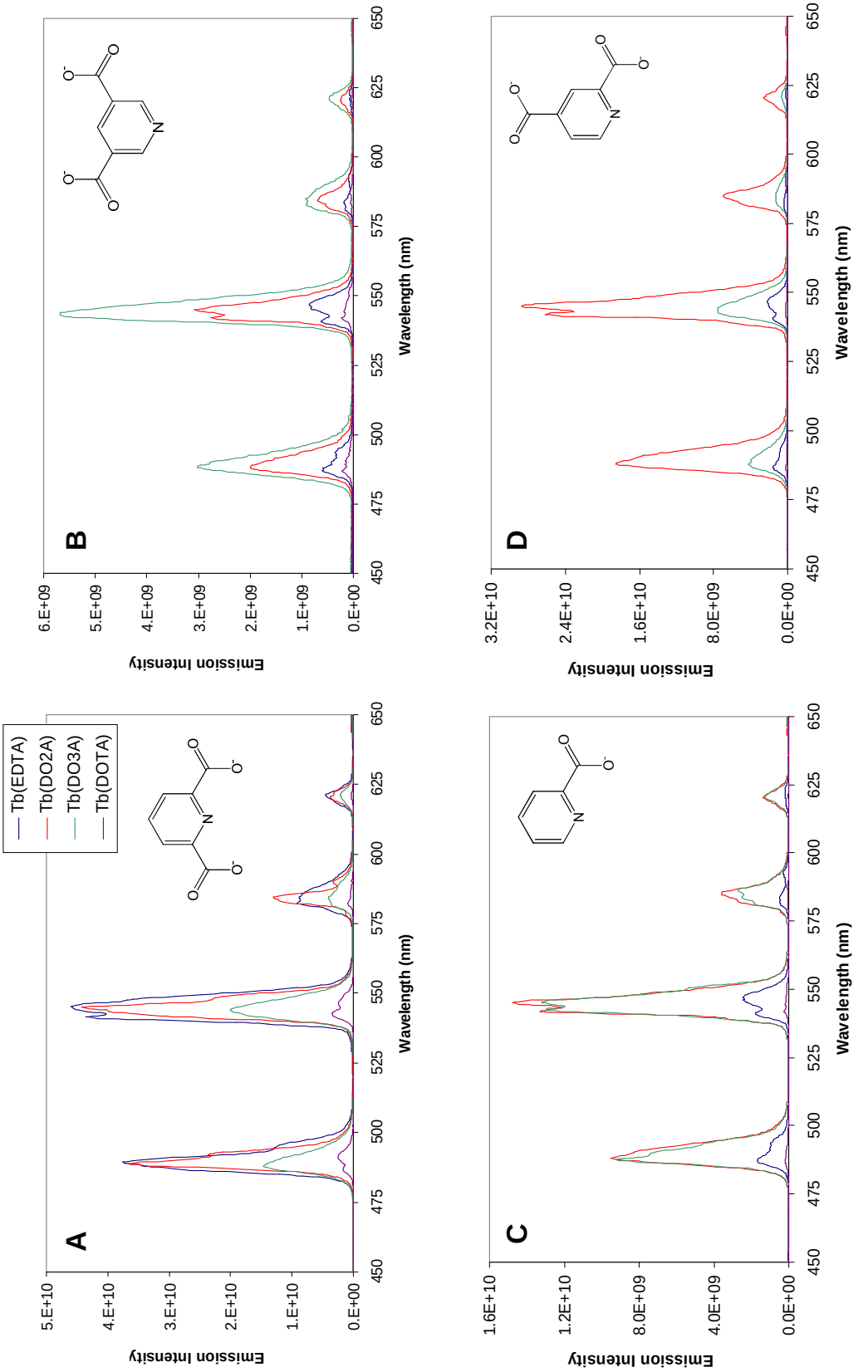

Figure 3.17. Emission spectra (λ_{ex} = 278 nm) of various terbium complexes in 50 mM MOPS buffer, pH 7.5. (A) DPA; (B) 3,5-DPA; (C) Pic; (D) 2,4-DPA.

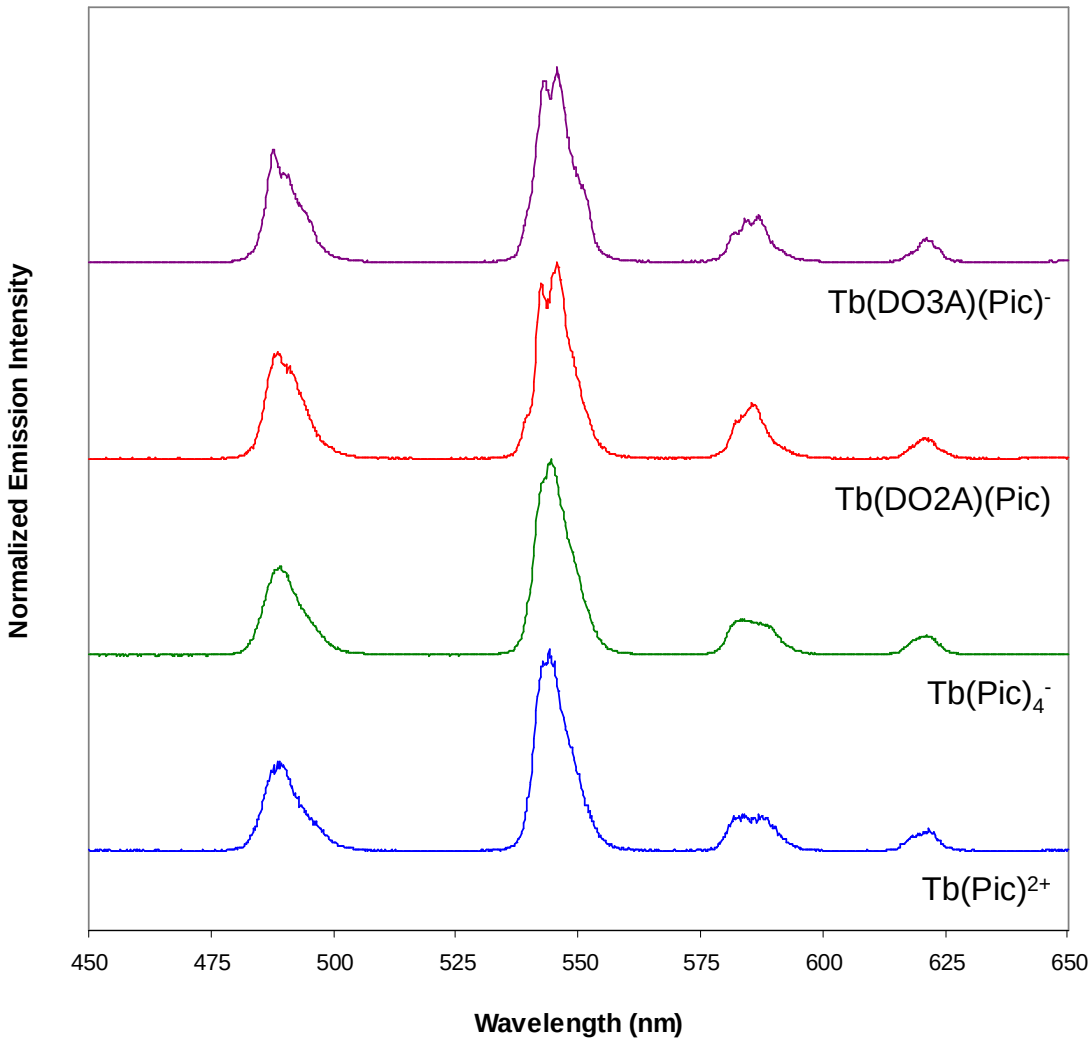

Figure 3.18. Emission spectra (λ_{em} = 274 nm) of various terbium picolinate complexes in 0.1 M MOPS buffer, pH 7.2. Charges and coordination numbers of Pic ligand assume deprotonation of carboxyl group (i.e., charge of -1) and bidentate coordination to Tb^{3+}.

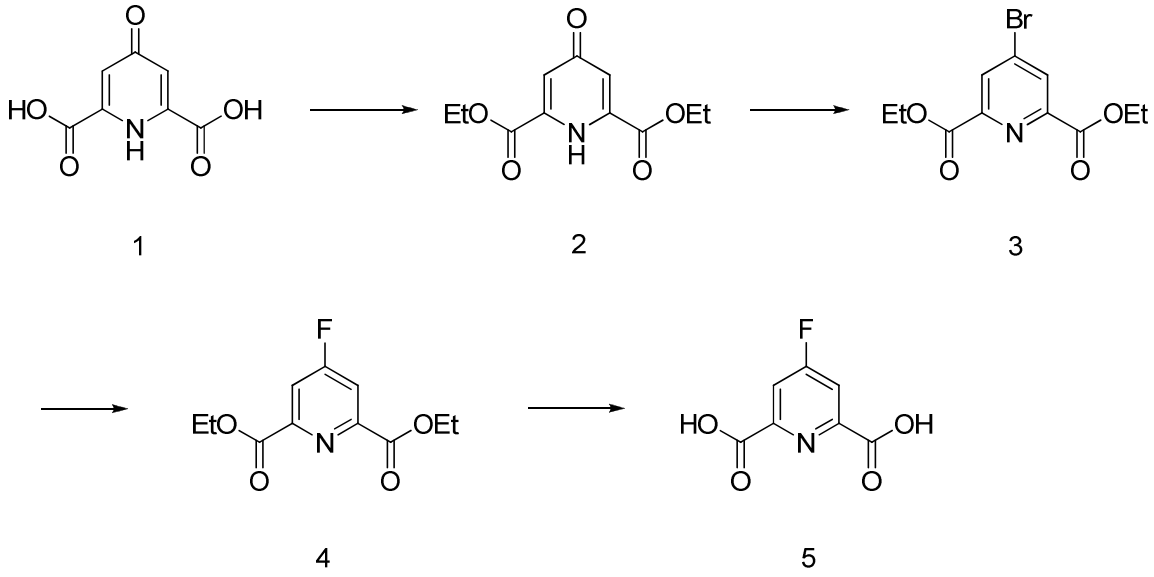

Figure 3.19. Protocol for synthesis of 4-fluoro-pyridine-2,6-dicarboxylic acid (F-DPA). Reproduced from CB Research & Development, Inc., personal communication.

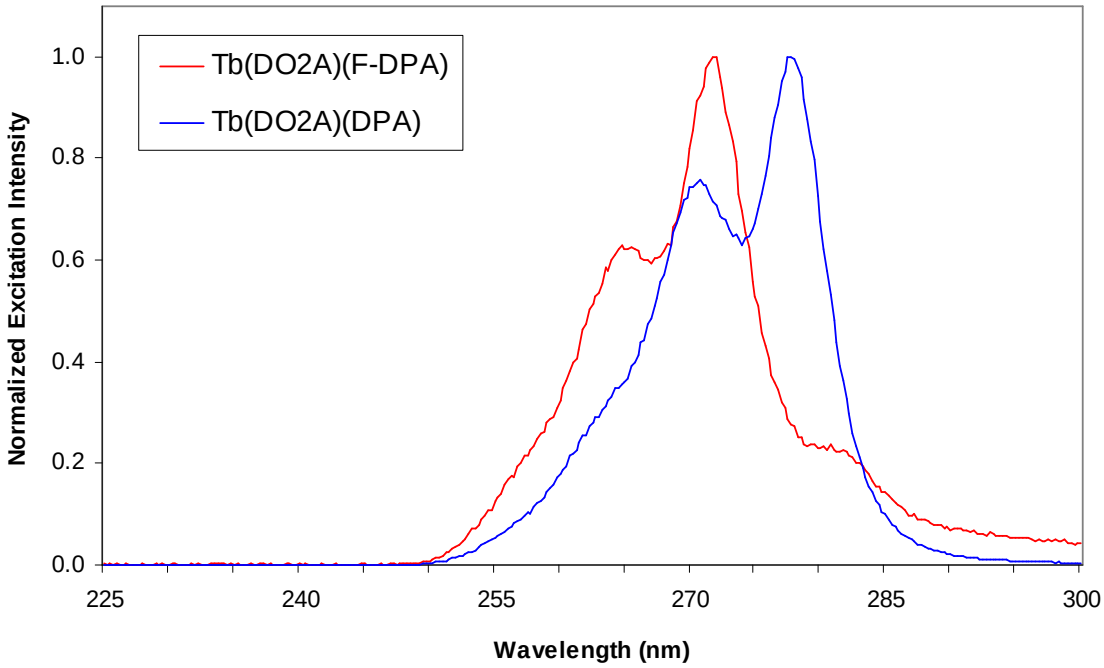

Figure 3.20. Normalized excitation spectra (λ_{em} = 544 nm) for $Tb(DO2A)(DPA)^-$ and $Tb(DO2A)(F\text{-}DPA)^-$, 10.0 μM in 1.0 mM NaOH, pH 9. The fluorinated dipicolinate complex is blue-shifted by approximately 5 nm, indicative of a shift of electron density away from the lanthanide.

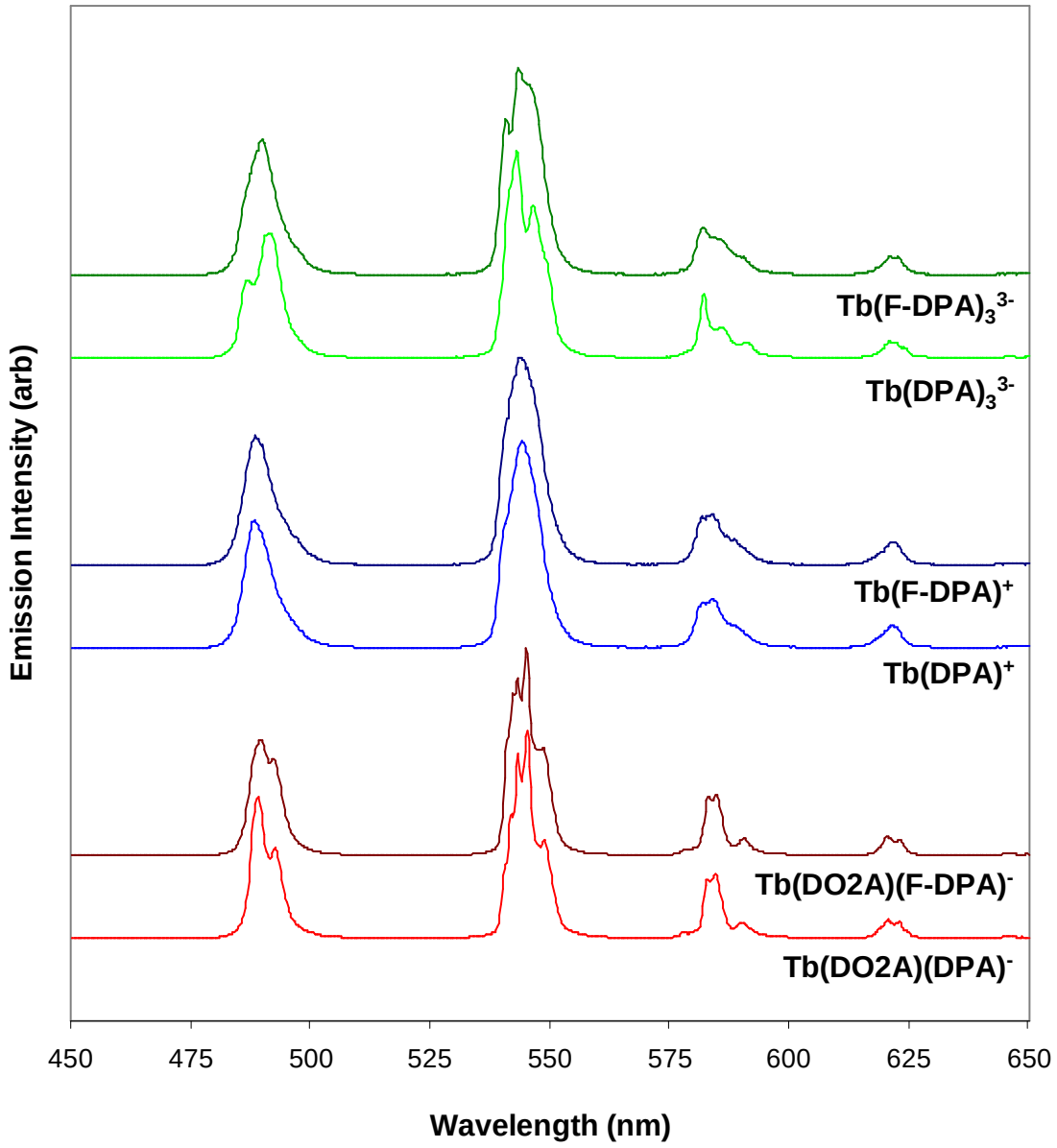

Figure 3.21. Normalized emission spectra (λ_{ex} = 278 nm) for various DPA and F-DPA complexes, 1.0 mM NaOH, pH 9. The F-DPA ternary complex (dark red) shows finer Stark splitting than its DPA counterpart (red), while the situation is reversed for the tris-dipicolinate species (light and dark green).

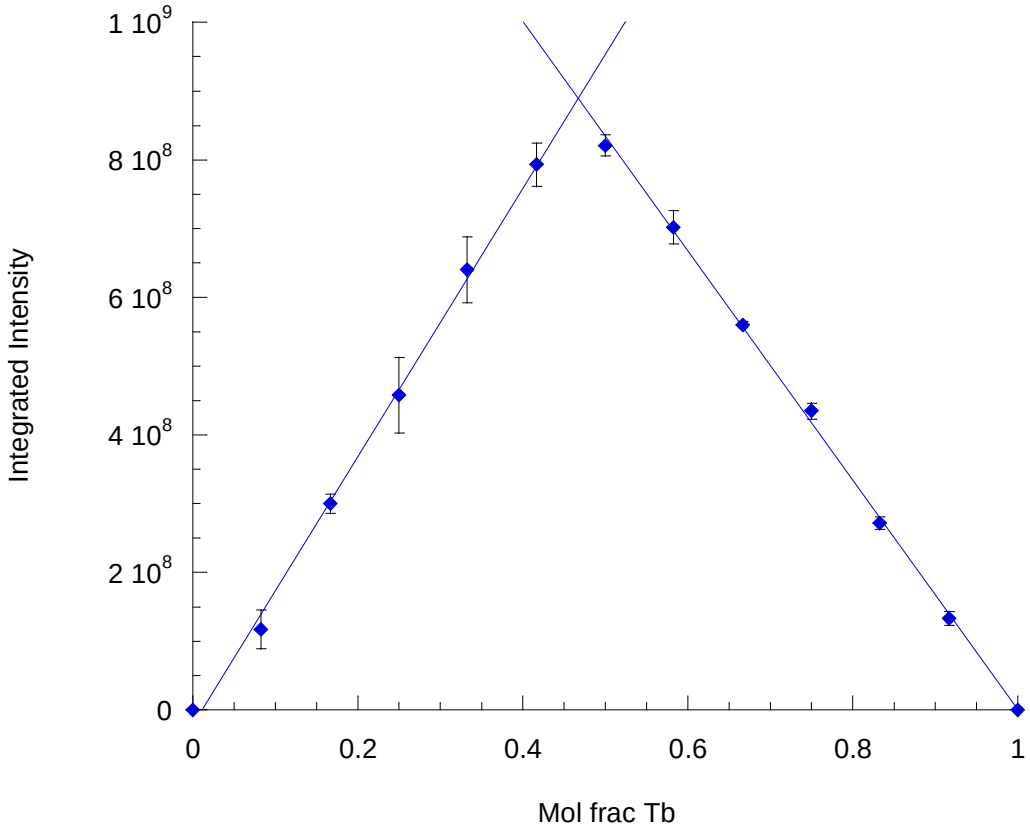

Figure 3.22. Jobs plot of $Tb(DO2A)^{+}$ with F-DPA in 1.0 mM NaOH, pH 9.0, indicating an optimal Tb mole fraction of 0.47 for complete binding of F-DPA.

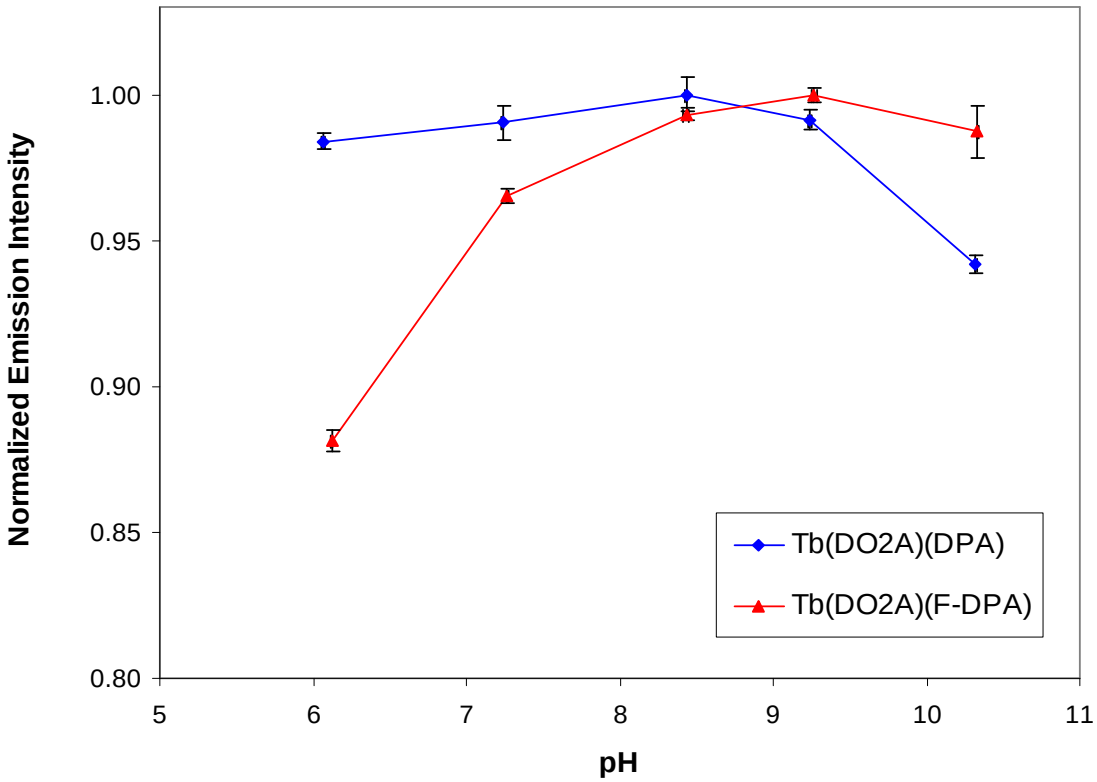

Figure 3.23. pH dependence of $Tb(DO2A)(DPA)^-$ and $Tb(DO2A)(F\text{-}DPA)^-$, 10.0 μM in 0.1 M buffer. Normalized emission spectra (λ_{ex} = 278 nm) are integrated from 530–560 nm.

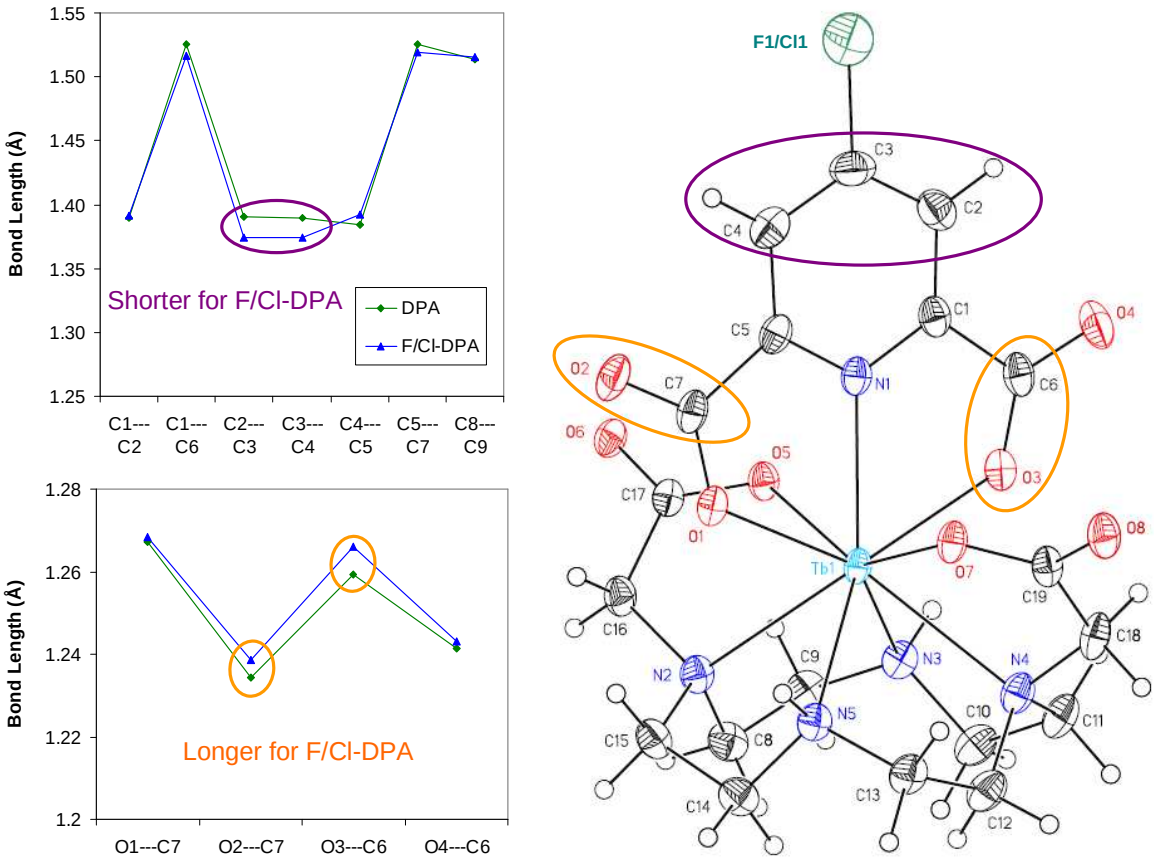

Figure 3.24. Various bond lengths (Å) for the dipicolinate of the TBA·Tb(DO2A)(F/Cl-DPA) crystal structure, where the 4-substituted dipicolinate species is 37% F-DPA and 63% Cl-DPA.

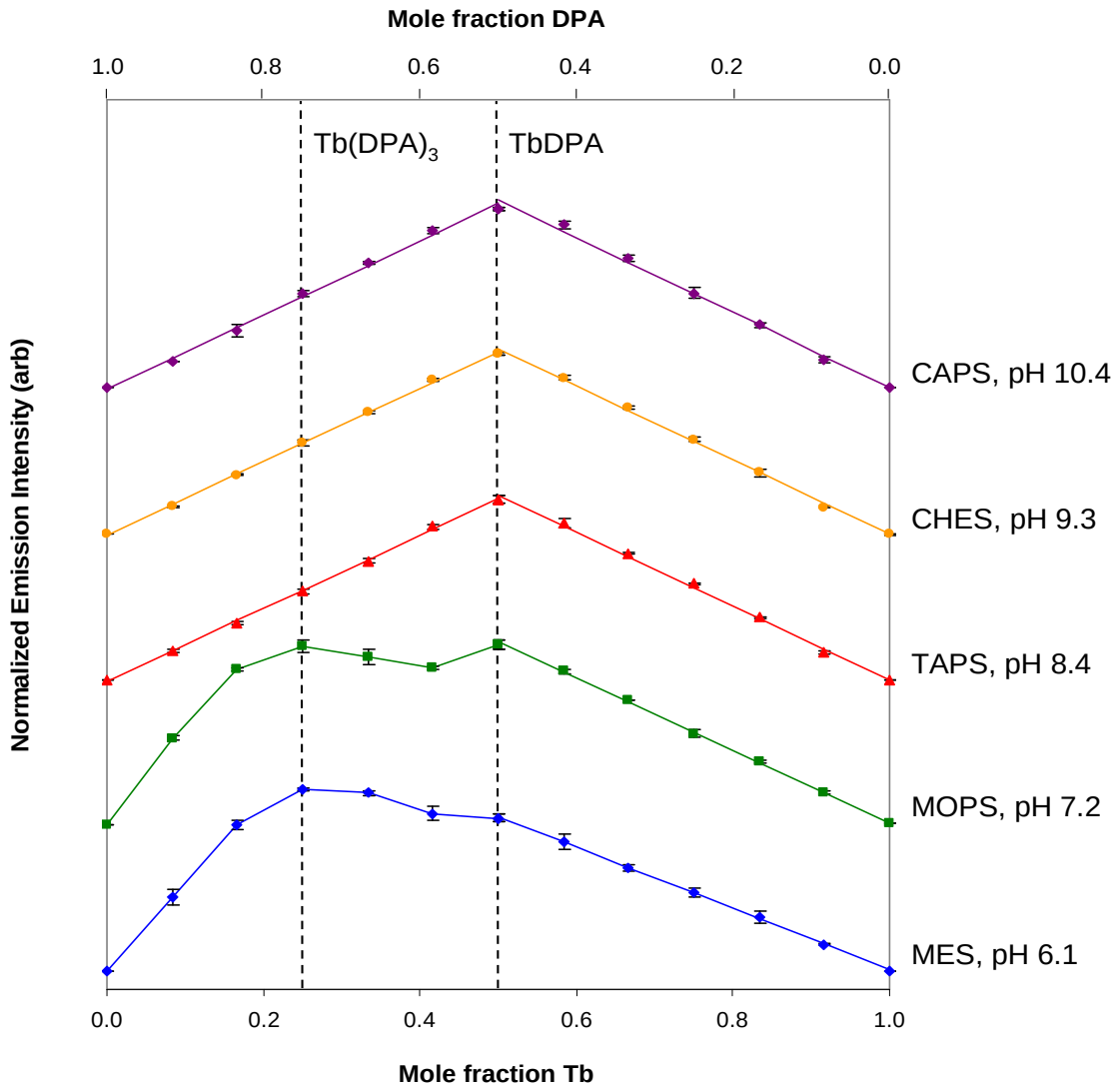

Figure 3.25. Jobs plots of Tb(DO2A)(DPA)$^-$ in 0.1 M buffer at various pH values. The concentrations of Tb and DPA are varied inversely from 0 to 12 μM in 1 μM increments, with the DO2A in excess (100 μM). Emission spectra (λ_{ex} = 278 nm) are integrated over 530–560 nm. Linear regions are fitted with trendlines, and significant Tb:DPA ratios are noted by dashed lines.

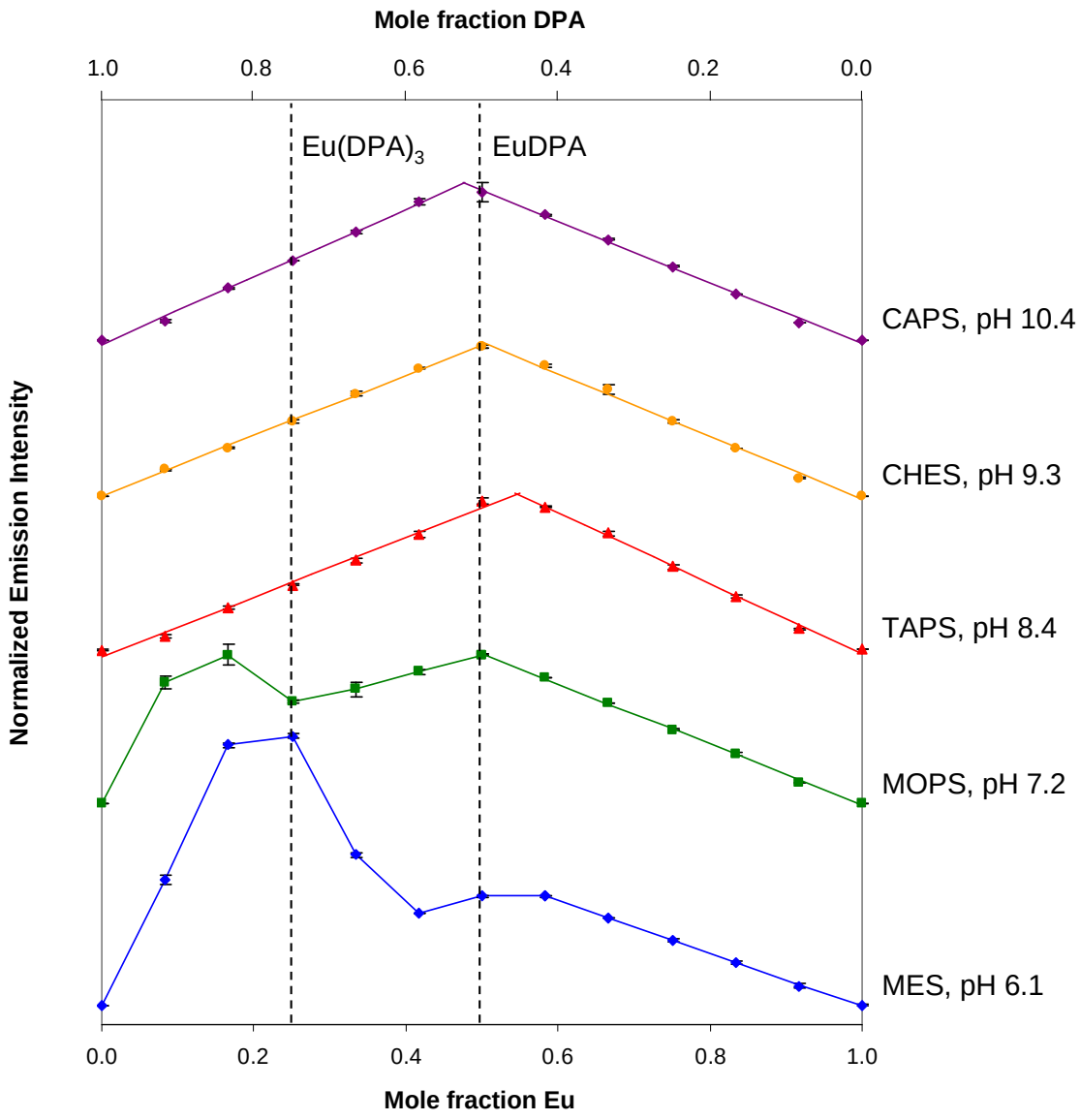

Figure 3.26. Jobs plots of Eu(DO2A)(DPA)$^{-}$ in 0.1 M buffer at various pH values. The concentrations of Eu and DPA are varied inversely from 0 to 12 μM in 1 μM increments, with the DO2A in excess (100 μM). Emission spectra (λ_{ex} = 278 nm) are integrated over 680–710 nm. Linear regions are fitted with trendlines, and significant Eu:DPA ratios are noted by dashed lines.

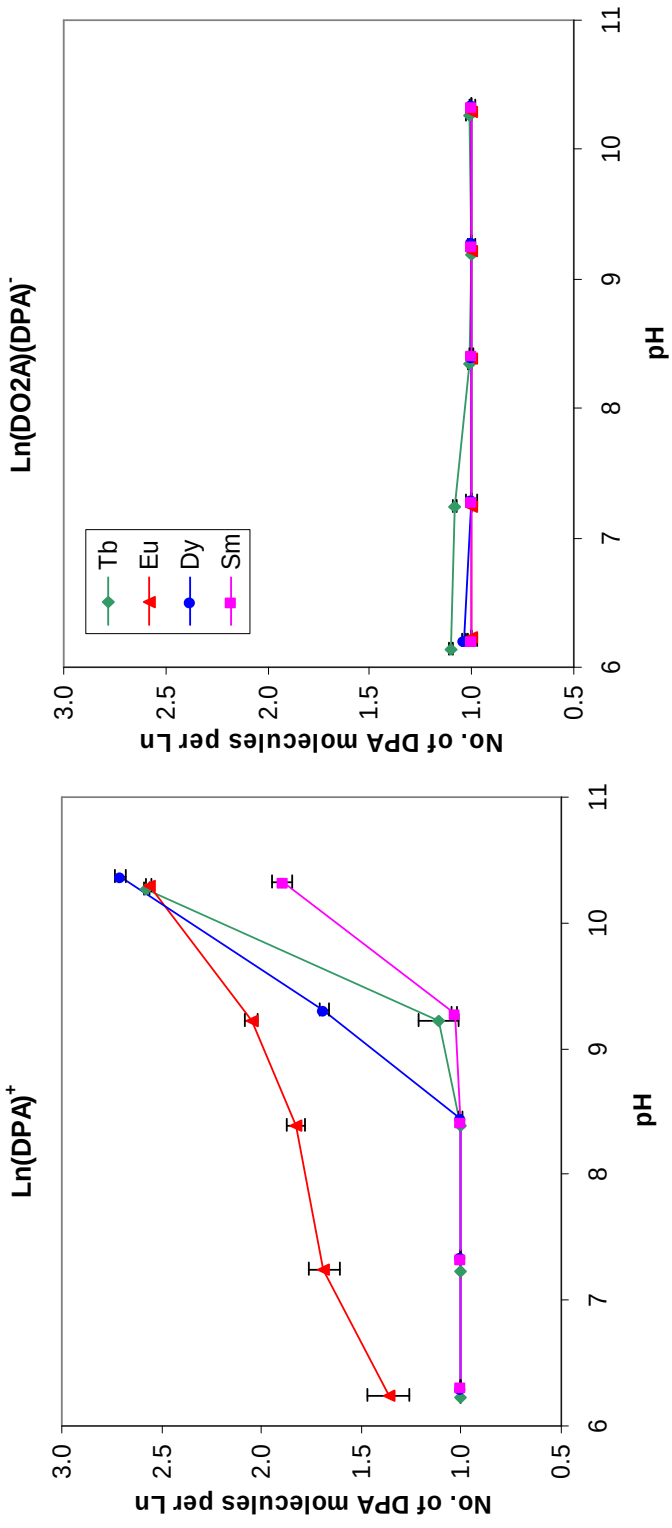

Figure 3.27. Number of DPA molecules bound per Ln^{3+} as a function of pH for $Ln(DPA)^{+}$ and $Ln(DO2A)(DPA)^{-}$ complexes (Ln = Sm, Eu, Tb and Dy), 10.0 µM in 0.1 M buffer (λ_{ex} = 278 nm).

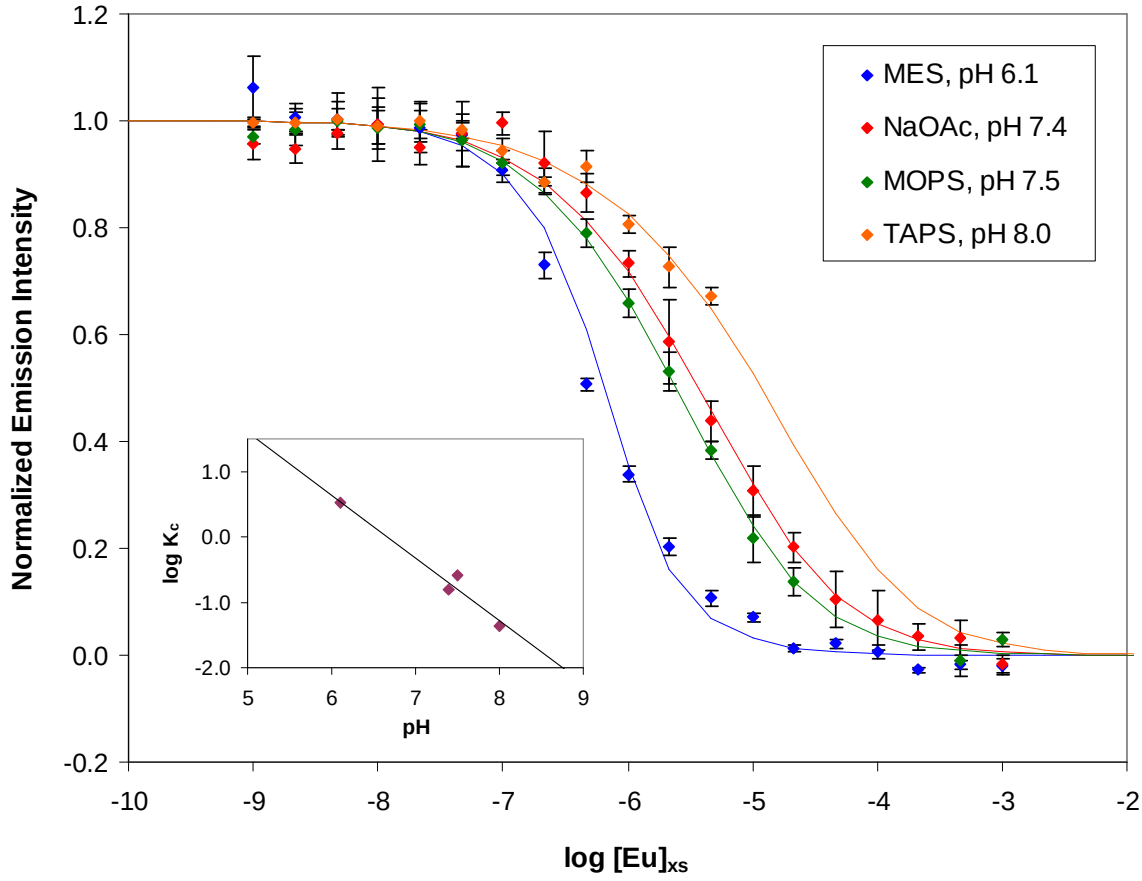

Figure 3.28. Binding affinity by competition (BAC) assay titration curves for Eu(DO2A)(DPA)$^{-}$ in 0.1 M buffer at various pH values. Emission spectra (λ_{ex} = 278 nm) integrated from 675–710 nm. Inset: Logarithm of competition constant (K_c) against pH.0

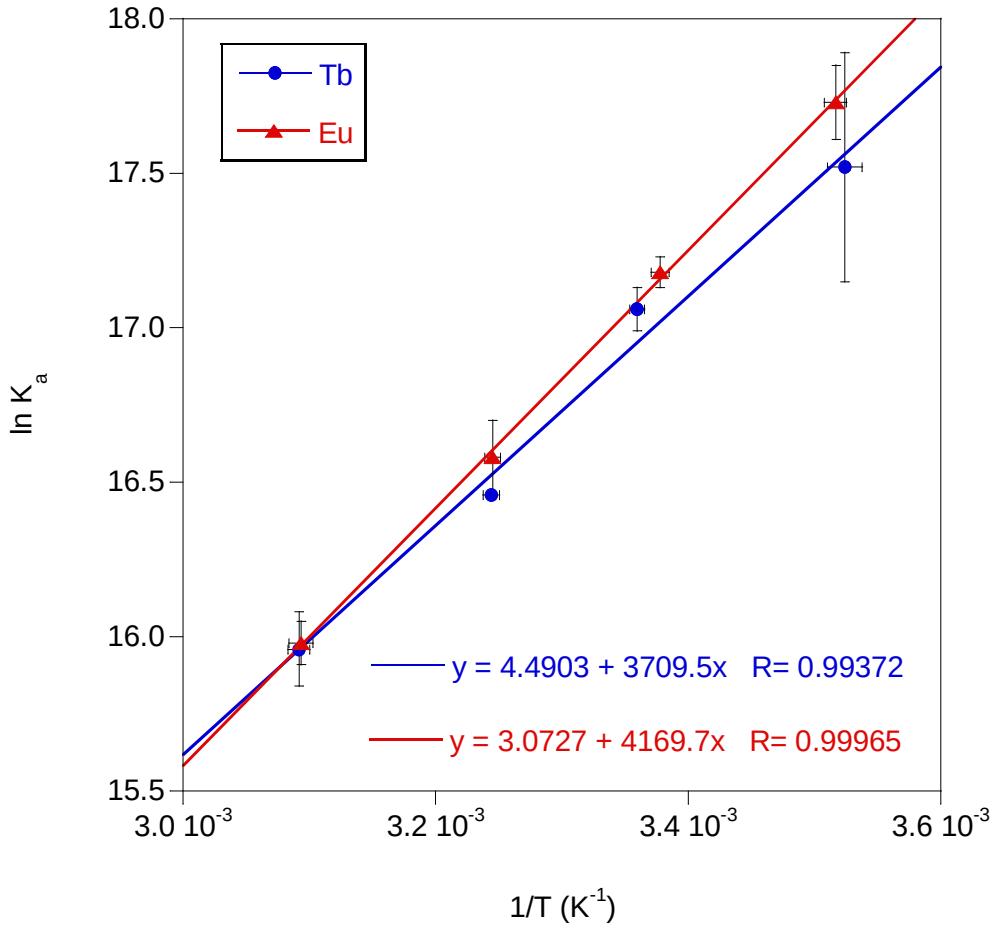

Figure 3.29. Plot of ln K_a against 1/T for $Tb(DPA)^+$ and $Eu(DPA)^+$ in 0.2 M NaOAc, pH 7.4. Slopes, y-intercepts and correlation coefficients (R) are shown for each linear fit.

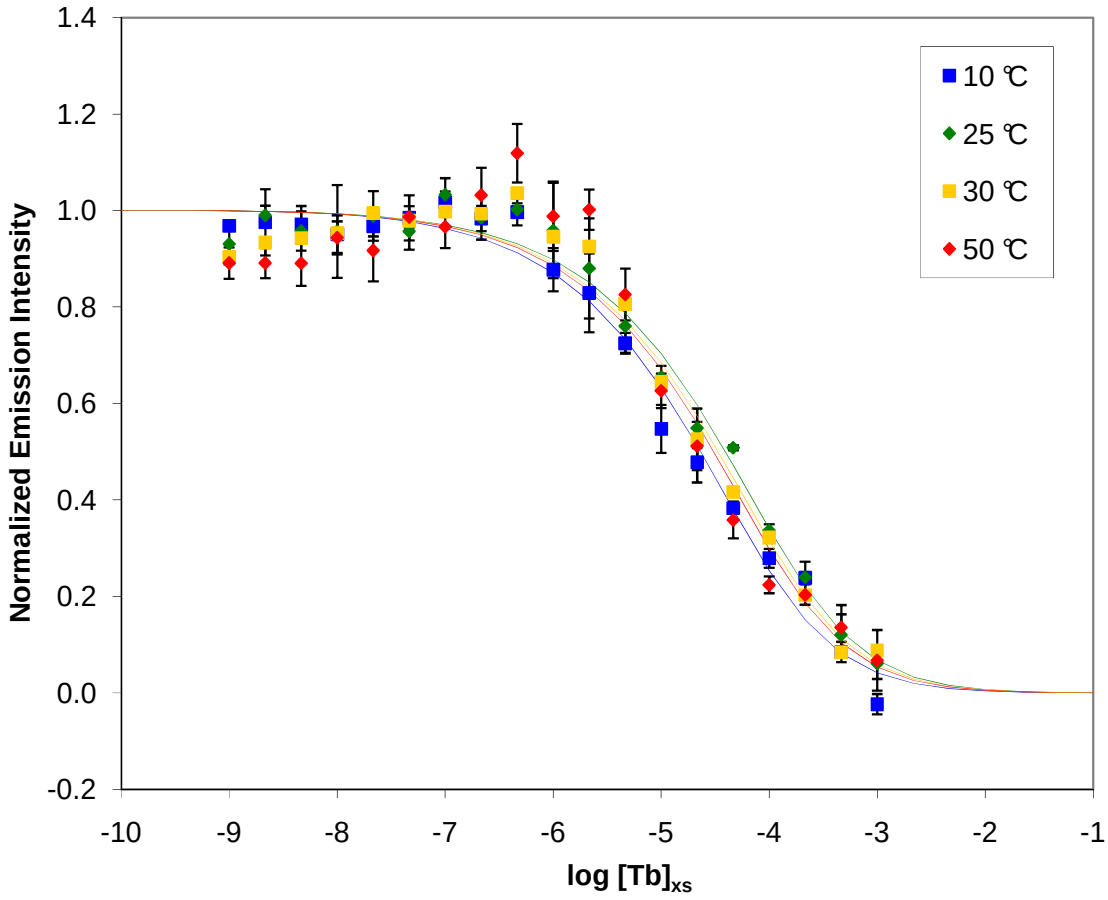

Figure 3.30. Binding affinity by competition (BAC) assay titration curves for Tb(DO2A)(DPA)$^{-}$ in 0.1 M buffer at various temperatures. Emission spectra (λ_{ex} = 278 nm) integrated from 570–600 nm.

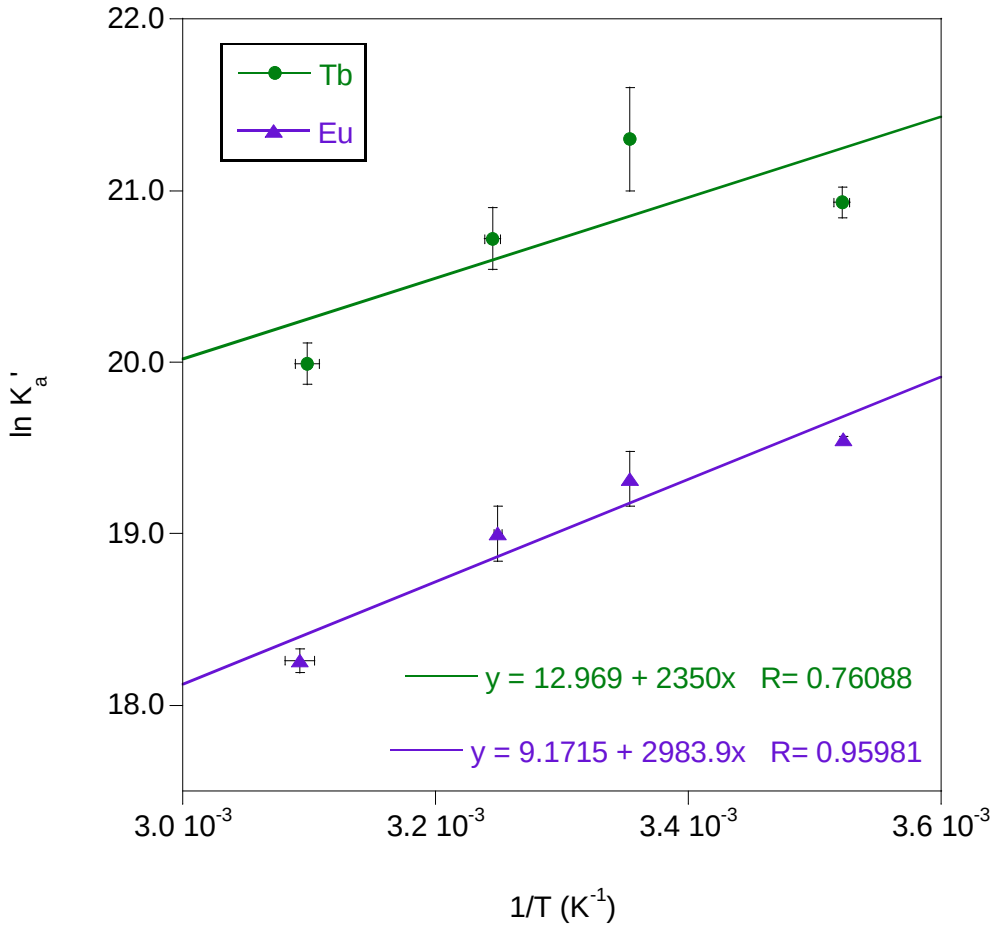

Figure 3.31. Plot of ln K_a' against 1/T for $Tb(DO2A)(DPA)^-$ and $Eu(DO2A)(DPA)^-$ in 0.2 M NaOAc, pH 7.4.

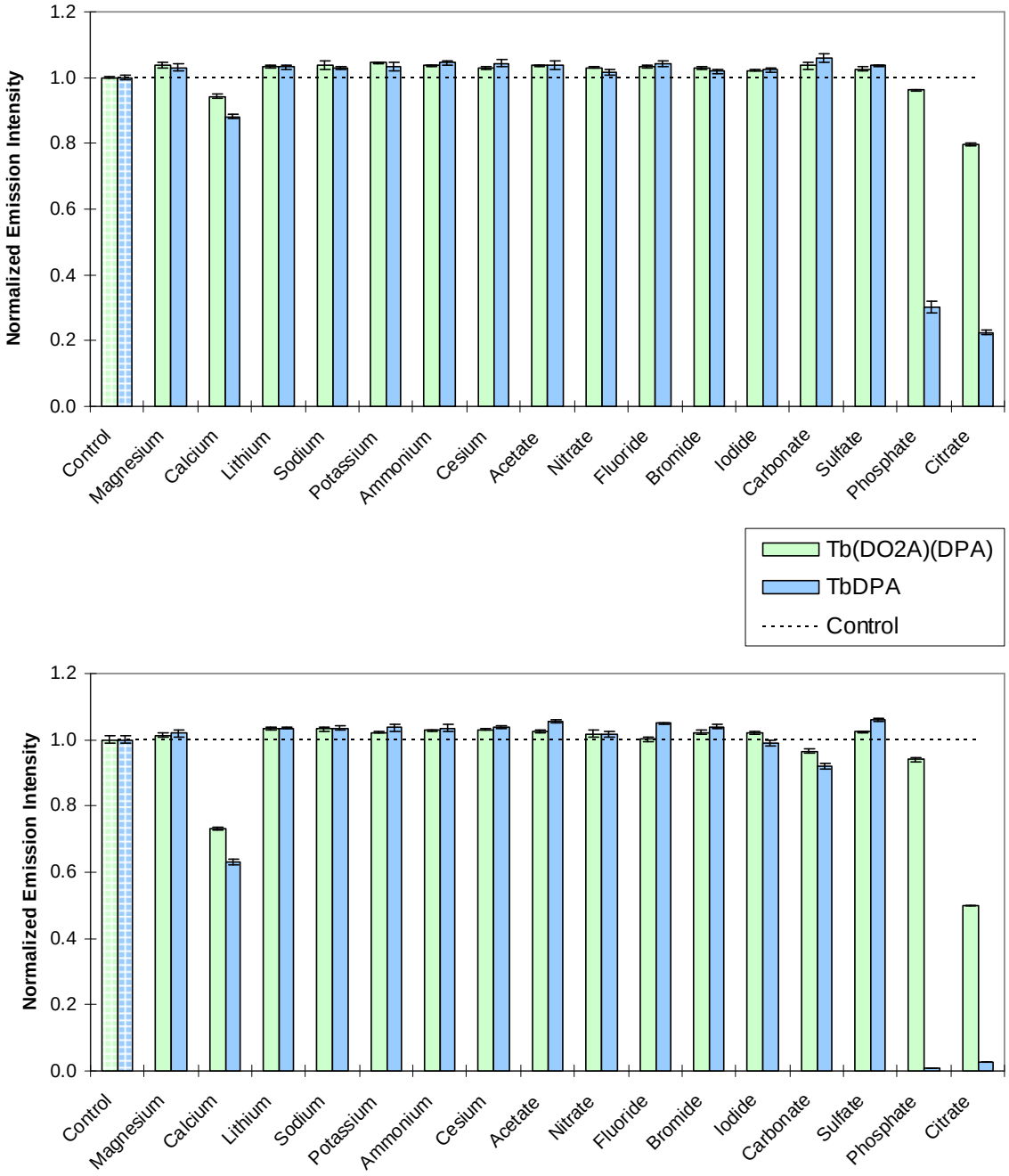

Figure 3.32. Emission intensity variation of 0.10 μM $Tb(DO2A)(DPA)^-$ or $Tb(DPA)^+$ complex with the addition of 100 μM (top) or 1.0 mM (bottom) of interfering ion, pH 5.2. Normalized integrated emission intensity, 530–560 nm; λ_{ex} = 278 nm.

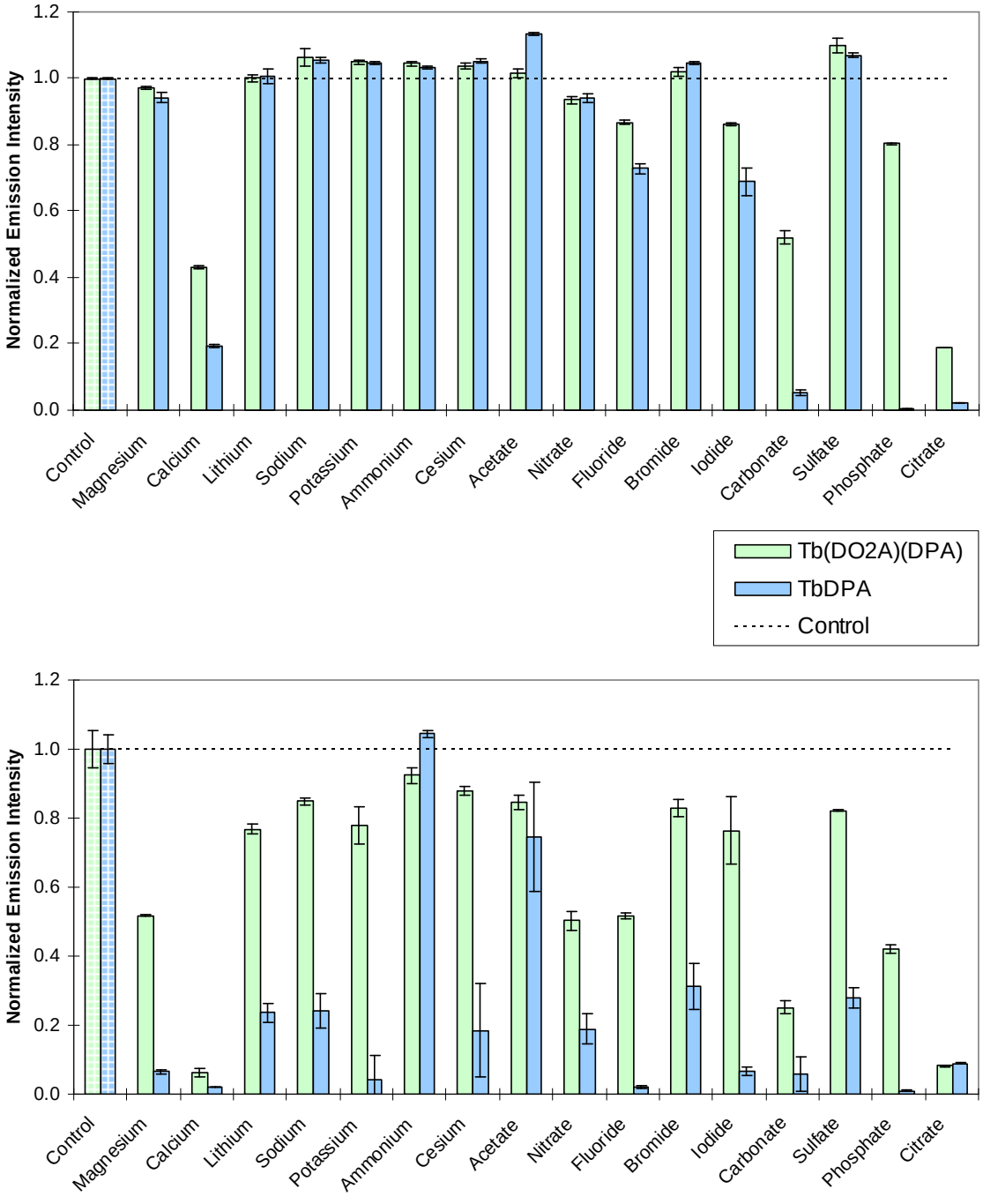

Figure 3.33. Emission intensity variation of 0.10 μM $Tb(DO2A)(DPA)^-$ or $Tb(DPA)^+$ complex with the addition of 10.0 mM (top) or 0.10 M (bottom) of interfering ion, pH 6. Normalized integrated emission intensity, 530–560 nm; λ_{ex} = 278 nm.

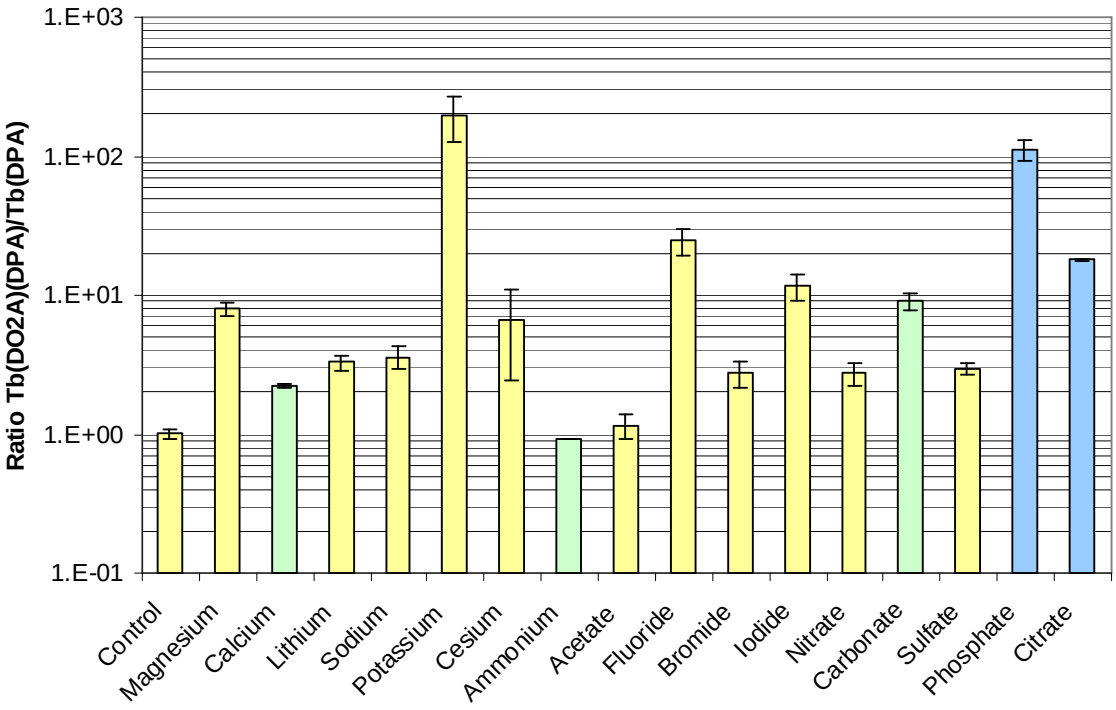

Figure 3.34. Ratio of 100 nM Tb(DO2A)(DPA)$^{-}$ to Tb(DPA)$^{+}$ emission intensity in 0.1 M (yellow), 10 mM (green) or 1 mM (blue) competing ion, pH 6.6. Ions are listed in order of charge from positive (left) to negative (right). Normalized integrated emission intensity, 530–560 nm; λ_{ex} = 278 nm.

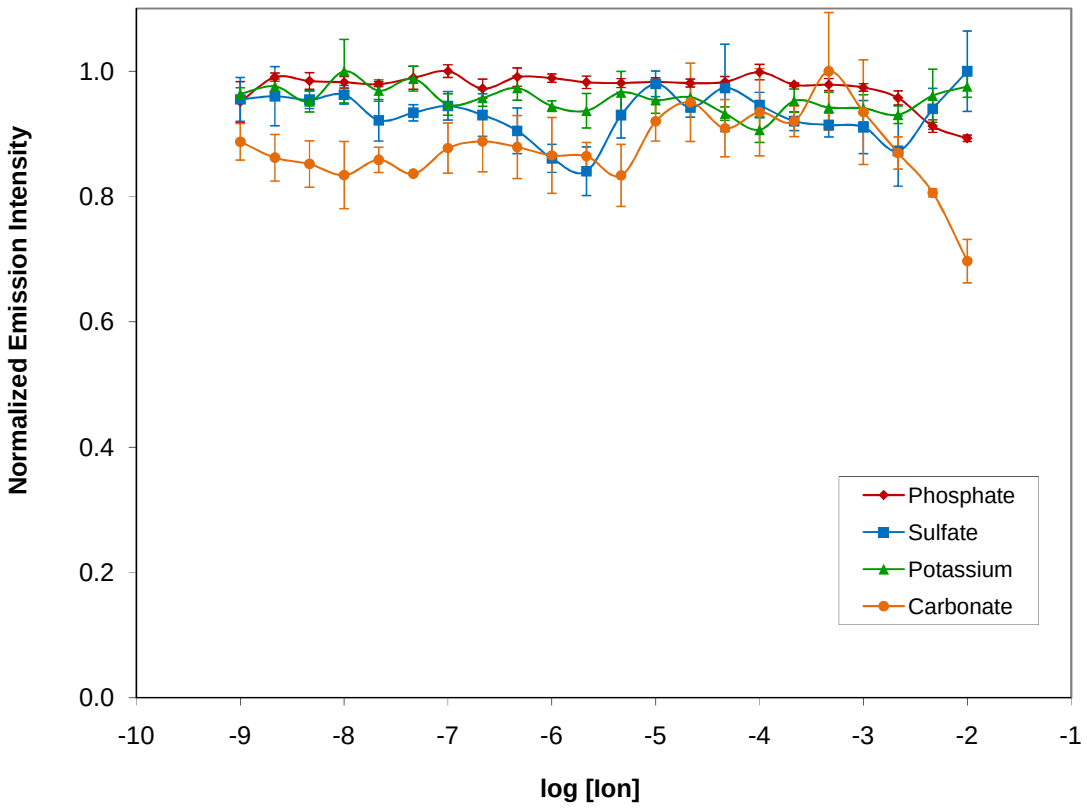

Figure 3.35. Ion competition experiment of 0.1 μM Tb(DO2A)(DPA)$^{-}$ titrated with phosphate (red), sulfate (blue), potassium (green) or carbonate (orange) over a concentration range from 1.0 nM to 100 mM, pH 7.5 (0.1 M MOPS). Carbonate appears to be the only ion that competes, and only at very high concentrations (1:10^5 [Tb(DO2A)(DPA)$^{-}$] : [CO_3^{2-}]).

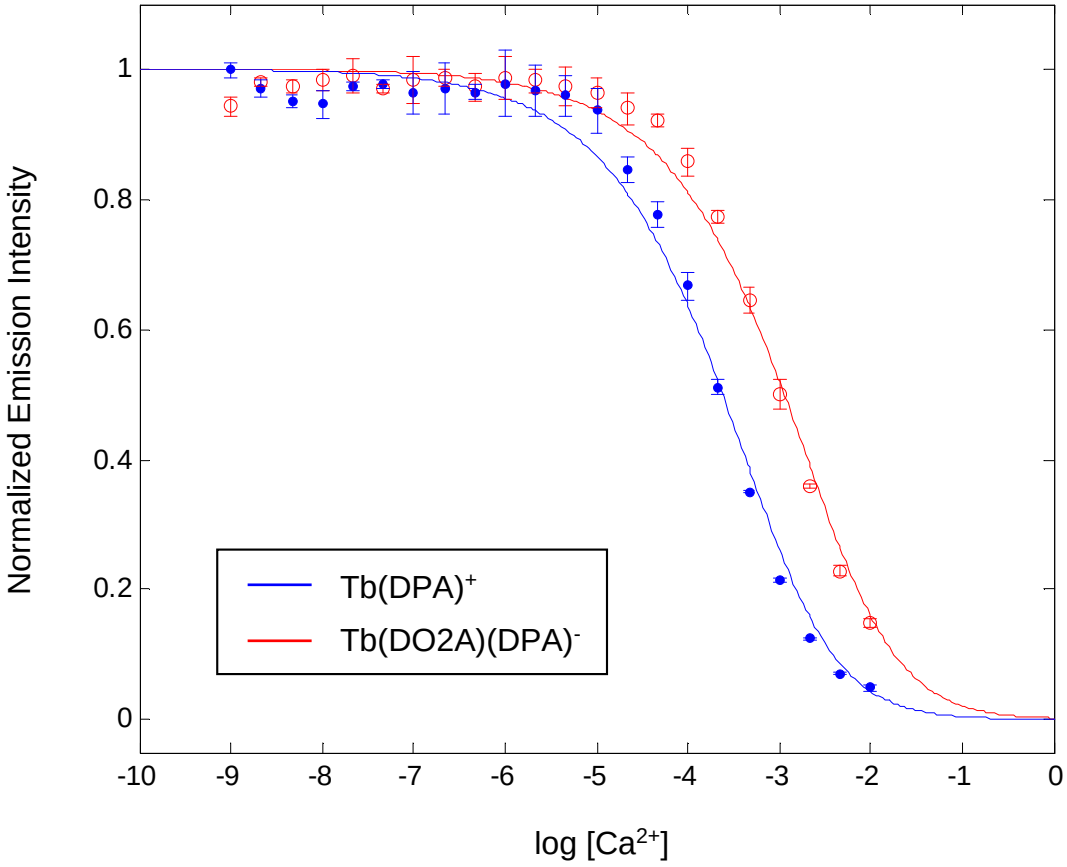

Figure 3.36. Cation competition experiment of 0.1μM $Tb(DO2A)(DPA)^-$ or $Tb(DPA)^+$ titrated with Ca^{2+} over a concentration range from 1.0 nM to 0.1 M, pH 7.5 (0.1 M MOPS). Emission intensity integrated from 530–560 nm, λ_{ex} = 278 nm.

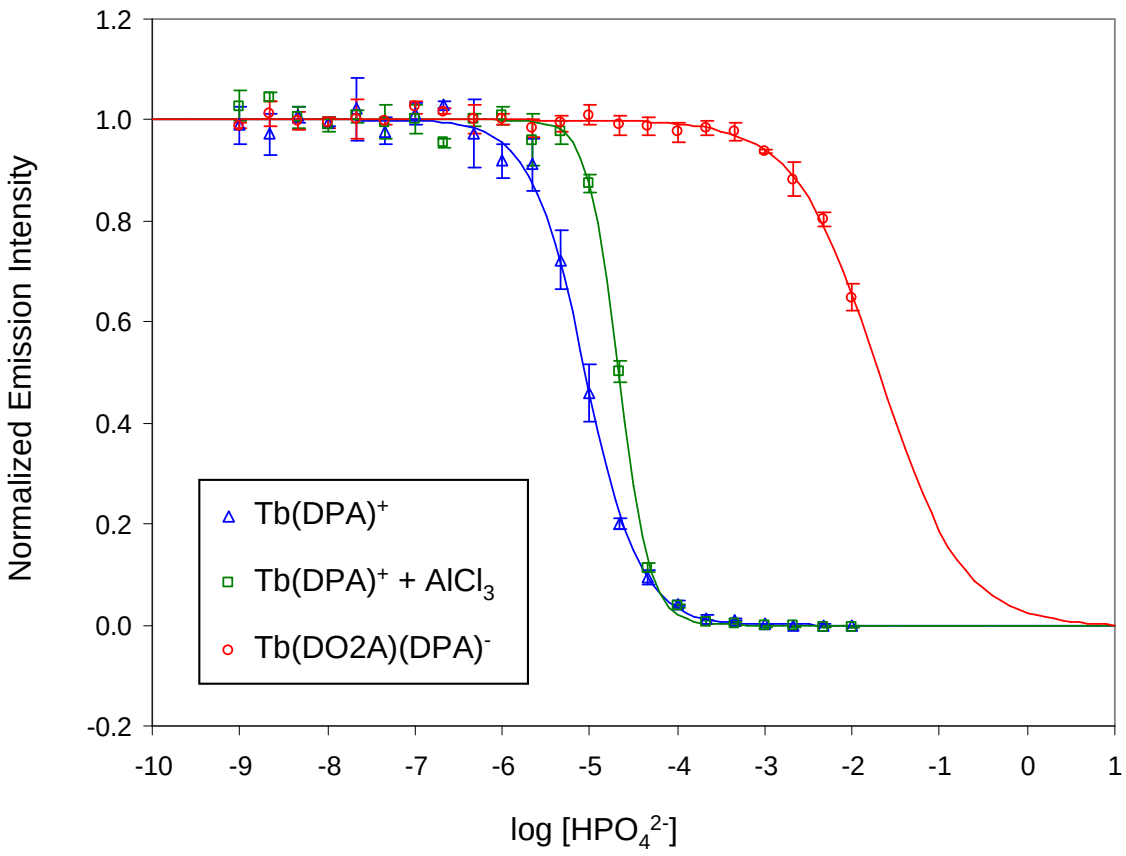

Figure 3.37. Anion competition experiment of 0.1μM Tb(DO2A)(DPA)$^{-}$, 0.1 μM Tb(DPA)$^{+}$ or 0.1 μM Tb(DPA)$^{+}$ with 100 μM aluminum chloride. Each was titrated with phosphate over a concentration range from 1.0 nM to 0.1 M, pH 7.3 (0.2 M NaOAc). Emission intensity integrated from 530–560 nm, λ_{ex} = 278 nm.

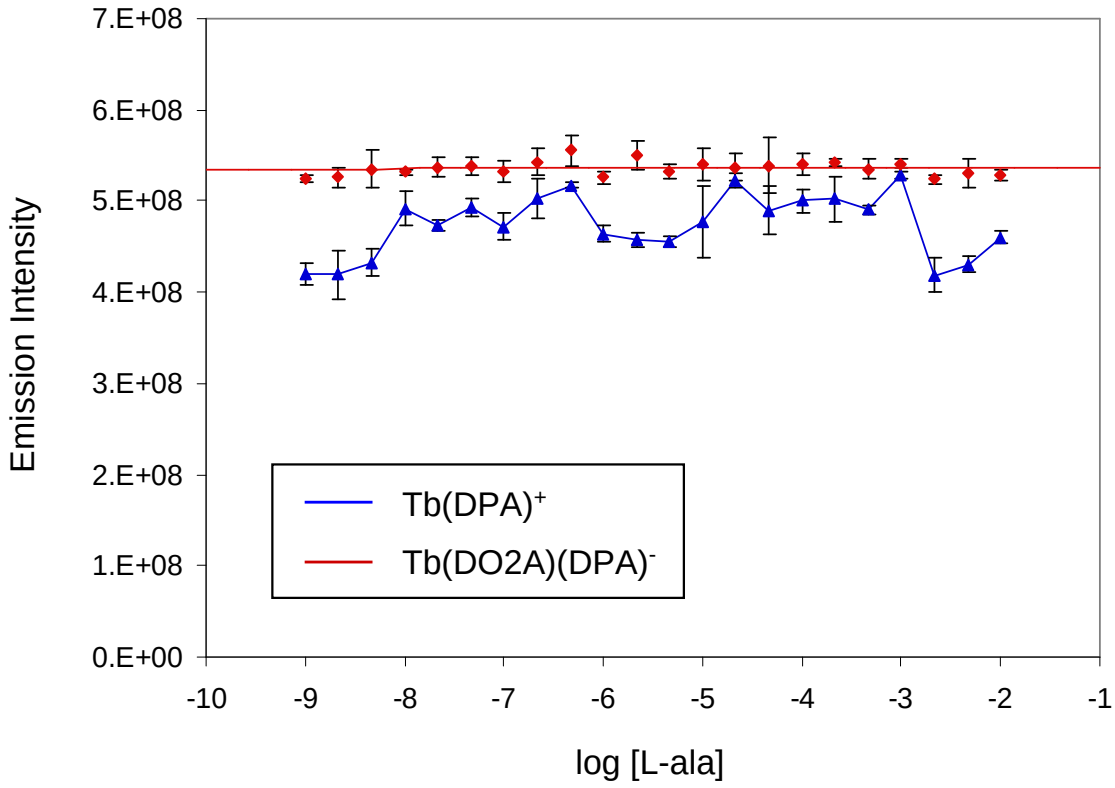

Figure 3.38. Germinant competition experiment of 0.1μM $Tb(DO2A)(DPA)^-$ or $Tb(DPA)^+$ titrated with L-alanine over a concentration range from 1.0 nM to 0.1 M, pH 7.5 (0.1 M MOPS). Emission intensity integrated from 530–560 nm, λ_{ex} = 278 nm.

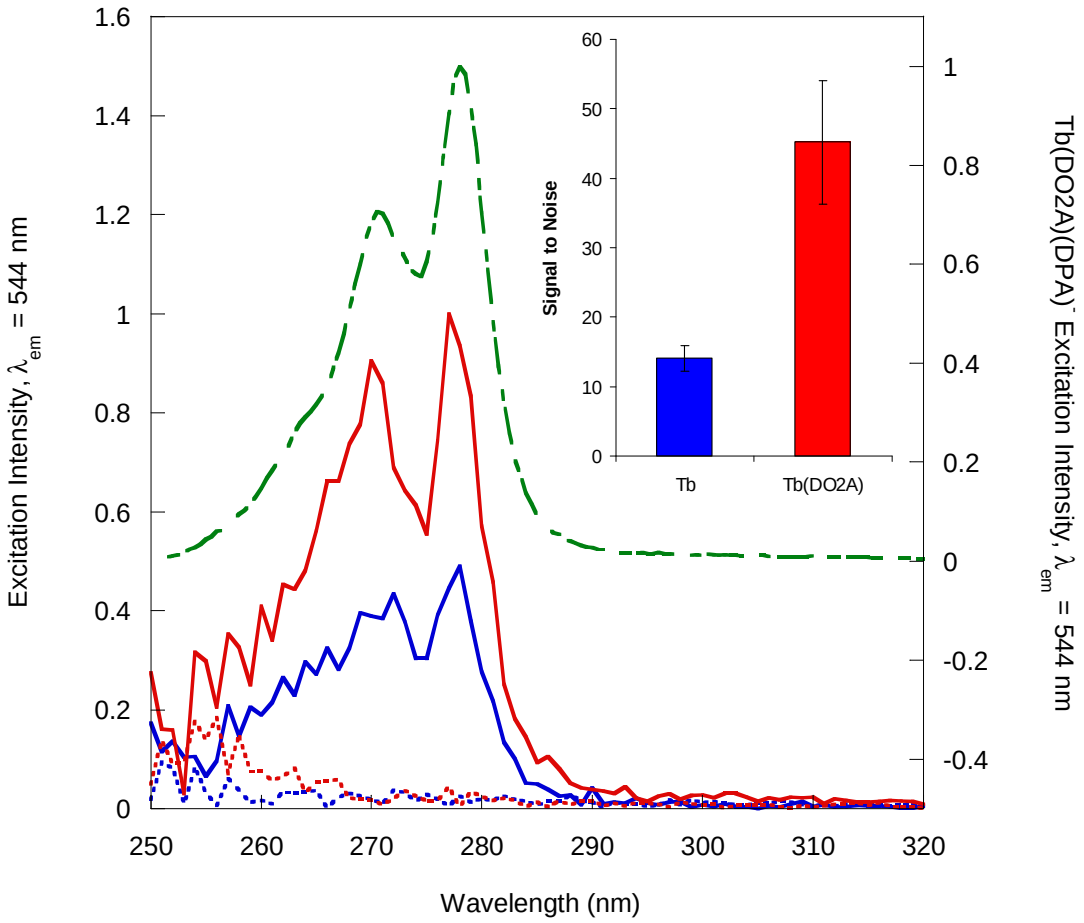

Figure 3.39. Excitation spectra of unfiltered samples of autoclaved *Bacillus atrophaeus* spores containing 10.0 μM of Tb^{3+} (blue) or the $Tb(DO2A)^{+}$ binary complex (red) in filter-sterilized nanopure H_2O. Dashed offset excitation spectrum (green) of 10 μM Tb(DO2A)(DPA) in 0.2 M sodium acetate, pH 7.4, confirms excitation profile as DPA. Concentration of bacterial spores approx. 10^5 spores/mL. Controls of Tb^{3+} or $Tb(DO2A)^{+}$ are shown in dotted blue and red, respectively. Inset: Signal-to-noise ratio of emission intensity, 530–560 nm, for Tb^{3+} (blue) and $Tb(DO2A)^{+}$ (red), showing a three-fold improvement in S/N with the use of DO2A.

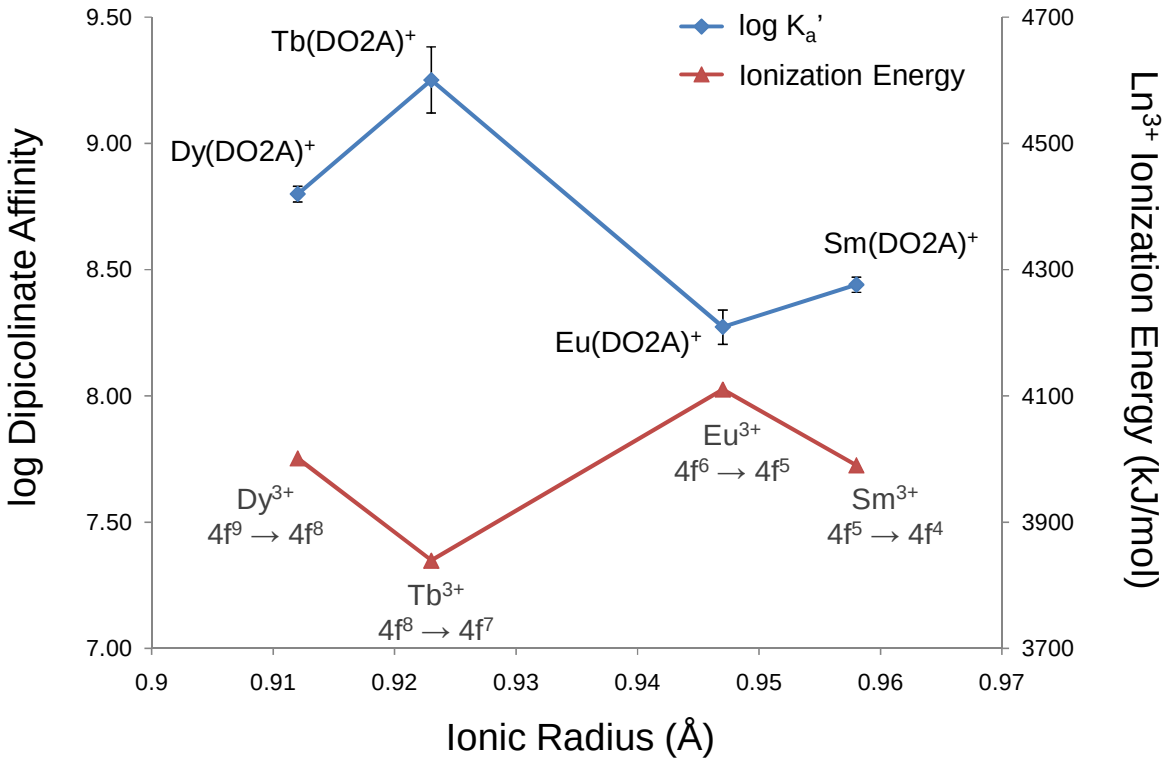

Figure 3.40. Relationship between Ln(DO2A)$^+$ dipicolinate binding affinity and $Ln^{3+} \rightarrow Ln^{4+}$ ionization energy with lanthanide ionic radius. The Tb(DO2A)$^+$ complex has the greatest affinity for DPA^{2-} because the low ionization energy of the Tb^{3+} ion makes it the most susceptible to perturbation by the DO2A ligand, shifting the electron density of the lanthanide and thereby generating the most positive binding site for the DPA^{2-} analyte. Ionization energies from reference 67.

TABLES

Table 3.1. Association constants of various lanthanide-macrocycle complexes.

Ln^{3+}	Macrocycle	log K	Ref
Gd	DO2A	19.42	8
	DO3A	21.0	▪
	DOTA	24.7	8
Sm	DOTA	23.0	5
Eu	DOTA	28.2	9
Tb	DOTA	28.6	9
Dy	DOTA	24.2	5

Table 3.2. Association constants of Ln^{3+} and $Ln(DO2A)^{+}$ with DPA^{2-}, calculated using a one-step equilibration model and the BAC assay, respectively, 0.2 M NaOAc, pH 7.5.

Ln	log K_a	log K_a'
Sm	7.64 ± 0.05	8.44 ± 0.03
Eu	7.46 ± 0.02	8.39 ± 0.07
Tb	7.41 ± 0.03	9.25 ± 0.13
Dy	7.57 ± 0.03	8.79 ± 0.03

Table 3.3. Crystallographic data for the TBA•Tb(DO2A)(F-DPA) structure.

Dipicolinate	**DPA**	**F-DPA**
Formula	$[C_{19}H_{25}N_5O_8Tb]^-[C_{16}H_{36}N]^+$• 0.47($C_3H_8O$) 0.53($C_3H_6O$) 3($H_2O$)	$[C_{19}H_{25}N_5O_8Tb]^-[C_{16}H_{36}N]^+$• ($C_3H_8O$) 2($H_2O$)
M_w	964.94	975.45
Crystal system	Monoclinic	Monoclinic
Space group	$P2_1/c$	$P2_1/c$
a (Å)	13.1047(5)	13.2324(6)
b (Å)	13.3397(5)	12.9812(6)
c (Å)	26.0901(9)	26.2126(11)
β (°)	90.0130(10)	90.528(2)
V ($Å^3$), Z	4560.9(3)	4502.4(3)
λ (Å)	0.71073	0.71073
D_c (Mg/m^3)	1.405	1.439
μ,Mo-Kα (mm^{-1})	1.613	1.671
T (K)	100(2)	100(2)
R_1, wR_2‡	0.0384, 0.0639	0.0285, 0.0499

‡ Structure refined on F^2 using all reflections: $wR_2 = [\Sigma[w(F^2 - F_c^2)^2]/\Sigma w(F^2)^2]^{1/2}$, where $w^{-1} = [\Sigma(F^2) + (aP)^2 + bP]$ and $P = [max(F^2,0) + 2F_c^2]/3$.

Table 3.4. Protonation constants of relevant ligands.

Ligand	pK_{a1}	pK_{a2}	pK_{a3}	pK_{a4}	pK_{a5}	pK_{a6}	Ref
DPA	-1.05	2.22	5.22	---------	---------	---------	15
DO2A	3.18	4.09	9.45	10.91	---------	---------	6
	2.55	3.85	9.55	10.94	---------	---------	5
DO3A	3.48	4.43	9.24	11.59	---------	---------	4
	3.39	4.40	9.51	10.72	---------	---------	5
DOTA	4.30	4.61	9.50	11.14	---------	---------	6
	4.00	4.60	9.90	11.34	---------	---------	5
Hexacyclen	~1	~2	4.09	8.73	9.23	10.19	7

Table 3.5. Calculated association constants for Ln^{3+} (K_a) and $Ln(DO2A)^{+}$ (K_a') for DPA^{2-} at various temperatures in 0.2 M NaOAc, pH 7.4 (Ln = Tb, Eu).

Temp (℃)	Tb		Eu	
	log K_a	log K_a'	log K_a	log K_a'
10.8	7.61 ± 0.16	9.09 ± 0.04	7.70 ± 0.05	8.49 ± 0.01
25.0	7.41 ± 0.03	9.25 ± 0.13	7.46 ± 0.02	8.39 ± 0.07
34.8	7.15 ± 0.01	9.00 ± 0.08	7.20 ± 0.05	8.25 ± 0.07
50.0	6.93 ± 0.05	8.68 ± 0.05	6.94 ± 0.03	7.93 ± 0.03

Table 3.6. Thermodynamic parameters calculated from the temperature dependence of K_a and K_a' for Tb and Eu in 0.2 M NaOAc, pH 7.4.

Reaction	ΔH (kJ/mol)	ΔS (J/mol·K)
$Tb^{3+} + DPA^{2-} \rightarrow Tb(DPA)^{+}$	-30.8	37.3
$Tb(DO2A)^{+} + DPA^{2-} \rightarrow Tb(DO2A)(DPA)^{+}$	-19.5	108
$Eu^{3+} + DPA^{2-} \rightarrow Eu(DPA)^{+}$	-34.7	25.5
$Eu(DO2A)^{+} + DPA^{2-} \rightarrow Eu(DO2A)(DPA)^{+}$	-24.8	76.3

Table 3.7. 'Ligand enhancement' in various lanthanide/analyte systems. Change in the analyte binding affinity (Δ log K)* due to the ligand in comparison to the lanthanide alone.

Ligand	Analyte	Δ log K	Ref
$DO2A^{2-}$	Dipicolinate	0.8 – 1.8	This work
$EDTA^{2-}$	Picolinate	0.2 – 1.5[†]	57, 58
L_1	Lactate	0.8 – 1.5[‡]	59, 60
L_2	Acetate	0.1 – 1.4[¥]	60, 61

*Δ log K = log K_a' – log K_a

[†] log K_a: 0.1 M KNO_3, 25 ℃; log K_a': 0.5 M $NaClO_4$, 25 ℃

[‡] log K_a: 0.1 M $NaClO_4$, 20 ℃; log K_a': 0.1 M collidine/HCl, 21.8 ℃, pH 7.4

[¥] log K_a: 0.1 M $NaClO_4$, 20 ℃; log K_a': 0.1 M collidine/HCl, 21.8 ℃, pH 7.4

L_1 = (*SSS*)-*1,4,7*-Tris[*1*-(*1*-phenyl)ethylcarbamoylmethyl]-*1,4,7,10*-tetraazacyclododecane, L_2 = (*SSS*)-*1,4,7*-Tris[*1*-(*1*-phenyl)ethylcarbamoylmethyl]-*10*-methyl-*1,4,7,10*-tetraazacyclo-dodecane

Table 3.8. Binding affinities for various Tb and Eu complexes for oxy-anions, pH 7.4–7.5, 295–298 K, showing the difference between the Tb and Eu species, Δ(Ln).

Ligand	Analyte	log K[†]		Δ(Ln)
		Tb	Eu	
DO2A	DPA	9.25	8.39	0.86
L_1	HCO_3^-	3.8	2.6	1.2
	$CH_3CO_2^-$	2.3	< 1.0	> 1.3
	HPO_4^{2-}	≥ 4.7	4.15	≥ 0.55
L_2	HCO_3^-	≥ 4.7	3.75	≥ 0.95
	$CH_3CO_2^-$	3.5	2.4	1.1
	HPO_4^{2-}	> 4.7	> 4.7	unknwn

[†] DPA values from this work, all others from reference 60 with errors ± 0.2

L_1 = (*SSS*)-*1,4,7*-Tris[*1*-(*1*-phenyl)ethylcarbamoylmethyl]-*1,4,7,10*-tetraazacyclododecane,
L_2 = (*SSS*)-*1,4,7*-Tris[*1*-(*1*-phenyl)ethylcarbamoylmethyl]-*10*-methyl-*1,4,7,10*-tetraazacyclo-dodecane